CFD Prediction and physical Mechanisms consideration of Thermal Separation and Heat transfer processes inside Divergent, Straight and Convergent Ranque-Hilsch Vortex Tubes

Adib Bazgir [a], Nader Nabhani [*a], Bahamin Bazooyar [b], Ali Heydari [a]

[a] *Ahvaz Faculty of Petroleum, Petroleum University of Technology (PUT), Ahvaz, P.O. Box 6198144471, Iran*

[b] *Post-Doctoral Researcher in Turbulent Combustion, Staffordshire University, Stoke-on-Trent, ST4 2DE, United Kingdom*

[*]Corresponding author

Nader Nabhani

Email: Nabhani@put.ac.ir

Tel: +989163060189

ABSTRACT: The design of Ranque-Hilsch vortex tube (RHVT) seems to be interesting for refrigeration and air conditioning purposes in industry. Improving thermal efficiency of the vortex tubes could increase the operability of these innovative facilities for a wider heat and cooling demand To this end, it is of a interest to understand the physical phenomena of thermal and flow patterns inside a vortex tube.. In the present work, the flow phenomena and the thermal energy transfer in Ranque-Hilsch vortex tube are studied for three RHVT: straight, divergent and convergent vortex tubes. A three-dimensional numerical analysis of swirling or vortex flow is performed, verified, and validated against previous experimental and numerical data reported in literature. The flow field and the temperature separation inside a RHVT for different configuration of straight, five angles of divergent hot-tube (1, 2, 3, 4 and 6 degree) and five angle of convergent hot-tube (0.5, 0.8, 1, 1.5 and 2 degree) are investigated. The thermal performance for all investigated RHVTs configuration is determined and quantitatively assessed via visualizing the stream lines for all three scenarios.

Keywords: *Heat Transfer enhancement; Divergent and convergent Ranque-Hilsch vortex tube; Physical flow structure; Secondary Circulation loop; Vortex formation; Thermal efficiency*.

Nomenclature	
ANN	Artificial Neural Network
CFD	Computational Fluid Dynamic
COP	Coefficient of Performance
LES	Large Eddy Simulation
RANS	Reynolds Average Navier Stokes
RHE	Ranque-Hilsch Effect
RHVT	Ranque-Hilsch vortex tube
RNG	Renormalized Group
RSM	Reynolds Stress Model
SC	Secondary Circulation
SOU	Second Order Upwind
VT	Vortex Tube

C_p	Specific heat capacity at constant absolute pressure ($J.kg^{-1}.K^{-1}$)
$C_{\varepsilon i}$	Coefficients (i = 1, 2) used in ε equation
C_μ	Constant in Eq.10
C_v	Constant in Eq.9
D	Diameter of the main tube (mm)
d_c	Diameter of the cold outlet (mm)
d_n	Diameter of the inlet nozzle (mm)
E	Total energy (kJ)
G_k	Generation of turbulence kinetic energy
K	Turbulence kinetic energy ($m^2.s^{-2}$)
k_e	Thermal conductivity ($W.m^{-1}.K^{-1}$)
L	Length of the vortex tube (mm)
L_h	Length of the hot-tube (mm)
Ma	Mach number
$\dot{m}$	Total mass flow rate ($kg.s^{-1}$)
P	Absolute total pressure (Pa)
Pr_t	Turbulent Prandtl number
ΔP	Pressure difference (Pa)
Q_c	Cooling rate
R	Specific constant of an ideal gas ($J.kgmol^{-1}.K^{-1}$)
R_{vt}	Radius of main tube (mm)
R	Radial distance (mm)
s_{ij}	Twice the strain rate tensor (s^{-1})
S_h	Energy source
T	Temperature (K)
T_H	Hot outlet temperature (K)
T_C	Cold outlet temperature (K)
u_i	Absolute fluid velocity component in i-direction ($m.s^{-1}$)
W	Mechanical energy
Y_M	Contribution of the fluctuating dilatation
z	Axial distance from the cold exit (mm)

Greek symbols	
α_k	Inverse effective Prandtl numbers for k equation (Eq.7)
α_ε	Inverse effective Prandtl numbers for ε equation (Eq.8)
δ_{ij}	Kronecker delta
τ	Shear stress ($N.m^{-2}$)
$(\tau_{ij})_{eff}$	Deviatoric stress tensor ($N.m^{-2}$)

$\boldsymbol{E}$	Turbulence dissipation rate ($m^{-2}.s^{-3}$)
$\boldsymbol{A}$	Cold mass fraction
$\boldsymbol{M}$	Dynamic viscosity ($kg.m^{-1}.s^{-1}$)
$\boldsymbol{\upsilon}$	Kinematic viscosity ($m^2.s^{-1}$)
$\boldsymbol{\hat{\upsilon}}$	Ratio of effective viscosity to the dynamic viscosity
$\boldsymbol{\Gamma}$	Specific heat ratio
$\boldsymbol{P}$	Density ($kg.m^{-3}$)
$\boldsymbol{\eta_0}, \beta, \boldsymbol{\eta}$	Coefficients in RNG k- ε model
$\boldsymbol{\lambda}$	Pressure loss ratio
$\boldsymbol{\eta_{is}}$	Isentropic efficiency

Subscripts	
a	Atmospheric
c	Cold gas
eff	Effective
h	Hot gas
in	Inlet gas
is	Isentropic
i , j ,k	Cartesian indicates
n	Nozzle
st	Static
t	Turbulent
vt	Vortex tube

1 .Introduction

Nowadays, the cooling process industries faces strict legal regulations requiring control of pollutants and fuel consumption. The design of innovative vortex tube is a great opportunity to comply with these regulations especially for low temperature applications because there is no need of any refrigerants and energy consumption (when compressed air is available). A vortex tube consists of a hollow cylinder, in which a compressed gas is admitted tangentially into its tube from

a side pipe wall and separate in a low and high total temperature flow region, as schematically shown in Fig. 1. On one side, the cold gas in the center exits through a central circular orifice with a temperature considerably lower than it had at the inlet, whereas on the other side, the hot gas flows through a ring orifice with a temperature much greater than the inlet. This could be done in the absence of any moving parts or work input, electrically or chemically. This somehow surprising temperature or energy separation is identified as the Ranque-Hilsch effect (RHE). This device was discovered by Ranque [1] in 1933 and examined experimentally in 1940's by Hilsch [2]. Since then, the device is called Ranque-Hilsch vortex tube. Vortex tube has low thermal efficiency and low coefficient of performance (COP) compared with other conventional cooling devices. However, this disadvantages is completely overshadowed by its lightweight, compactness, low cost, environmentally friendly (no need for refrigerant), maintenance free (no moving part) and no need of input work or heat. The energy separation inside vortex tube has been examined by many researchers both experimentally or numerically with respect to geometric and thermo-fluid physical parameters. These studies can be further summarized in two groups according to previous efforts on the vortex tube. The first is concerned with investigation of the performance of the vortex tube. The second is focused on the flow structure or physical pattern occurring inside the vortex tube. A literature review on the studies of RHVTs is listed in Table (1). Details review on Ranque-Hilsch effect can be found in Eiamsa-ard and promvonge [3], Gutsol [4], Thakare et al. [5], Xue et al. [6] and Yilmaz et al. [7].

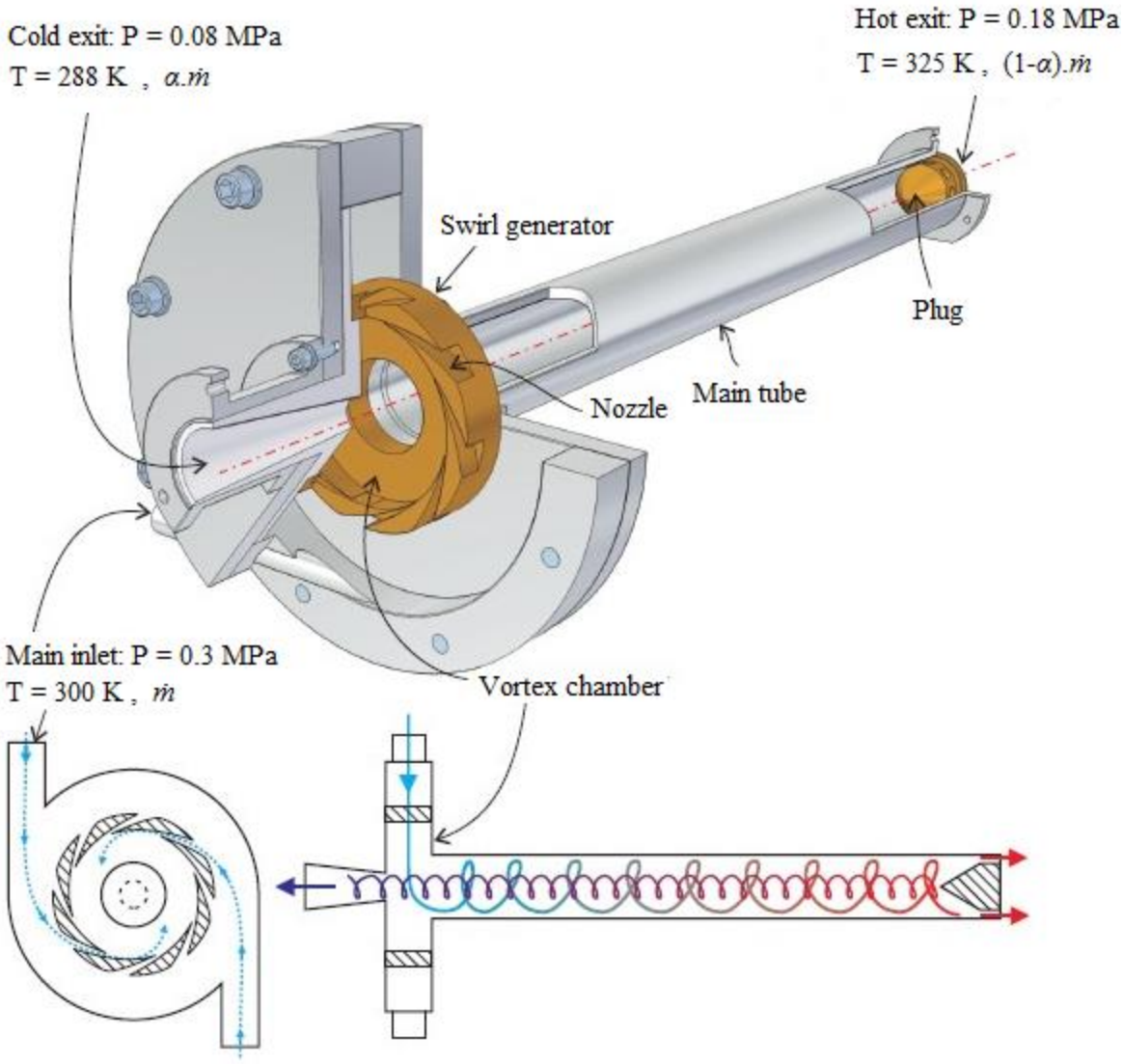

Fig. 1. Geometry structure of the counter-flow Ranque-Hilsch vortex tube.

Table 1. A literature overview on the studies of vortex tubes.

Author	Year	Investigation	Ref.
Ranque	1933	First temperature separation in VT	[8]
Hilsch	1946	First detailed parameter study of temperature separation in VT	[2]
Knoernschild	1948	Explanation of the RHE	[9]
Elser and Hoch	1951	Separation of gases in VT	[10]
Deissler and Perlmutter	1960	Analysis of energy separation	[11]
Reynolds	1961	Mechanism of energy separation	[12]
Erdelyi	1962	Explanation of the RHE	[13]
Sibulkin	1962	Unsteady, viscous, circular flow	[14]
Gulyaev	1965	RHE at low temperatures	[15]
Bruun	1969	Experimental energy separation in VT	[16]

Linderstrom-Lang	1971	3D calculations of velocity and temperature in VT	[17]
Takahama and Yokosawa	1981	Energy separation in divergent VT	[18]
Kurosaka	1982	Acoustic streaming in swirling flow	[19]
Stephan et al.	1983	Experimental investigation of energy separation	[20]
Stephan et al.	1984	Mathematical formulation of energy separation	[21]
Eckert	1986	Energy separation in VT	[22]
Balmer	1988	RHE in liquids	[23]
Ahlborn et al.	1994	Temperature separation limits	[24]
Ahlborn and Groves	1997	Secondary flows in VT	[25]
Gutsol	1997	RHE review	[4]
Gutsol and Bakken	1998	Explanation of RHE	[26]
Fröhlingsdorf et al.	1999	CFD analysis of VT (standard k-ε)	[27]
Mischner and Bespalov	2002	Entropy production in RH-tube	[28]
Shannak	2004	Temperature separation in VT	[29]
Aljuwayhel et al.	2005	Numerical study of VT (RNG k-ε, standard k-ε)	[30]
Behera et al.	2005	Numerical study of RHVT (RNG k-ε)	[31]
Gao et al.	2005	Experimental study of RHVT	[32]
Piralishvili and Fuzeeva	2005	Analytical and experimental study of RHVT	[33]
Piralishvili and Fuzeeva	2006	Criteria for energy separation	[34]
Sky et al.	2006	Numerical study of VT (RNG k-ε, standard k-ε)	[35]
Sohn et al.	2006	Experimental and numerical study of VT	[36]
Eiamsa-ard and Promvonge	2006	Numerical study of VT	[37]
Eiamsa-ard and Promvonge	2007	Numerical study of RHVT	[38]
Eiamsa-ard and Promvonge	2008	Review of RHVT	[3]
Dincer et al.	2008	Experimental study of RHVT	[39]
Behera et al.	2008	Numerical study of RHVT (RNG k-ε)	[40]
Xue and Arjomandi	2008	Effect of vortex angle in RHVT	[41]
Yilmaz et al.	2009	Review on design criteria for VT	[7]
Secchiaroli et al.	2009	Numerical study of RHVT (RANS and LES)	[42]
Zin et al.	2010	Numerical study of VT (RNG k-ε)	[43]
Xue et al.	2010	Review of temperature separation	[6]
Liew et al.	2012	Experimental study of RHVT	[44]
Liew et al.	2012	Theory of energy separation in RHVT (Maxwell's demon)	[45]
Xue et al.	2013	Experimental study of temperature separation	[46]
Liu et al.	2014	Numerical study of VT (standard k-ε)	[47]

Xue et al.	2014	Energy analysis in VT	[48]
Kobiela	2014	Analytical derivation of the RHE from the conservation equations	[49]
Thakare et al.	2015	Review of experimental, numerical and optimization studies of VT	[5]
Manimaran	2016	Computational analysis of energy separation	[50]

Several numerical and experimental works have been done to investigate the performance of the VT. Among these, Takahama [51] studied the energy separation efficiency, velocity distribution, and temperature distribution inside the tube, experimentally. Later, Takahama et al. [52] studied the effects of divergent tube with a divergent angle of 1.75^{o} on the performance of VT. They reported that the performance of divergent vortex chamber is better than the straight tube with the same length of tube. However, they studied only one divergent vortex chamber without changing the angle of the divergent. Saidi et al. [53] studied the effects of parameter on the performance of VT by changing diameter and length of main tube, diameter of cold exit, shape of entrance nozzle, and types of working gas. They used a tube with an inner diameter of 18 mm. They reported the optimum value of length to inner diameter ratio ($^{L}/_{D}$) is 55.5, cold exit diameter is 50% of inner diameter of tube, and diameter of inlet nozzle is 3.5 mm with 3 inlets. They also report that helium is better than oxygen or air as the working gas for a higher performance of VT. Nimbalkar et al. [54] performed a CFD analysis and experimental investigation to optimize the geometry of VT. They reported that the optimum size of the cold exit is 58% of the diameter of tube, which is same as Saidi et al. [53] but 8% smaller than the result of Behera et al. [31]. Chang et al. [55] studied the effect of a divergent vortex chamber on the performance of the VT, similar to Takahama et al. [52], with variation of divergent angle of tube. They reported that the performance of the VT can be improved by using the divergent tube with a divergent angle not more than 6^{o}. Uluer et al. [56] used an artificial neural network (ANN) for modelling the performance of the vortex tube. They performed an experiment using a VT with 2, 3, 4, 5 and 6 inlet nozzles. They estimated the temperature gradient by using the ANN mode. Korkmaz et al. [57] also used ANN to estimate the performance of VT. They modeled the VT with ANN using experimental data to study the effects of conical valve angle, inlet pressure and length of the tube to the performance of VT. They reported that ANN is a reliable option in modelling of the thermo-fluids systems. Khazaei et al. [58] investigated the effects of gas properties and geometrical parameters on performance of a vortex tube using a CFD model. They reported that the cold temperature difference increases by using working gas with a larger specific heat ratio, and the hot exit dimension and its shape have

a negligible effect on temperature distribution in a VT. An overview of important design criteria for vortex tubes are summarized by Behera et al. [31] and Yilmaz et al. [7].

In parallel with the investigation of performance of vortex tubes, several researchers studied the flow structure inside VT numerically and experimentally to explain the reasons behind the physical behavior of the flow. For example, Xue et al. [59] recently studied the flow structure in VT, which is immerged under water, using air bubble as seeding particle. They used water as the working fluid, so no compression and expansion occur inside the tube. They reported the axial and swirl velocity of the flow inside the tube and the image of flow visualization inside the tube. Later, Xue et al. [60] used a cobra probe to measure the pressure inside a large VT with an inner diameter of 60 mm and a length 2000 mm. They calculate the velocity of flow inside VT based on the measured pressures. They reported that the gradually changed static pressure distributions along the VT axis indicates the transformation of a forced vortex at cold exit side to a free vortex at hot exit side. They also proposed a flow pattern with a stagnation point exists inside VT. Aljuwayhel et al. [30] and Behera et al. [31] presented a computational analysis to explain the flow behavior and energy separation. They reported that the cause of the energy separation is primarily due to the thermodynamic work resulting from the viscous shear stress. Gao et al. [32] presented an experimental investigation of the flow pattern inside vortex tube. They reported that the secondary circulation flow and different pressures, temperature and velocity fields appears in the VT.. Farouk and Farouk [61] discussed the application of large eddy simulation (LES) method in a numerical investigation of temperature field inside vortex tube. Eiamsa and Promvonge [62] attempted to perform an algebraic stress model and k-ε model to study the energy separation numerically. Liu et al. [47] presented a numerical method taking the effect of fluid compressibility using CFD code. They reported that the multi-circulation flow is an important factor in Ranque-Hilsch effect. More recently, Manimaran [50] experimentally investigated the effect of the inlet shape of rectangular and trapezoidal, addressing the importance of turbulent kinetic energy in energy separation inside vortex tube. Bianco et al. [63] represented a numerical method of the performance of RSM and LES turbulence methods to predict the internal flow features in a double-circuit RHVT. Xue et al. [6] published a critical review of temperature separation in RHVT. They summarized the theories and the main factors of physical behavior of the flow and proposed the important point for Ranque-Hilsch effect. They showed that the available explanations in the literature are not in consensus with a general physical mechanism of energy separation. Further attention, elevation and research of different physical factors are needed. Moreover, the above cited research clearly indicates that the optimal geometry to obtain a higher performance of RHVT is experimentally well known. On the contrary, the flow physical pattern inside the tube, which is the key point of RHE, is still

remaining unclear. A three-dimensional computational method is therefore necessary to obtain an more reliable and accurate information and to fully understand the exact flow behavior of the complex thermo-hydraulic phenomena. Moreover, only relative few experimental studies have focused on the divergent vortex tube and none on the convergent vortex tube type. Therefore, additional research efforts are still required in order to find which one is able to give the optimal geometry corresponds to the highest efficiency.

The aim of this paper is:

1- To perform a detailed comparison, analysis and finally finding the optimal performance of straight, divergent and convergent vortex tube geometries with similar operational range. This is accomplished under different divergent and convergent angles of hot (main)-tube, and

2- To document and explain the relationship between the velocity and thermal fields in order to capture and demonstrate the major physical mechanism occurring inside vortex tube. Indeed there is a complex flow established in vortex tubes such as the existence of secondary flow circulation and vortex formation..

Moreover, a three-dimensional computational technique utilizing the RNG k-ε turbulence model was established in order to provide a clear information and detailed insight into vortex tube separation mechanism. In addition, the numerical model was verified and validated with previous experimental and numerical data reported in literature.

2. Schematic of the geometry

The Schematic of the three different types of the vortex tubes; (a) straight tube, (b) divergent tube and (c) convergent tube are shown in Fig. 2. Vortex tube with eleven angles is employed for investigation in both diverging and converging mode with the same length. Detailed geometrical parameters of the vortex tubes are given in Table (2). The straight model has an inside diameter of D = 10 mm aluminum tube. Air enters the main tube tangentially through six nozzles with $d_n = 2\,mm$. Vortex tubes are considered with constant parameters (except the angle of divergence), inner diameter of the cold tube is $d_c = 6\,mm$.

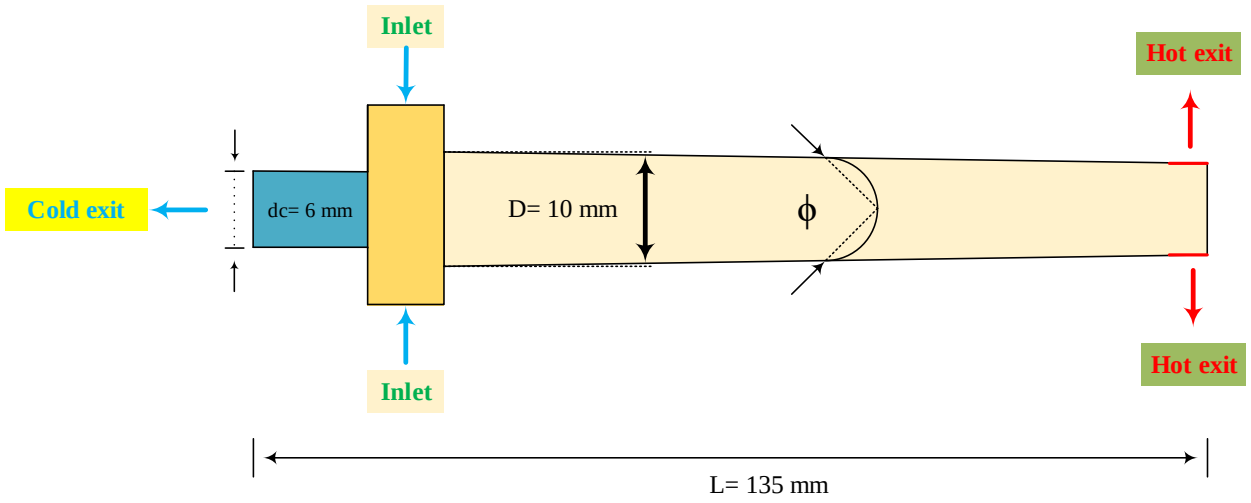

(a)

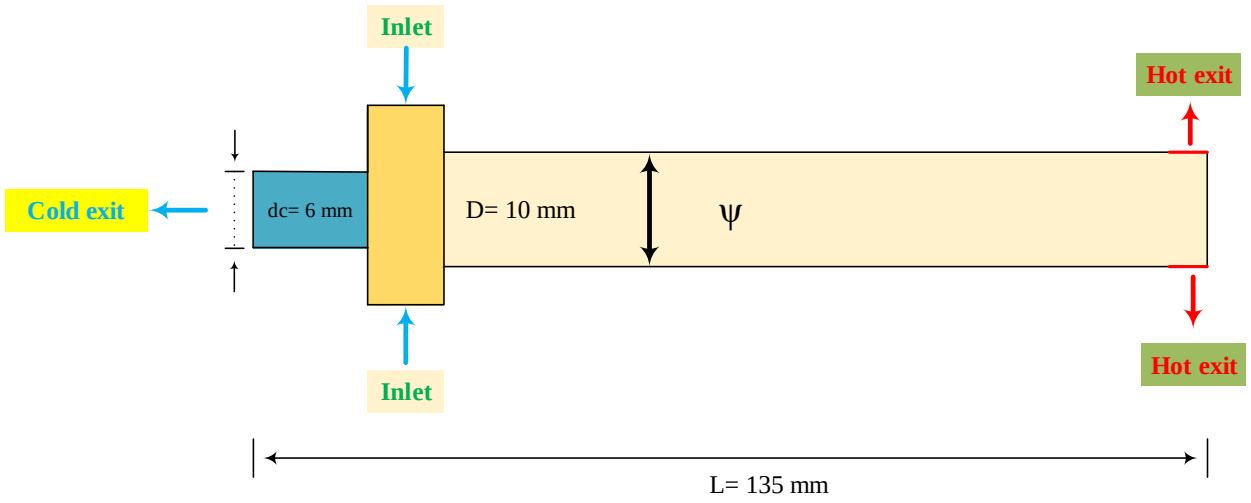

(b)

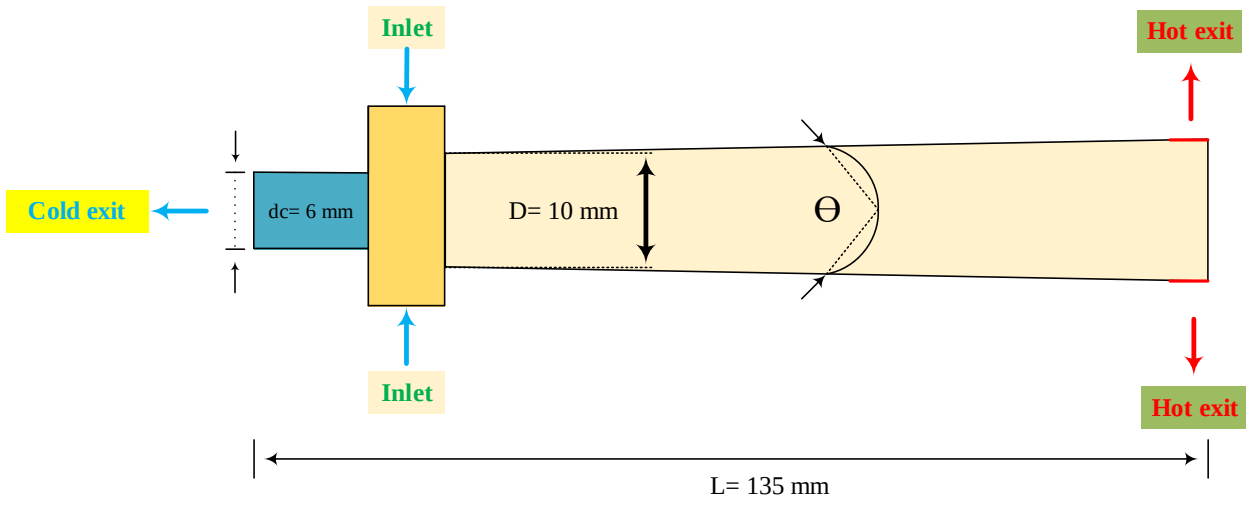

(c)

Fig. 2. Schematic of the investigated vortex tubes: (a) Convergent vortex tube, (b) Straight (β = 0) vortex tube and (c) Divergent vortex tube.

3. Numerical simulation

3.1. Problem description

A vortex tube with characteristics of Liu et al. [47] is numerically studied. The working fluid is purposed to be compressible, turbulent . Investigation of the temperature separation phenomenon inside Ranque-Hilsch vortex tube is the main target of this simulation. A computational fluid dynamic (CFD) software Ansys Fluent 16.1 is utilized to implement the present numerical simulation.

3.2. Governing equations and turbulence model

The compressible turbulent flows in the vortex tubes are determined by solving the conservation of all three equations of momentum, mass and energy. The RNG k-ε turbulence model is represented to solve the flow complexity. All equations are mentioned below:

Continuity equation:

$$\frac{\partial}{\partial x_i}(\rho u_i) = 0 \tag{1}$$

Momentum equation:

$$\frac{\partial}{\partial x_i}(\rho u_i u_j) = -\frac{\partial P}{\partial x_i} + \frac{\partial}{\partial x_j}(\mu\left(\frac{\partial u_i}{\partial x_j} + \frac{\partial u_j}{\partial x_i} - \frac{2}{3}\delta_{ij}\frac{\partial u_k}{\partial x_k}\right) + \frac{\partial}{\partial x_j}(-\rho\bar{u}_i\bar{u}_j) \tag{2}$$

Equations. (1) and (2) are well-known as Reynolds-averaged Navier – Stokes (RANS) equations.
Energy equation:

$$\frac{\partial}{\partial x_i}[u_i(\rho E + P)] = \frac{\partial}{\partial x_j}\left[\left(k_e + \frac{c_p\mu_t}{Pr_t}\right)\frac{\partial T}{\partial x_j} + u_i(\tau_{ij})_{eff}\right] + S_h \tag{3}$$

$$(\tau_{ij})_{eff} = \mu_{eff}\left(\frac{\partial u_j}{\partial x_i} + \frac{\partial u_i}{\partial x_j}\right) - \frac{2}{3}\mu_{eff}\frac{\partial u_k}{\partial x_k}\delta_{ij} \tag{4}$$

Ideal gas equation:

$$P = \rho RT \tag{5}$$

We employ the Boussinesq hypothesis [64] to relate the Reynolds stress:

$$-\rho\bar{u}_i\bar{u}_j = \mu_t\left(\frac{\partial u_i}{\partial x_j}+\frac{\partial u_j}{\partial x_i}\right)-\frac{2}{3}\left(\rho k+\mu_t\frac{\partial u_k}{\partial x_k}\right)\delta_{ij} \tag{6}$$

The RNG k-ε turbulence model is obtained from the Navier – Stokes equations, employing a mathematical procedure which is known as renormalization group (RNG) methods. In addition, more expansive details and descriptions of RNG theory and its applications to turbulence can be found in ref. [65].

Transport equations for the RNG k-ε turbulence model are mentioned below:

$$\frac{\partial}{\partial x_i}(\rho k u_i) = \frac{\partial}{\partial x_j}\left(\alpha_k\mu_{eff}\frac{\partial k}{\partial x_j}\right)+G_k+\rho\varepsilon-Y_M \tag{7}$$

$$\frac{\partial}{\partial x_i}(\rho\varepsilon u_i) = \frac{\partial}{\partial x_j}\left(\alpha_\varepsilon\mu_{eff}\frac{\partial \varepsilon}{\partial x_j}\right)+C_{1\varepsilon}\frac{\varepsilon}{k}G_k-C_{2\varepsilon}^{*}\rho\frac{\varepsilon^2}{k} \tag{8}$$

The effective viscosity is acquired by:

$$d\left(\frac{\rho^2 k}{\sqrt{\varepsilon\mu}}\right) = 1.72\frac{\hat{\upsilon}}{\sqrt{\hat{\upsilon}^3-1+C_\upsilon}}d\hat{\upsilon}, \qquad \hat{\upsilon} = {}^{\mu_{eff}}/_{\mu}\ ,\ C_\upsilon \approx 100 \tag{9}$$

$$C_{2\varepsilon}^{*} = C_{2\varepsilon}+\frac{C_\mu\eta^3(1-\frac{\eta}{\eta_0})}{1+\beta\eta^3}$$

$$\eta = (2\,S_{ij}.S_{ij})^{1/2}\,\frac{k}{\varepsilon} \tag{11}$$

$$S_{ij} = \left(\frac{\partial u_i}{\partial x_j}+\frac{\partial u_j}{\partial x_i}\right) \tag{12}$$

Eq. (9) is modulated to acquire an exacting explanation of how the effective turbulent transport and Reynolds number (or eddy scale) can vary with each other.

The definition of production of turbulence kinetic energy is calculated by:

$$G_k = -\rho \bar{u}_i \bar{u}_j \frac{\partial u_i}{\partial x_i} \tag{13}$$

The dilatation dissipation term, Y_M, is included in the k equation. This term is modeled based on a suggestion by Sarkar [66]:

$$Y_M = 2\rho\varepsilon {Ma_t}^2 \quad , \quad Ma_t = \sqrt{\frac{k}{\gamma RT}} \tag{14}$$

The model constants are:

$$C_\mu = 0.0845, C_{1\varepsilon} = 1.44, C_{2\varepsilon} = 1.44, \alpha_k = \alpha_\varepsilon = 1.39, Pr_t = 0.85, \beta = 0.012, \eta_0 = 4.377 \tag{15}$$

Further information and details base on the governing equations and RNG k-ε turbulence model can be found in ref. [67].

3.3. Geometry of models

Five kinds of divergent and convergent and a straight vortex tubes with same geometry features such as: length of tube, diameter of main tube and etc. are modeled by Gambit 2.4.6 mesh generator software for CFD simulation. Table (2) shows the vortex tube's dimensions. Straight models have an inside diameter of D = 10 mm aluminum tube but diameter of both divergent and convergent vortex tubes vary with their different angles. Air entered the main tube through six inlet nozzles of d_n = 2 mm diameter tangentially. The schematic diagram of vortex tubes are shown in Fig. 3. The flow rates of hot and cold streams are adjusted by hot control valve. Vortex tubes are designed with constant parameters: inner diameter of cold end tube is d_c = 6 mm.

No.	θ (°)	L (mm)	D (mm)	L/D

Table 2

1	2º convergent	120	5.811	20.6512
2	1.5º convergent	120	6.858	17.49
3	1º convergent	120	7.9055	15.1793
4	0.8º convergent	120	8.324	14.41
5	0.5º convergent	120	8.952	13.40
6	Straight	120	10	12
7	1º divergent	120	12.0946	9.9217
8	2º divergent	120	14.1892	8.4571
9	3º divergent	120	16.282	7.3689
10	4º divergent	120	18.375	6.5285
11	6º divergent	120	22.5779	5.31

Geometry characteristics of vortex tubes.

3.4. Solution scheme and boundary conditions

The CFD code was applied for the RNG k-ε simulations reported in this research paper. Finite volume method is a kind of numerical scheme which is implemented to solve the governing equations base on this analysis. For convective-diffusive terms in the (RANS) equations, continuity and momentum equations (Equation. (1) and (2)), the energy equations (Equation. (3) and (4)), together with an RNG k-ε turbulence model equations (Equation. (7) and (8)), and a second order upwind (SOU) scheme [68] are applied. For the pressure-velocity coupling, the SIMPLE is utilized. All vortex tubes have same type of meshing. The three-dimensional meshing of straight vortex tube is presented in Fig. 3. The analysis was proceeded in an Intel CORE ™ i7, Processor 2.30 GHz and 8.00 GB RAM (DDR3) system.

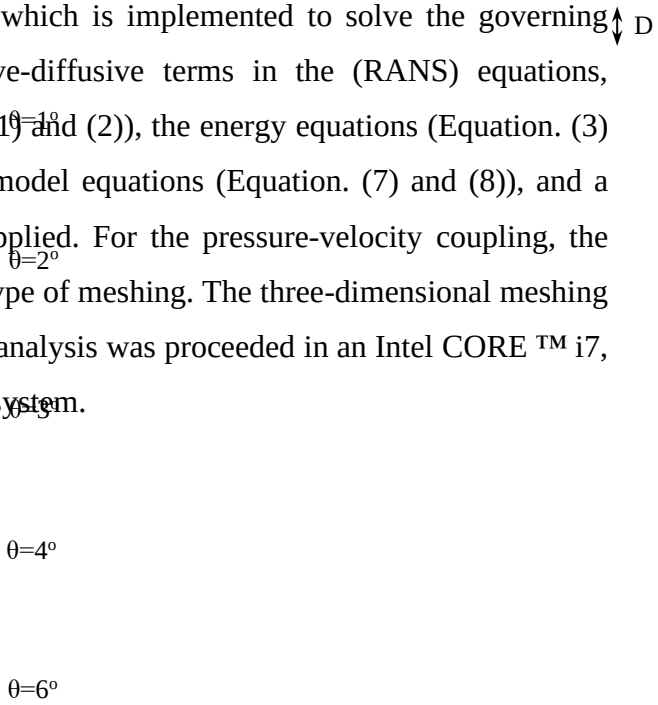

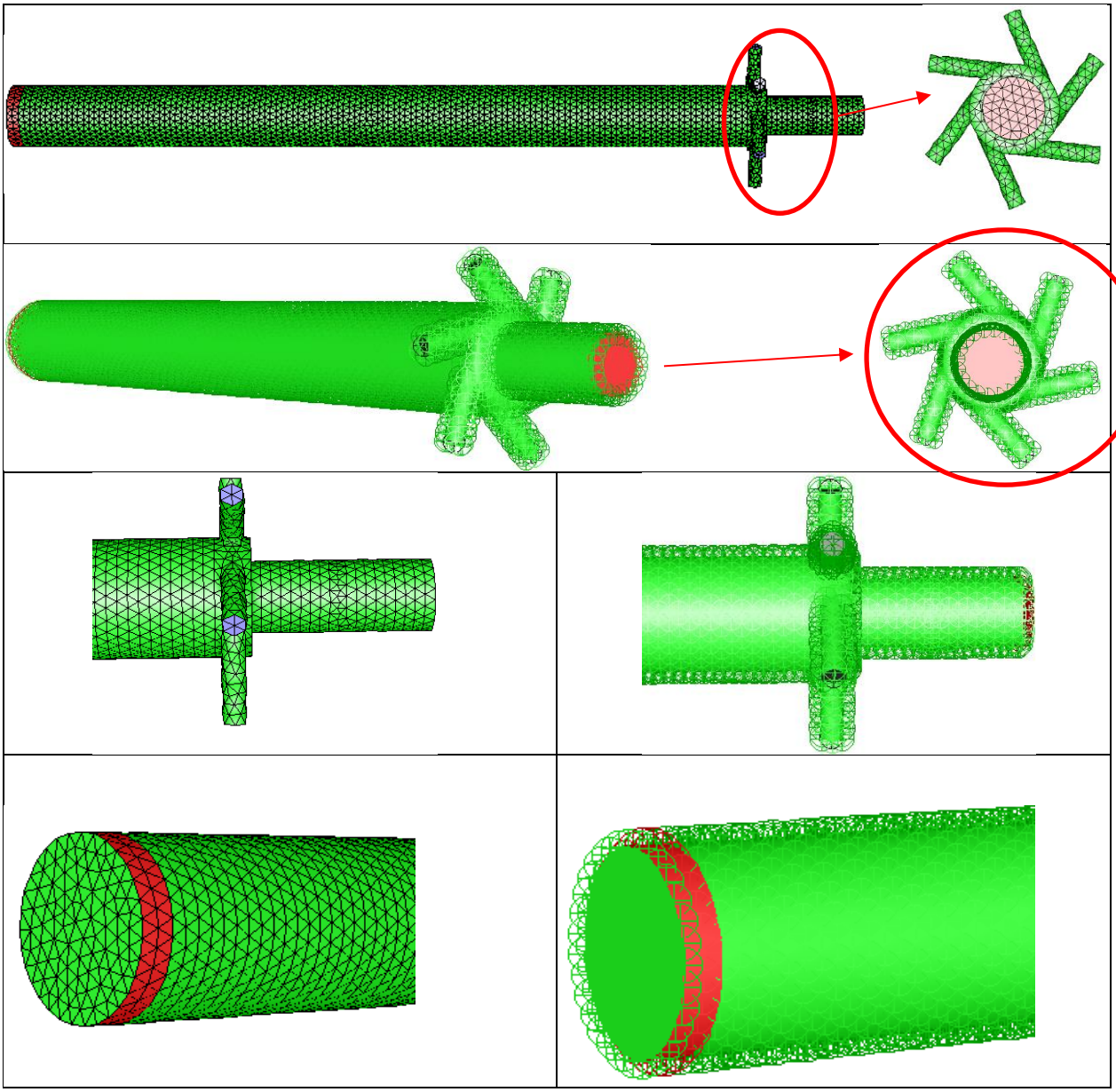

Fig. 3. Three-dimensional meshing of straight vortex tube

The numerical analysis is investigated to describe the flow stream pattern, velocity gradients temperature, pressure distributions of the present models and finally to comment on the energy separation within the VT. Because of the geometry complexity of the flow, information data for all boundary conditions need to be chosen base on real experimental results and data which used in different literatures. Boundary conditions' information for the vortex tube flows are mentioned following:

Inlet: Features and properties of the inlet flow usually obtained from experimental data, numerical analysis or some estimations but all the boundary conditions which are necessary for simulation are rarely available just from experiments. Compressed gas enters the main tube of vortex tube tangentially through six inlet nozzles. Most of experimental studies provide inlet data as inlet

pressure (P_{in}), inlet temperature (T_{in}) and mass flow inlet ($\dot{m}_{in}$) for the nozzles. In this simulation, the assumptions for inlet boundary condition are pressure and total temperature with known values and constants for compressed air.

Wall: Since the shell of vortex tube is made of aluminum and covered with a layer which is insulator, then walls are assumed to be no slip and adiabatic boundary condition.

Outlets: Both of cold and hot exits are assumed to be pressure outlet boundary condition with pressure range of 0.12 and 0.25 MPa. Variation in hot outlet pressure regulating by moving hot control valve can lead to different cold mass fraction [31].

3.5. Grid independence study and validation:

To decrease error due to unmapped grids by using the changing of grid size, the variations of cold temperature difference versus pressure loss ratio with different number of cells are reported in Table (3). The difference between case 6 and 7 in cold mass fraction, pressure loss ratio and cold temperature difference for straight and 2° divergent vortex tube are less than 1%. It is observed that there is no significant difference in cold mass fraction, pressure loss ratio and cold temperature difference with increasing number of cells more than 264,000 grid cells with respect to refinement at inlet and both of cold and hot outlets. Thus, according to grid-independency, the grid which is used in case 6 (for straight and 2 degree divergent vortex tube) was chosen as the basic mesh for this analysis. This numerical analysis is validated with experimental and numerical data of Liu et al. [47] to ensure that flow is simulated accurately. The variation of total temperature difference versus pressure loss ratio is reported in Fig. 4.

Table 3 Effect of grid size, Pressure loss ratio and cold mass fractions on the cold temperature difference at constant inlet pressure P = 0.3 MPa.

Cases	Number of cells		λ		α	ΔT_c (k)
	θ = 0°	θ = 2°	θ = 0°	θ = 2°		

					θ = 0°	θ = 2°	θ = 0°	θ = 2°
1	35000	50000	0.76	0.81	0.73	0.76	9.87	11.1
2	62350	86415	0.75	0.79	0.71	0.75	10.5	11.86
3	111225	137468	0.73	0.77	0.68	0.72	11.1	12.34
4	140000	175256	0.71	0.74	0.66	0.7	11.51	12.94
5	181214	210000	0.7	0.71	0.64	0.68	11.7	13.4
6	200000	264000	0.69	0.70	0.63	0.67	11.8	13.6
7	224358	310000	0.68	0.69	0.62	0.66	11.83	13.66

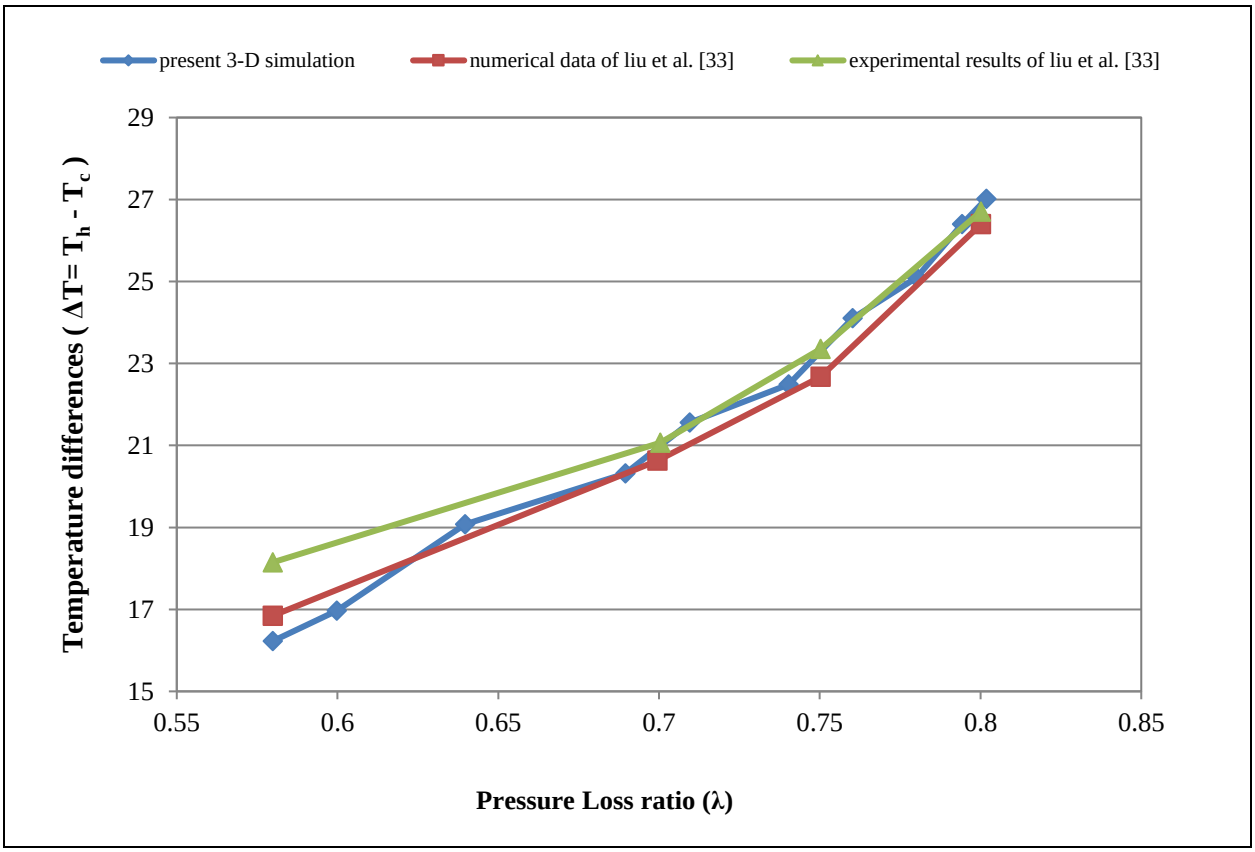

Fig. 4. Experimental and numerical variation of total ($\Delta T = T_H - T_C$) temperature difference with pressure loss ratio.

4. Operative parameters

Some parameters which are effective on the performance of vortex tube are defined below:

• Cold mass fraction:

$$\alpha = \frac{\dot{m}_c}{\dot{m}_{in}} \tag{16}$$

where $\dot{m}_c$ (kg/s) is cold the mass flow rate and $\dot{m}_{in}$ (kg/s) is the inlet mass flow rate.

• Cold temperature difference:

$$\Delta T_c = T_{in} - T_c \tag{17}$$

in which T_{in} (K) is the inlet air temperature and T_c (K) is the cold air temperature.

• Pressure loss ratio:

$$\lambda = \frac{\Delta P_c}{P_{in}} = \frac{P_{in} - P_c}{P_{in}} \tag{18}$$

• Isentropic efficiency:

According to adiabatic expansion of ideal gas, the refrigeration efficiency of the vortex tubes can be acquired. Base on isentropic expansion in vortex tube, the isentropic efficiency is:

$$\eta_{is} = \frac{\Delta T_c}{\Delta T_{is}} = \frac{T_{in} - T_c}{T_{in}(1 - {}^{P_a}/_{P_{in}})^{\frac{\gamma-1}{\gamma}}} \tag{19}$$

where$\eta_{is}, \Delta T_{is}$ $(K), P_{in}$ $(bar), P_a$ and $\gamma$are the isentropic efficiency, isentropic temperature difference, inlet air pressure, atmosphere pressure and specific heat ratio, respectively.

• Coefficient of performance:

By using the principle of isentropic expansion of ideal gas, the coefficient of performance is calculated by below equation:

$$Cop = \frac{Q_c}{W} = \frac{\alpha C_p (T_{in} - T_c)}{(\frac{\gamma}{\gamma - 1}) R T_{in} [(^{P_{in}}/_{P_c})^{\frac{\gamma-1}{\gamma}} - 1]} \quad (20)$$

in which Q_c is cooling rate and W is mechanical energy which are effected on refrigerating of air inlet.

5. Results and discussion

5.1. Velocity and pressure pattern at nozzle section

This section provides a comparative analysis for the relationship between flow behavior and the energy separation with diverging and converging vortex tubes. High pressure flow enters main tube through the inlet nozzles of the vortex tube. Due to the vortex tube has no external source of work or heat, pressure at the inlet is the only availability source of energy. The majority of the pressure drop occurs in the nozzle where the magnitude velocity increases sharply and a swirling flow is established. Fig. 5 (a-c) shows the contours of the total pressure and velocity magnitude fields at inlet cross section of 2°, convergent, straight and 2° divergent vortex tubes respectively. The total pressure drops down to 107.5, 93.69, 87.30 KPa from 300 KPa at inlet of 2° convergent, straight and 2° divergent vortex tubes respectively while the velocity increases very sharply. Because of ideal gas law, the density distribution is similar to total pressure inside vortex tube.

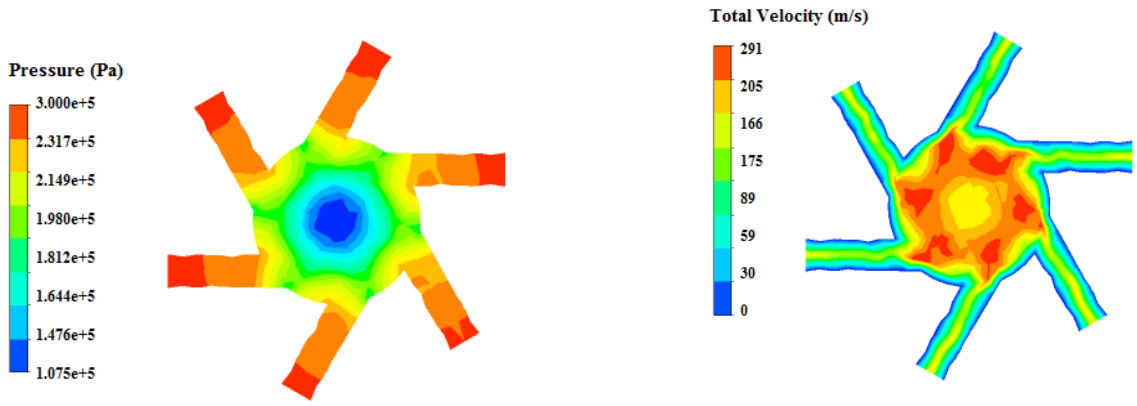

(a)

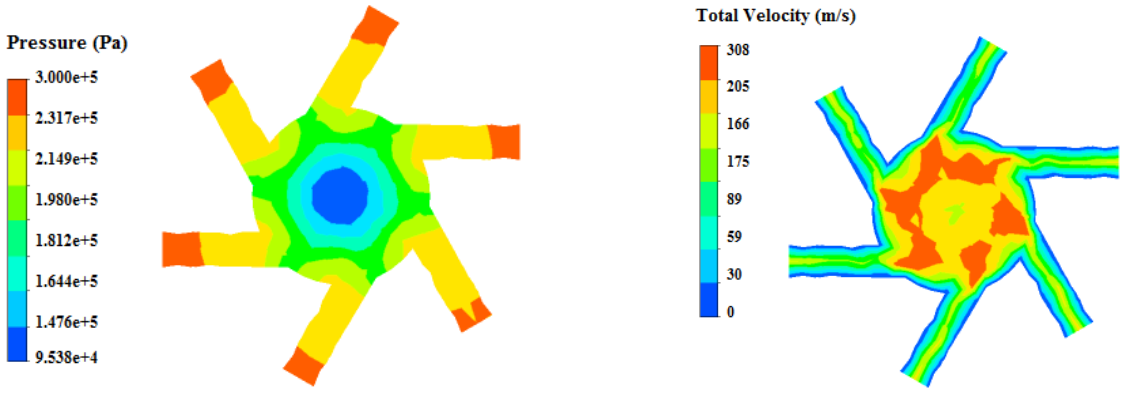

(b)

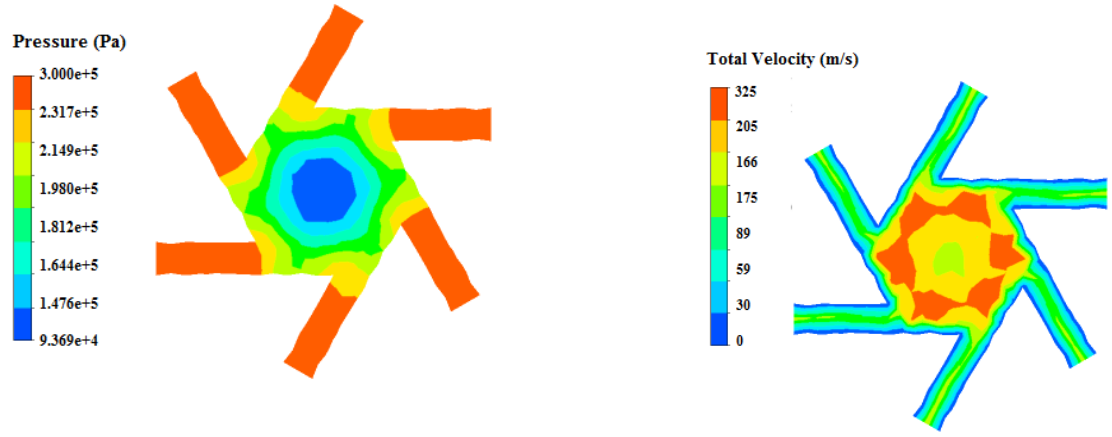

(c)

Fig. 5. Contours of the pressure and velocity at inlet section for (a) 2° convergent, (b) straight and (c) 2°divergent vortex tubes at P = 0.3 MPa.

5.2. Velocity and pressure distribution

To experimentally measure and plot velocity, pressure and temperature contours within the tube in order to gain a better insight into the mode of energy migration is very difficult. A similar alternative is to employ CFD. The radial distributions of velocity components in direction of axial, radial and tangential are shown respectively in Fig. 6 (a-c) for 2°, 1.5°, 1°, 0.8° and 0.5° , convergent, straight and 1°, 2°, 3°, 4° and 6° divergent vortex tubes at different cross section n locations of Z = 0, 10, 50 and 110 mm. In every cross sections, the tangential velocity is predominant velocity component. The magnitude of the tangential velocity decreases towards the hot outlet. A free vortex is observed near the wall based on the radial profile of the tangential velocity and the values become very small at the core

flow. The numerical results for straight vortex tube are in confirm with the observations of Behera et al. [31], Korosaka [19] and Gutsol [4]. The fluid flow which is located at the core stream of the vortex tube has a negligible kinetic energy because of the minimum tangential velocity at the central zone of the main tube. The maximum value of tangential velocity component is about 290 m/s which occurs at the inlet zone. The tangential velocity in the core region gradually increases to critical value and it decreases abruptly due to the friction of the wall. Results show in region - 1 < r/R_{vt} < 1, the tangential velocity gradient for 2° divergent vortex tube is higher than the other vortex tubes except at cross section of Z = 110 mm. At Z = 110 mm and in range of r/R_{vt} > 0.5 and r/R_{vt} < - 0.5, the maximum tangential velocity gradient is for 6° divergent vortex tube.

The axial velocity profiles show that this component reached to zero in a specific radius of main tube. This radius is located in a place which the direction of axial velocity changes to opposite direction of the previous state. The negative zones of axial velocity are covered with cold flow regimes and the positive zones are specified for hot flow regimes, therefore stagnation point is defined a point where the axial velocity leads to zero value. The axial velocity value in core flow for 2° divergent vortex tubes is higher than the straight and 2° convergent vortex tube except at Z = 110 mm. Furthermore, the results showed that the increase in angle of divergence, the cold core flow in each section increased compared with the straight vortex tube, and for all range of convergent angles, the cold core flow in each section decreased compared with the straight vortex tube, under similar operational condition. The radial velocity is significantly low in magnitude in comparison with the tangential and axial components. Radial velocity for all vortex tubes at different radial distances are almost symmetric, as well.

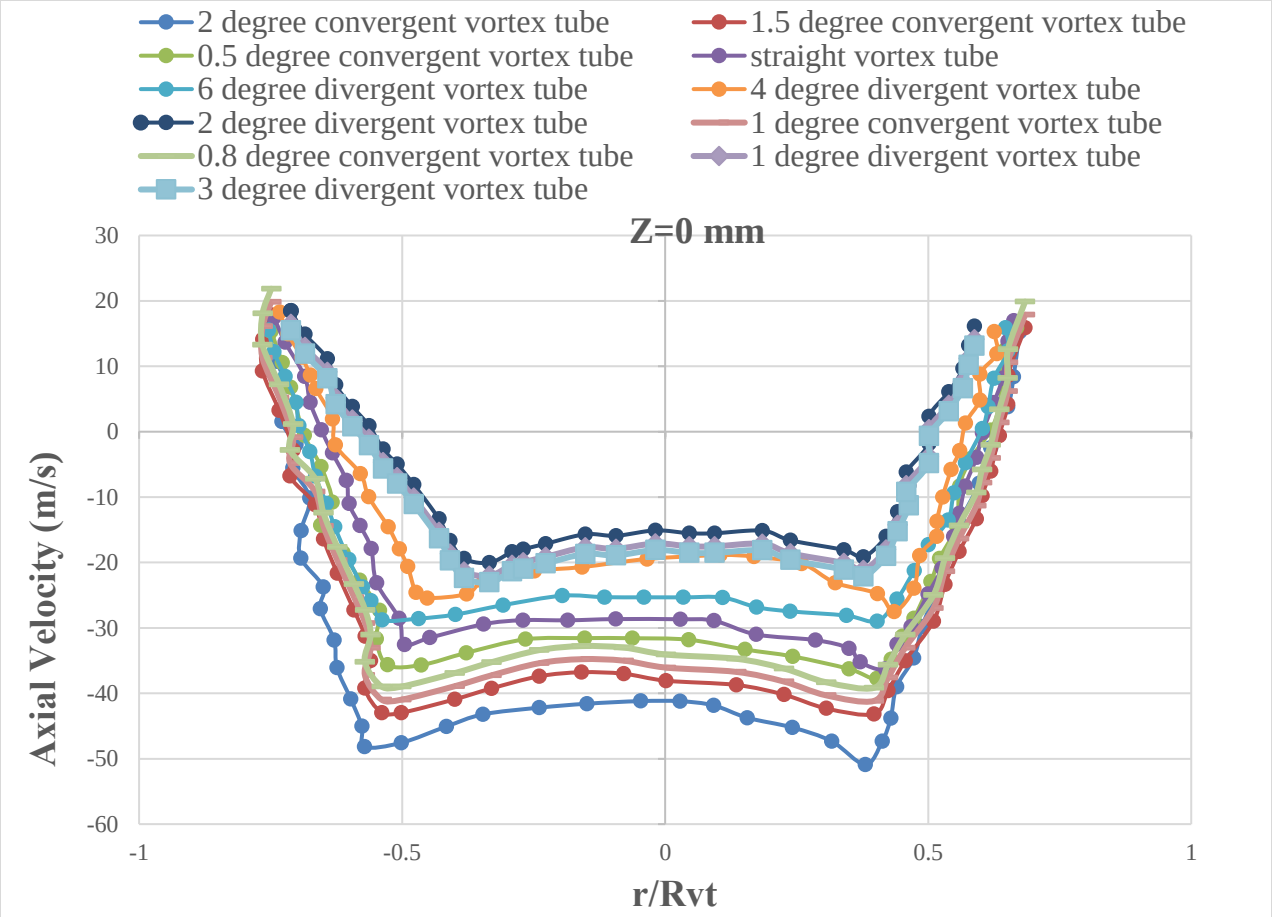

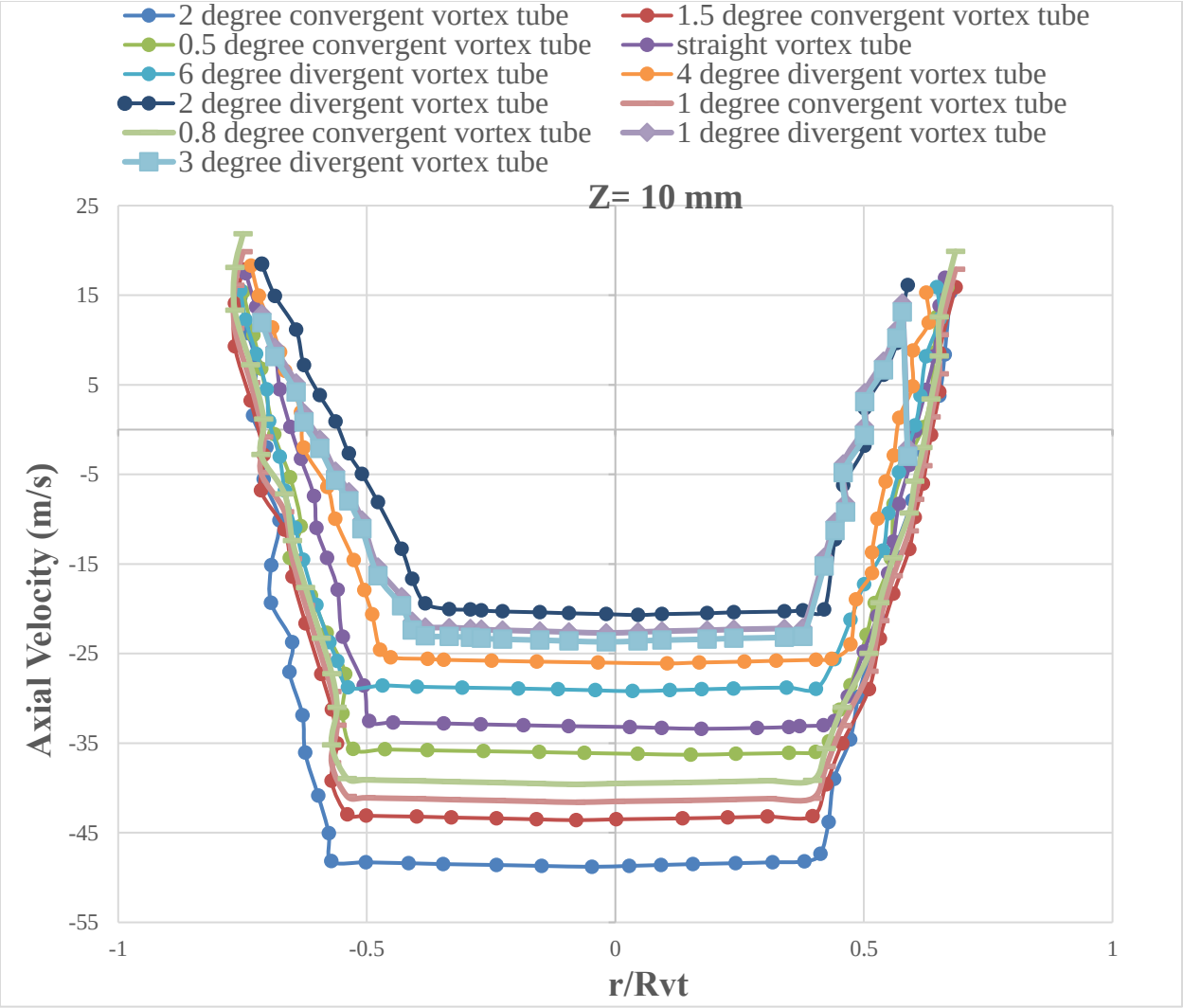

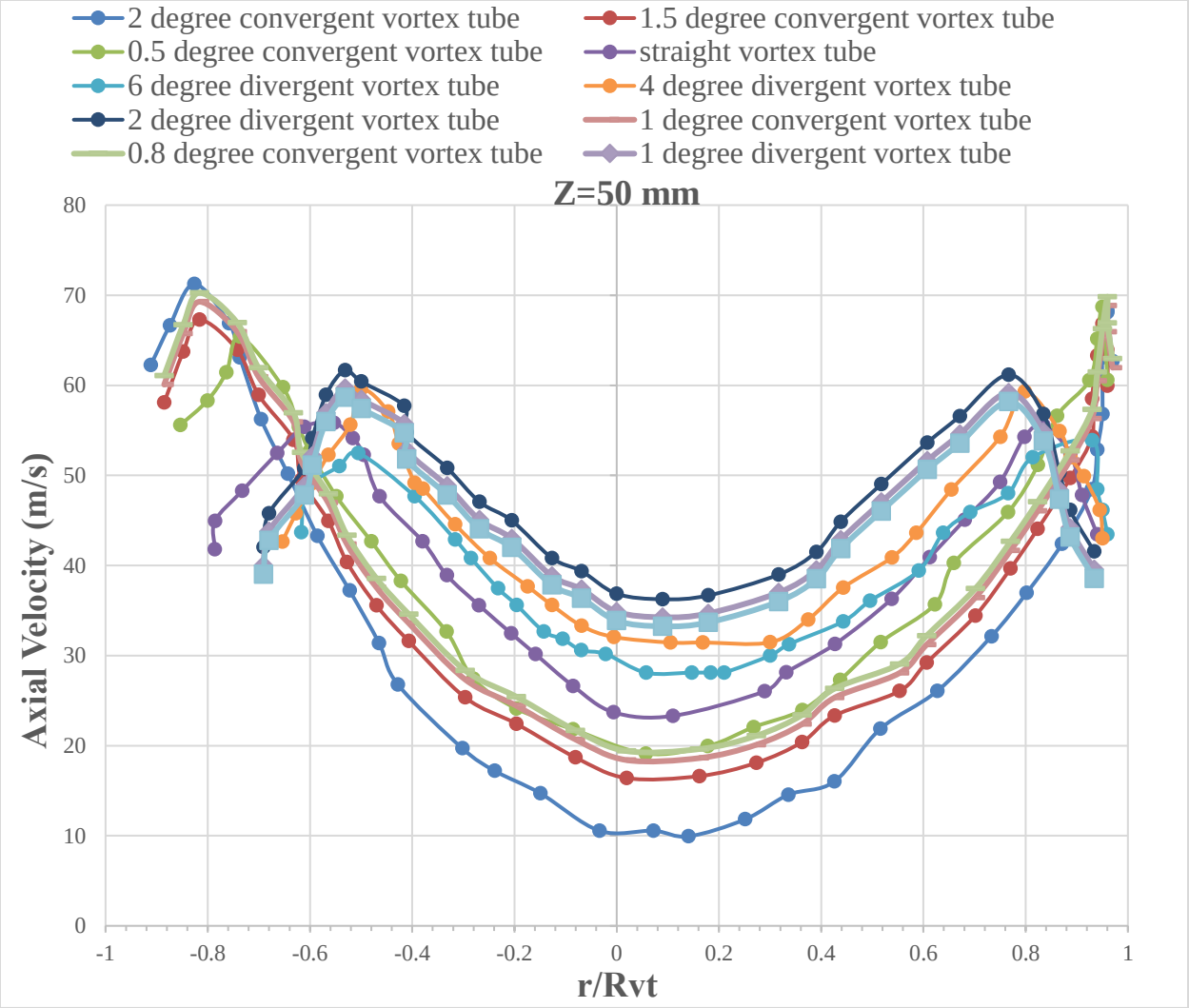

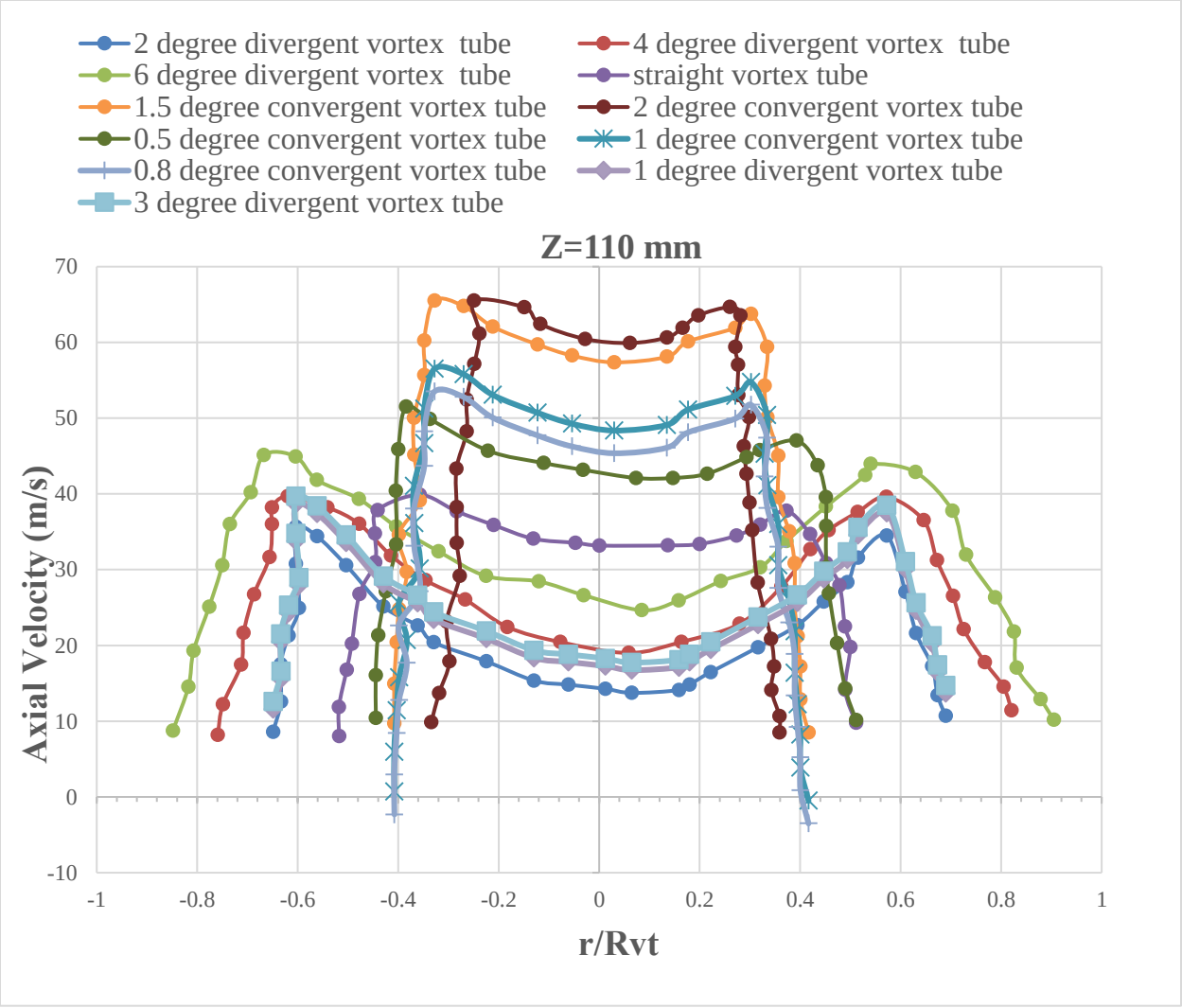

(a)

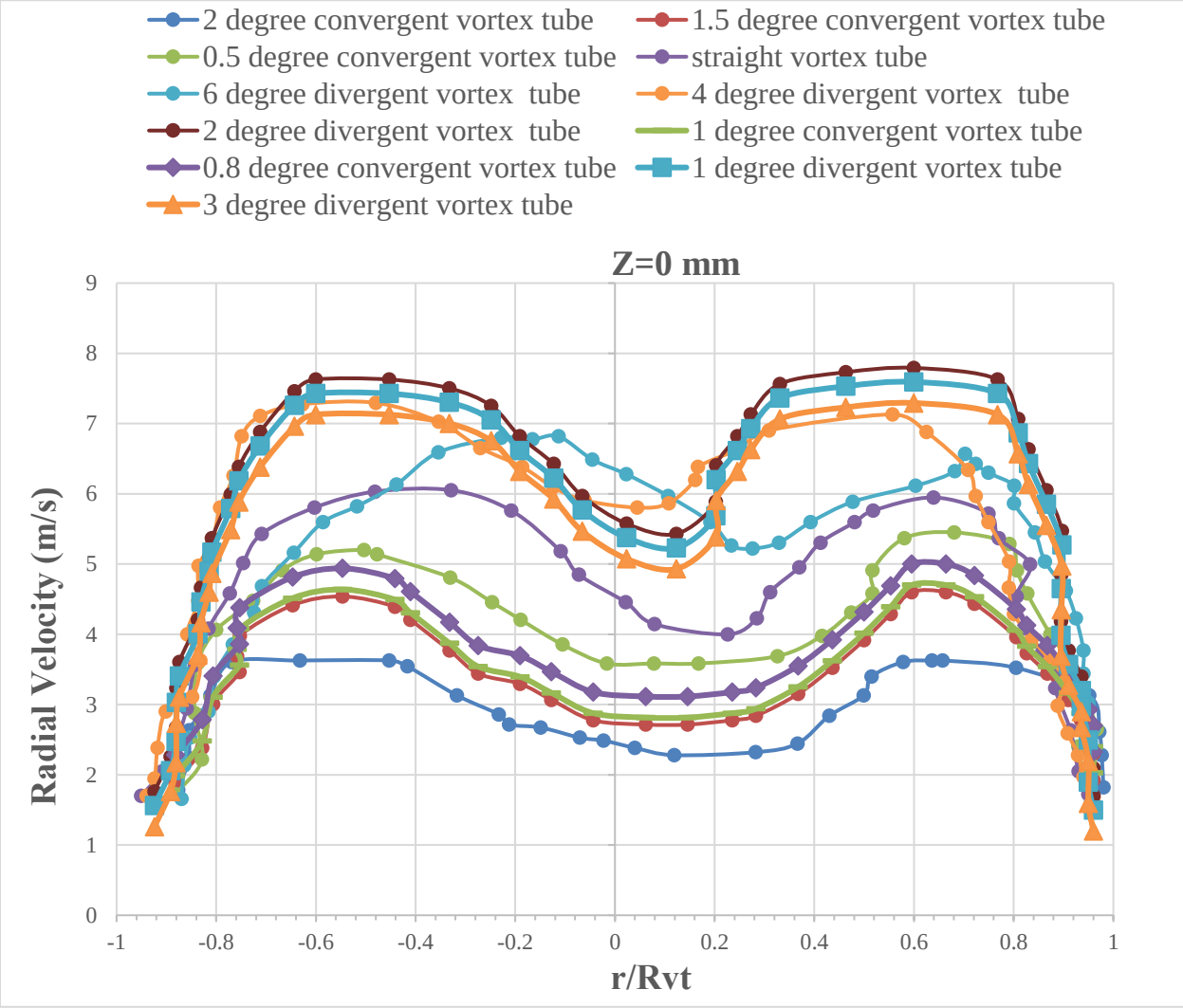

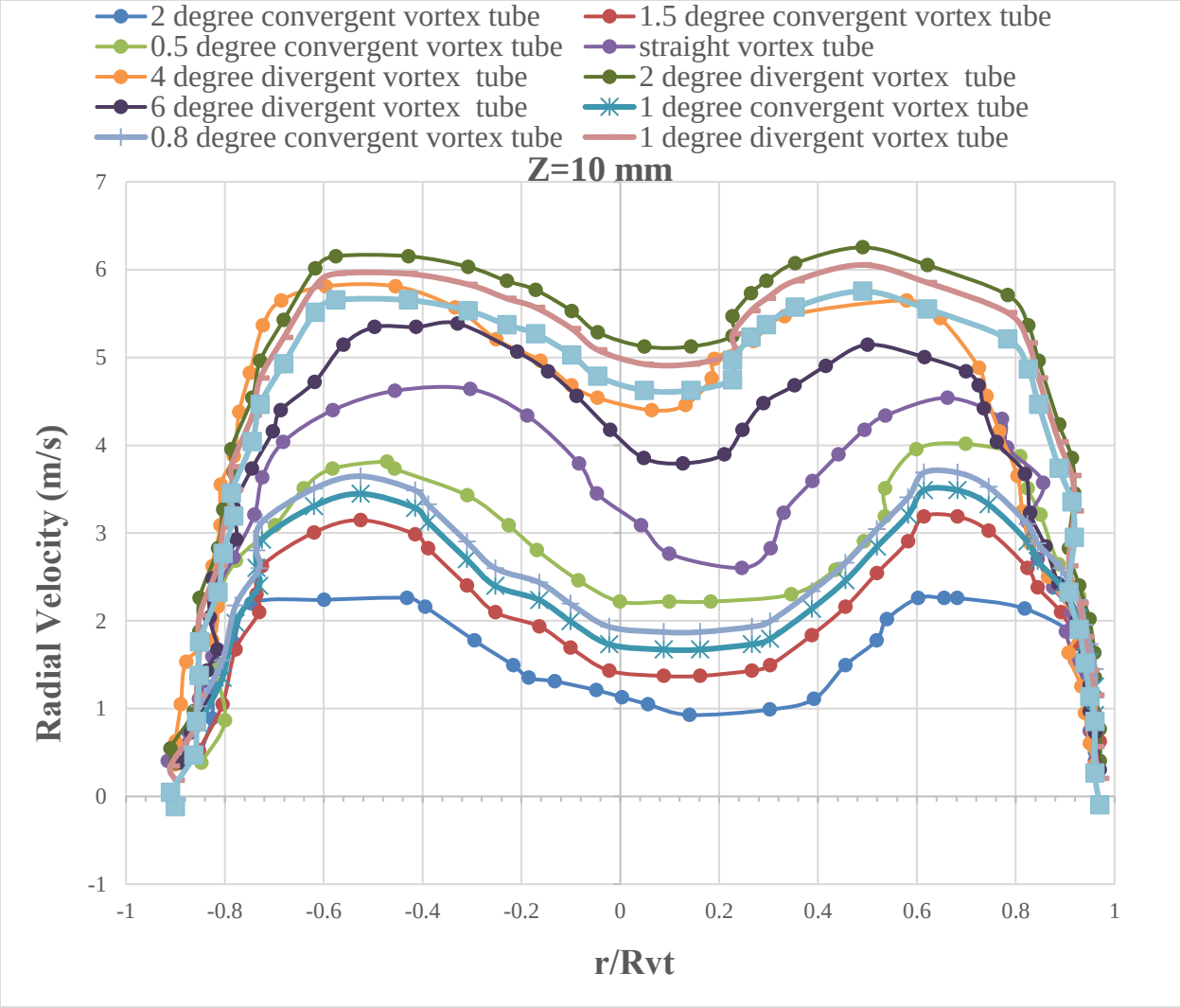

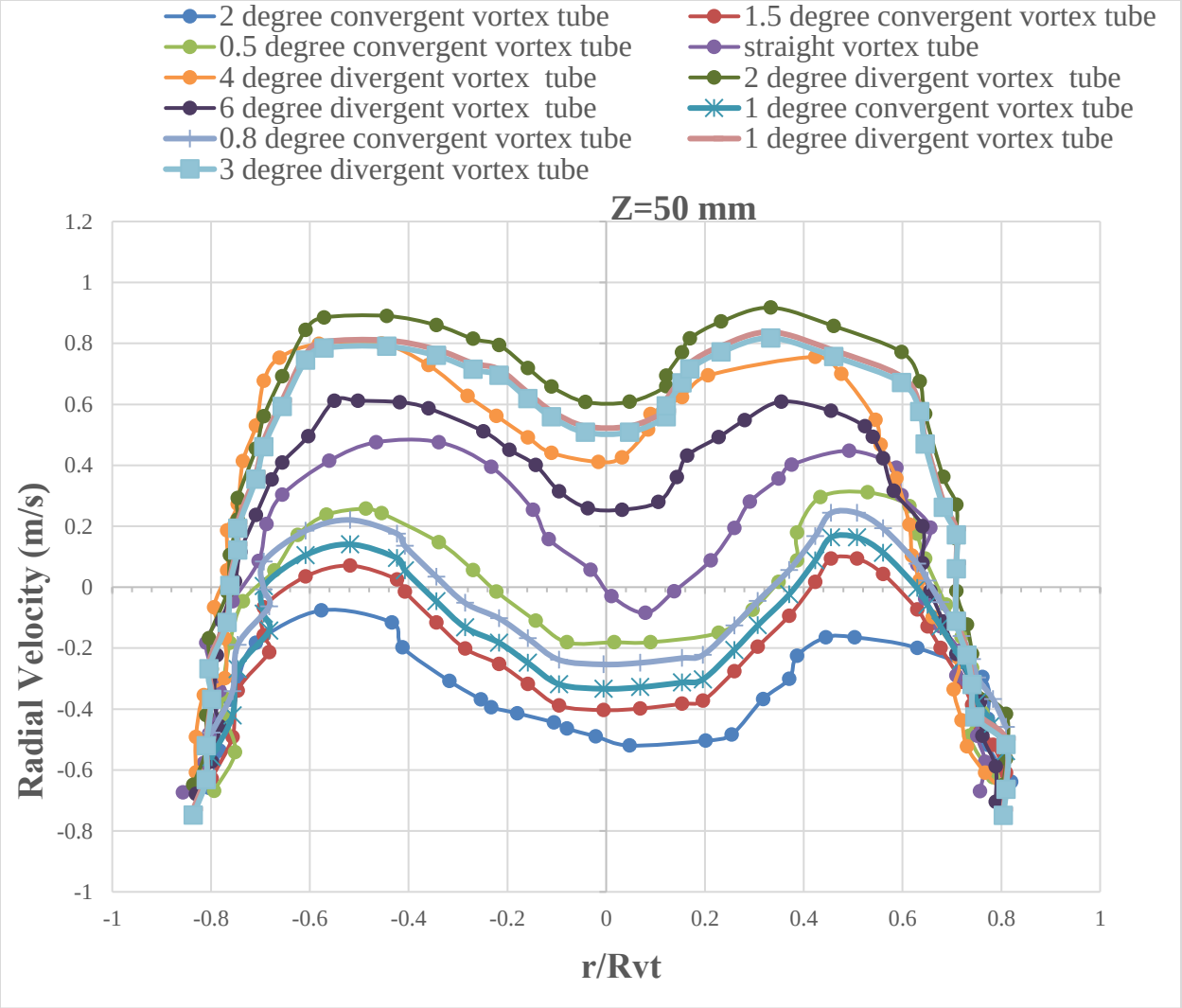

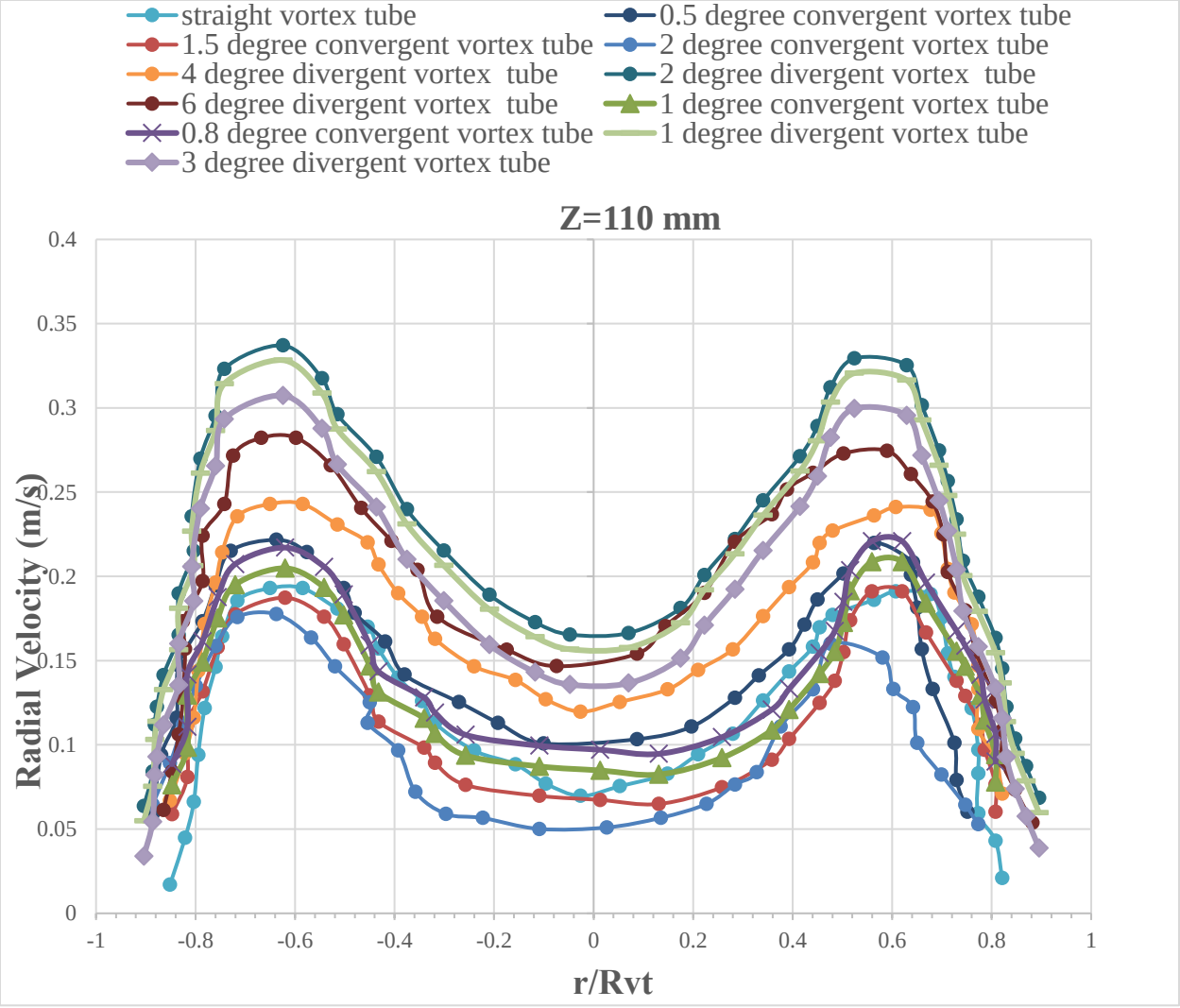

(b)

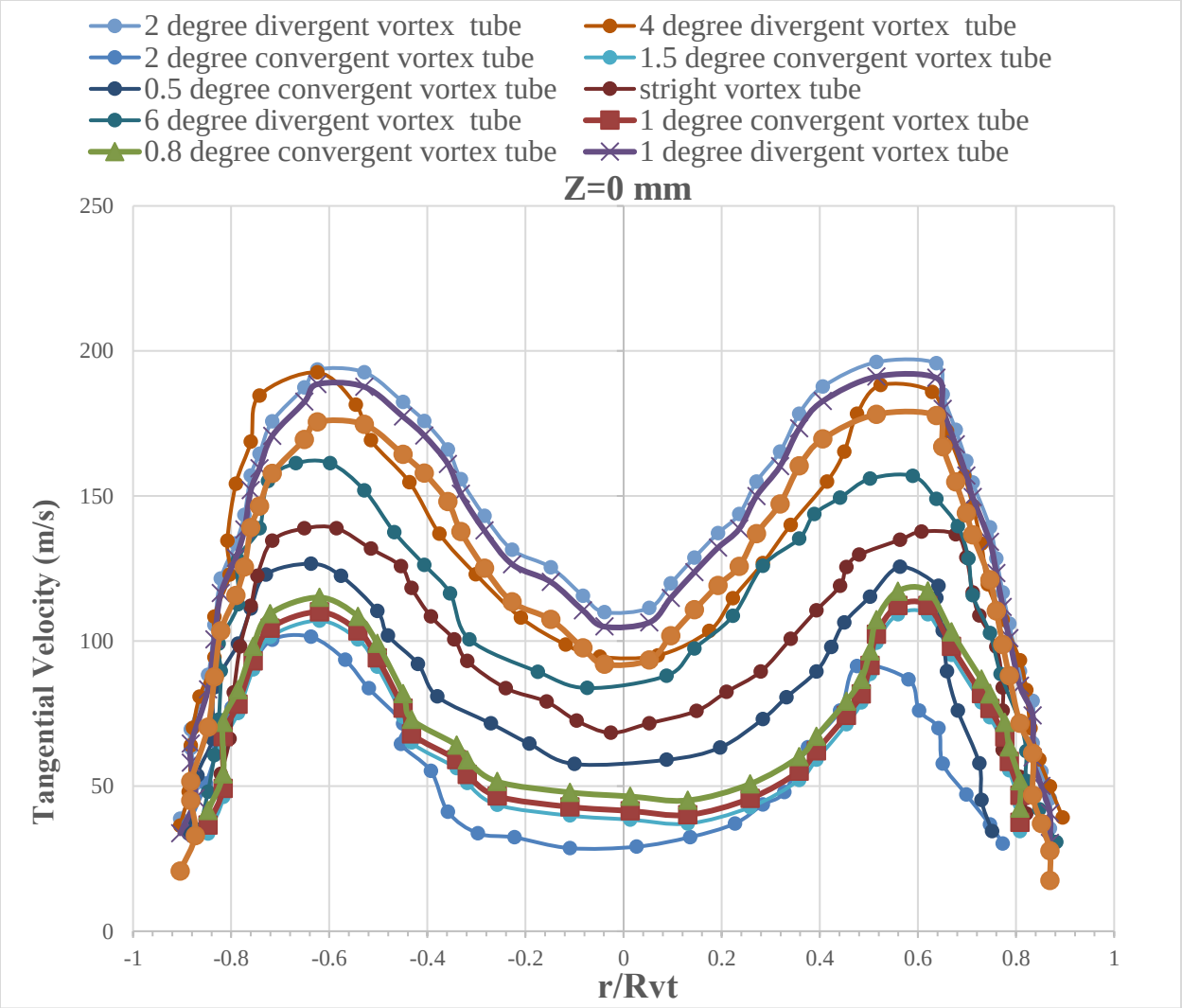

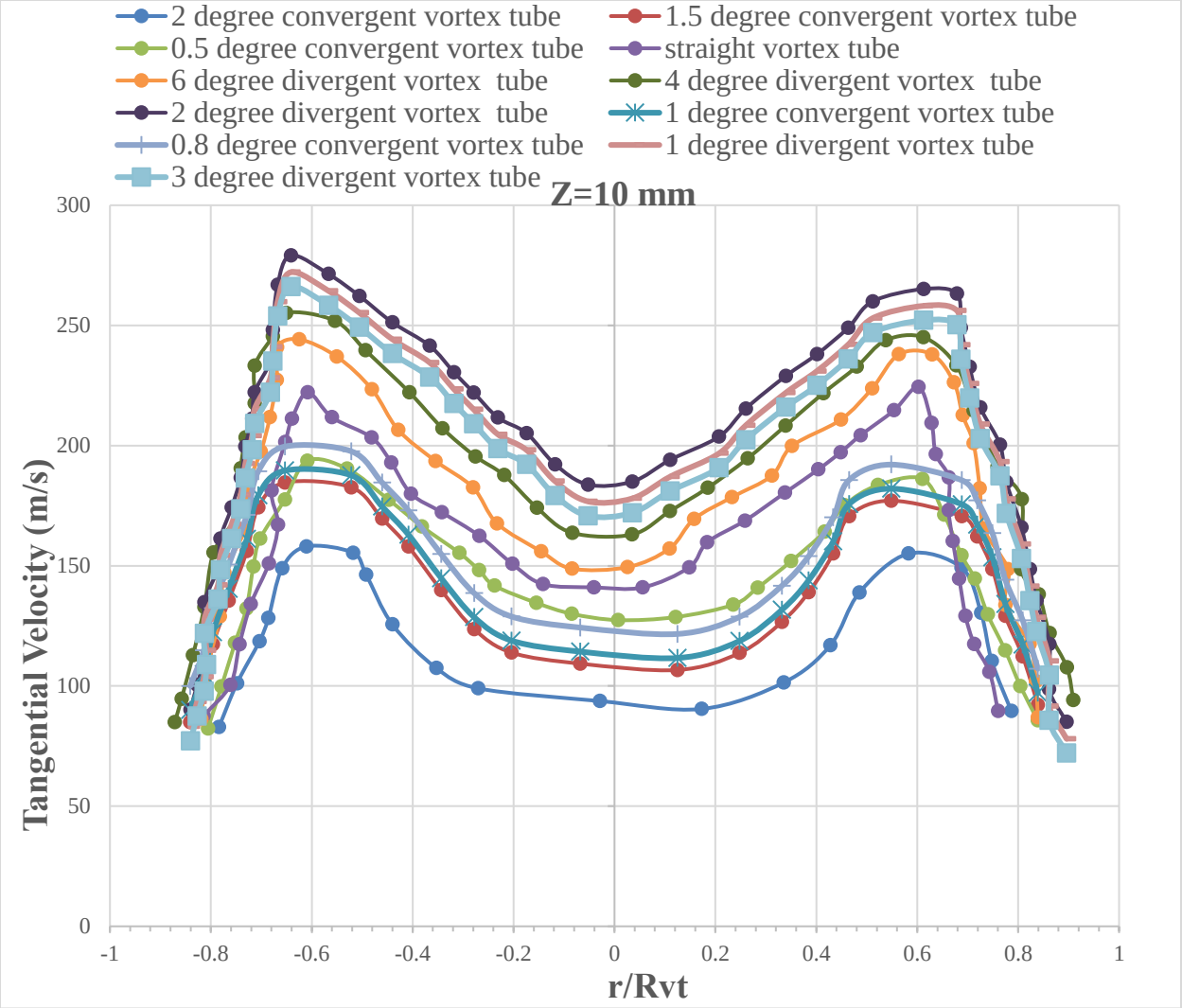

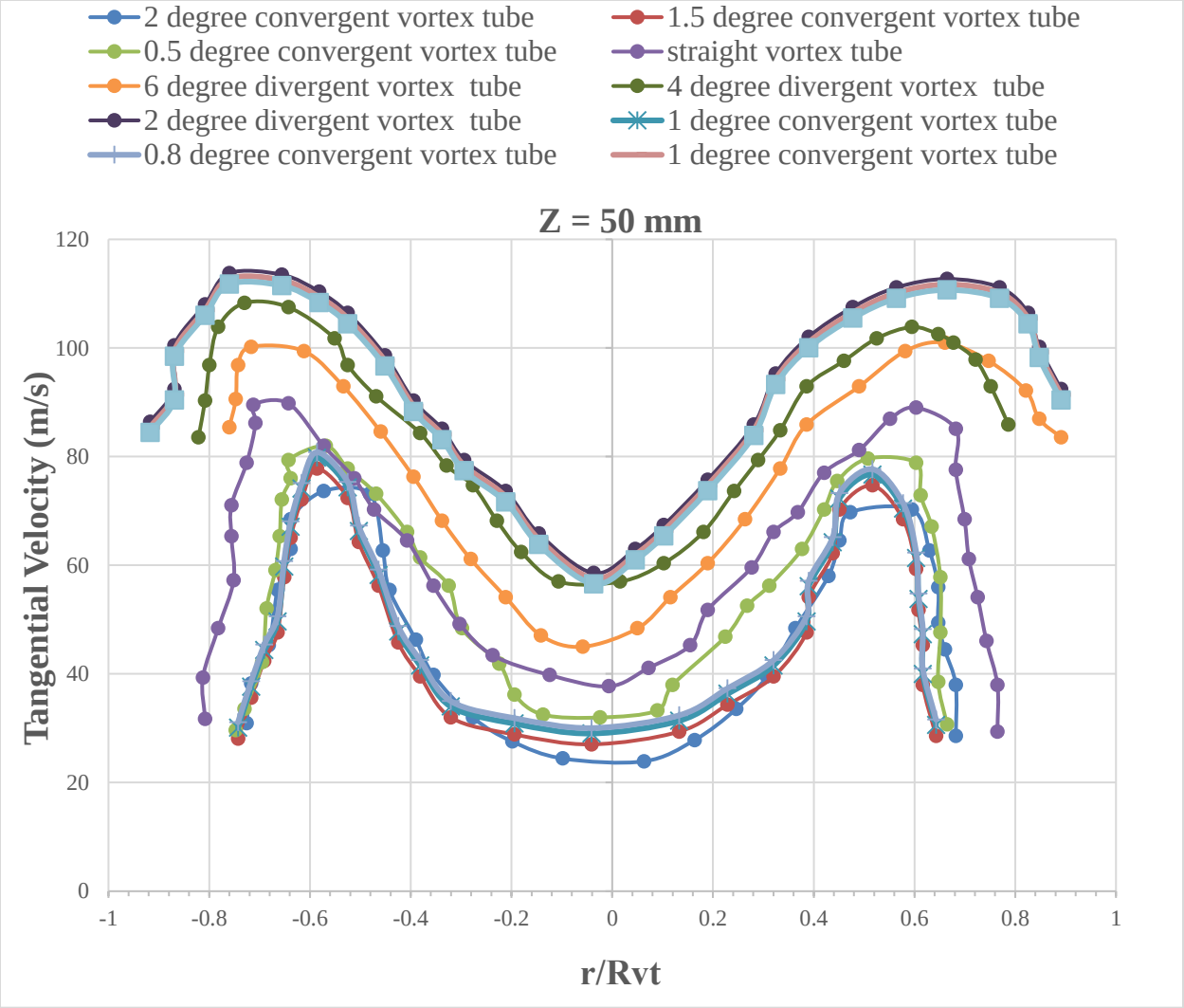

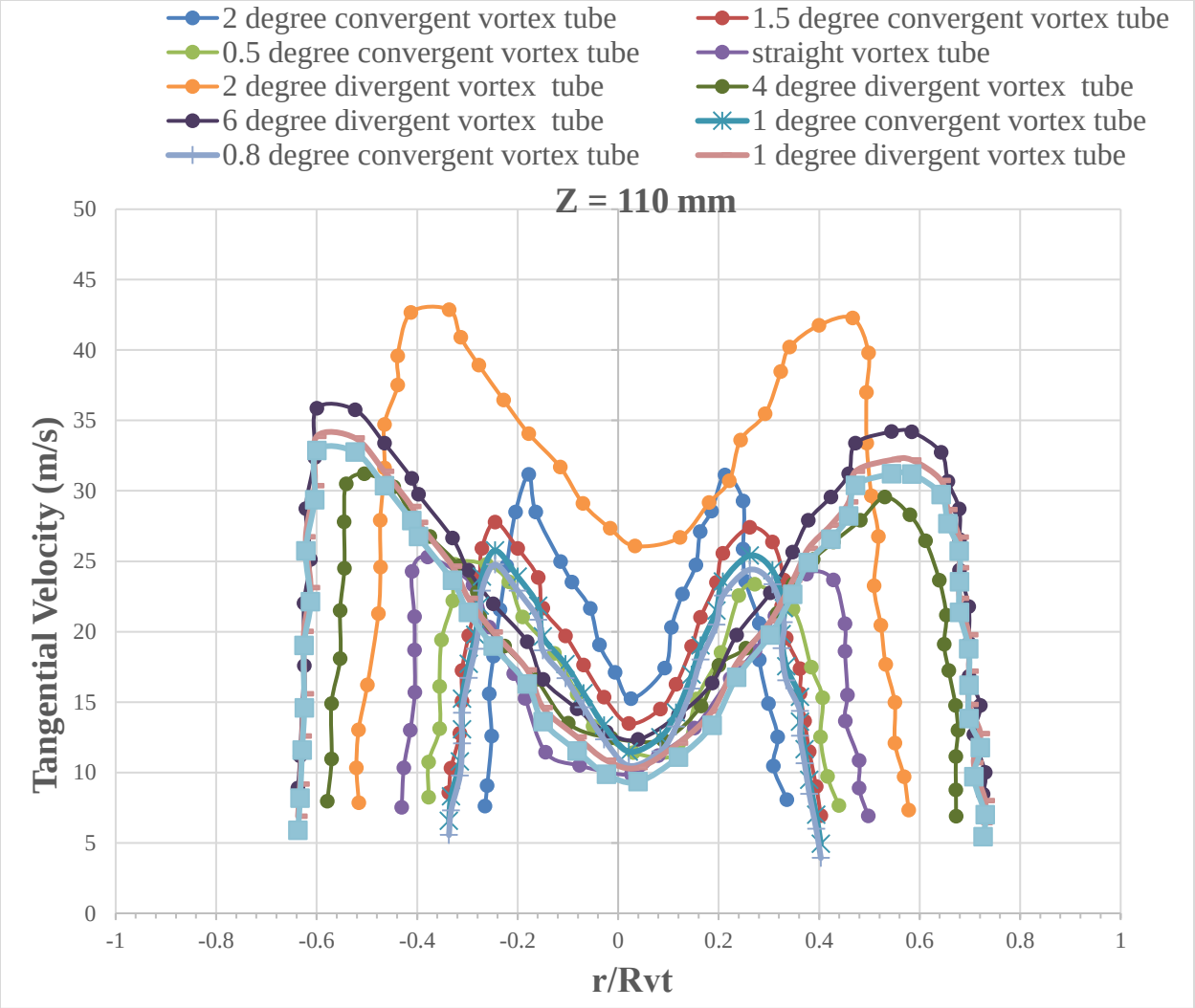

(c)

Fig. 6. Radial profiles of (a) Axial, (b) Radial and (c) Tangential velocities for 2°, 1.5°, 1°, 0.8° and 0.5° convergent, straight and 1°, 2°, 3°, 4° and 6° divergent vortex tubes at different cross section locations Z = 0, 10, 50, and 110 mm with inlet pressure P = 0.3 MPa.

The radial profile of static pressure is shown in Fig. 7 for convergence angles of 2°, 1.5° and 0.5°, straight (0°), and divergence angles of 2°, 4° and 6°, respectively at different locations Z = 0, 10, 50 and 110 mm. The maximum pressure occurs at maximum radius while the minimum pressure is seen at minimum radius. The particle in core flow has the negative value of axial velocity and take a reverse (negative) direction. The particle in peripheral region along the tube wall moves toward the hot end discharge. Also it can be observed that the axial velocity in the cold core increase with a decrease in the axial distance.

As the presented results (Fig. 7), the angle of divergent and convergent hot-tubes has a considerable effect on the value of the static pressure. As seen from this figure, for divergent angle of hot-tube can lead to a decrease in static pressure and as result the cold flow velocity is increased which will be higher than that of straight one. For the case of convergence angle, the cold flow velocity is less than that of straight one. Moreover, from Fig. 4, one can see clearly that the total temperature difference, ΔT, increases singularly with the pressure loss ratio, λ. This proves that separating process within the vortex tube is a direct result of pressure loss ratio and the larger the pressure loss ratio, the larger the temperature drop or energy separation is. Further, it confirms the reliability of created 3-D CFD model for predicting the energy migration or separation phenomenon in the counter-flow vortex tubes.

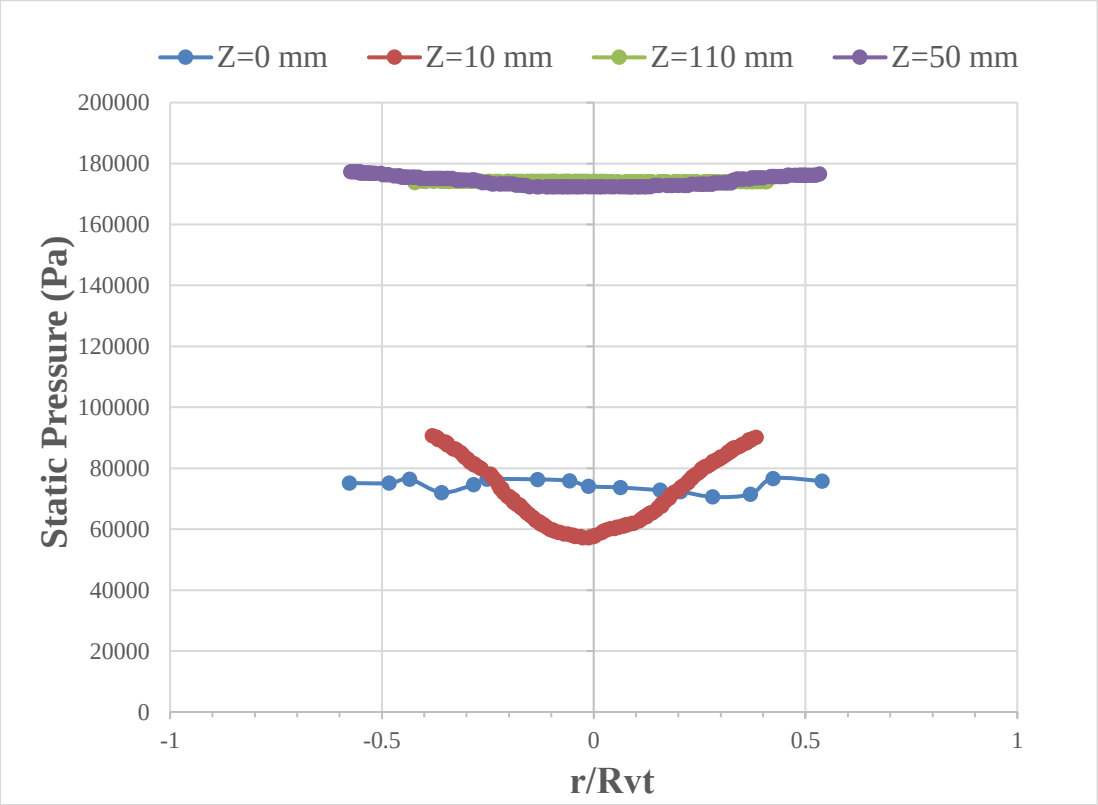

(a)

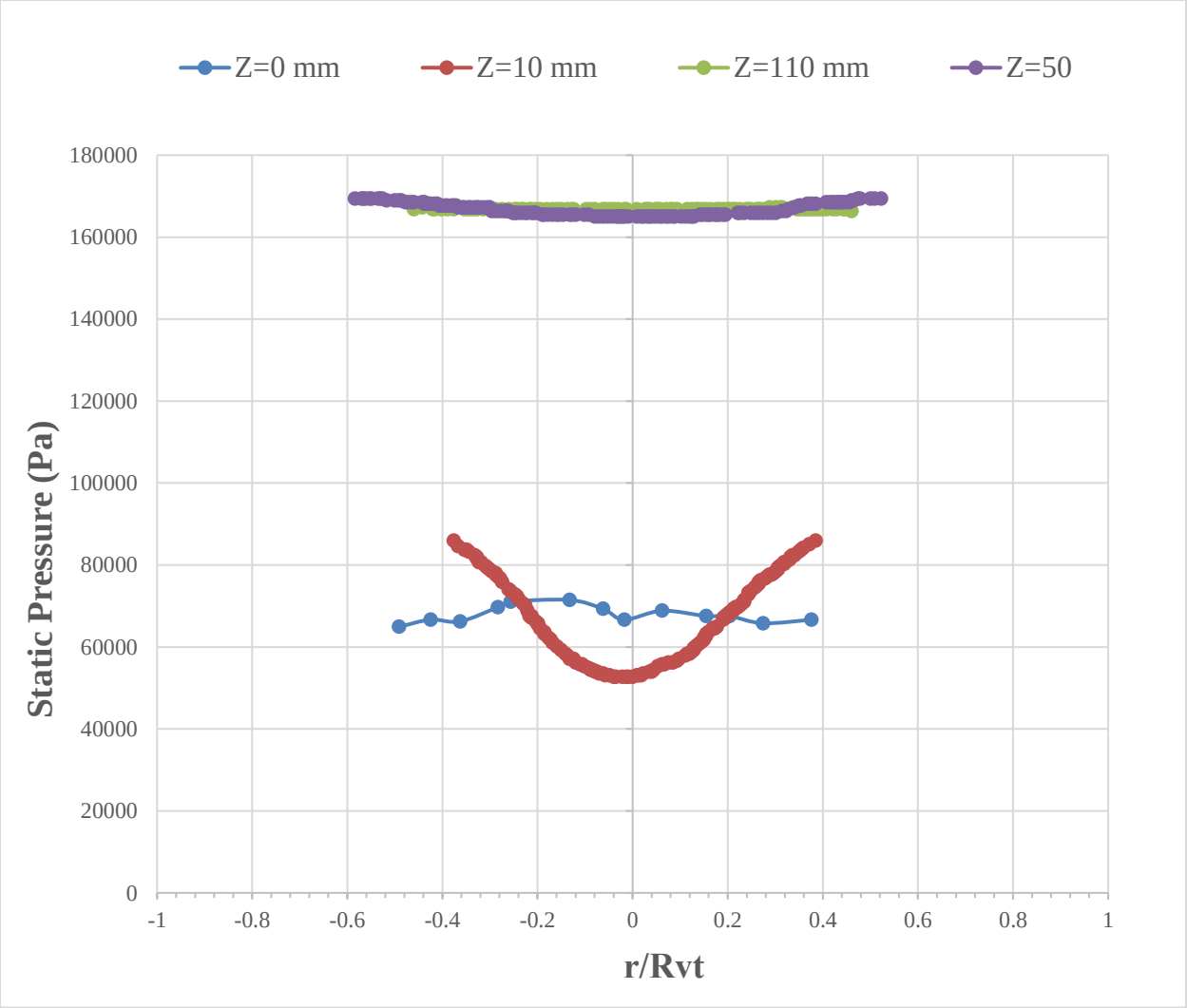

(b)

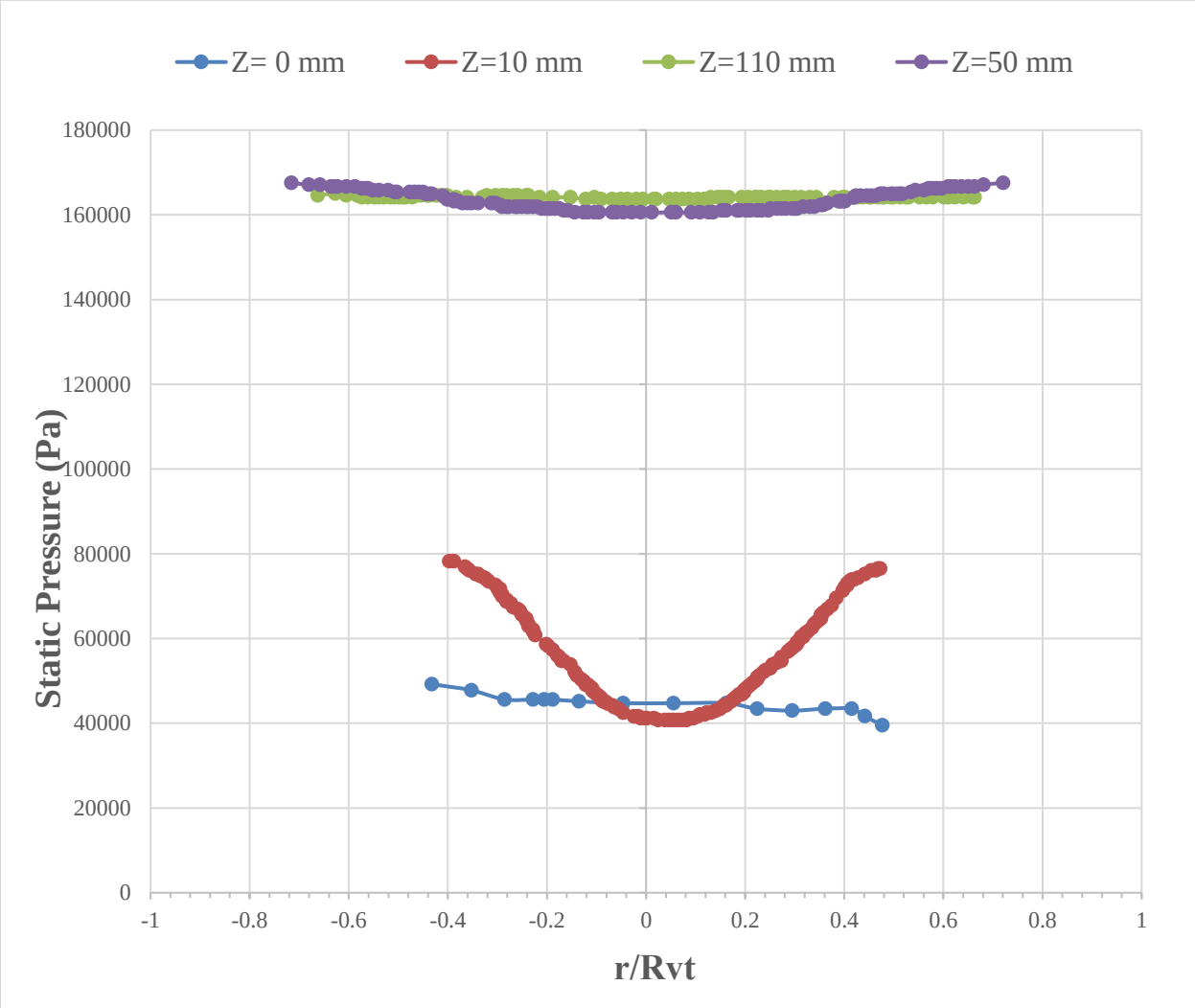

(c)

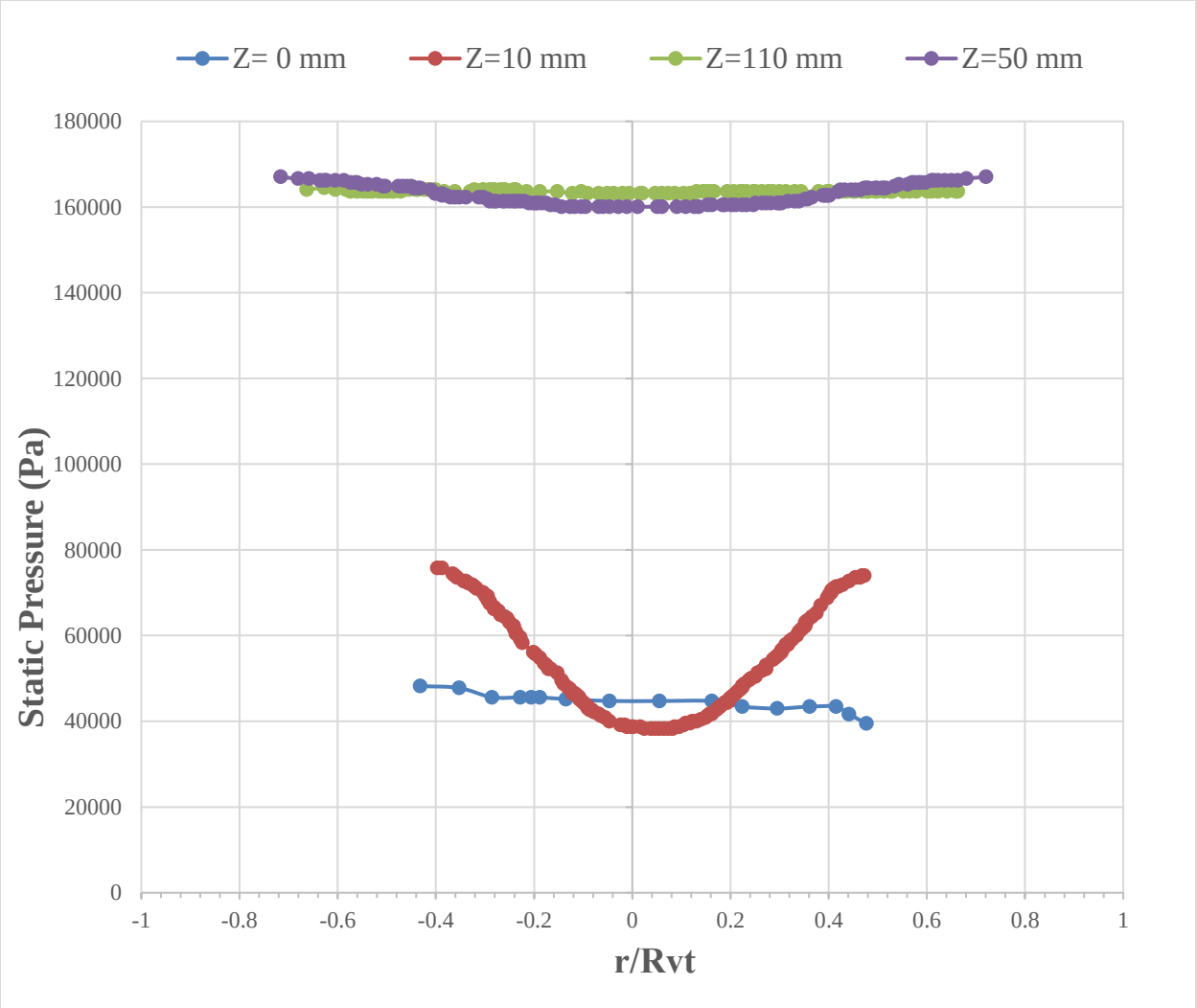

(d)

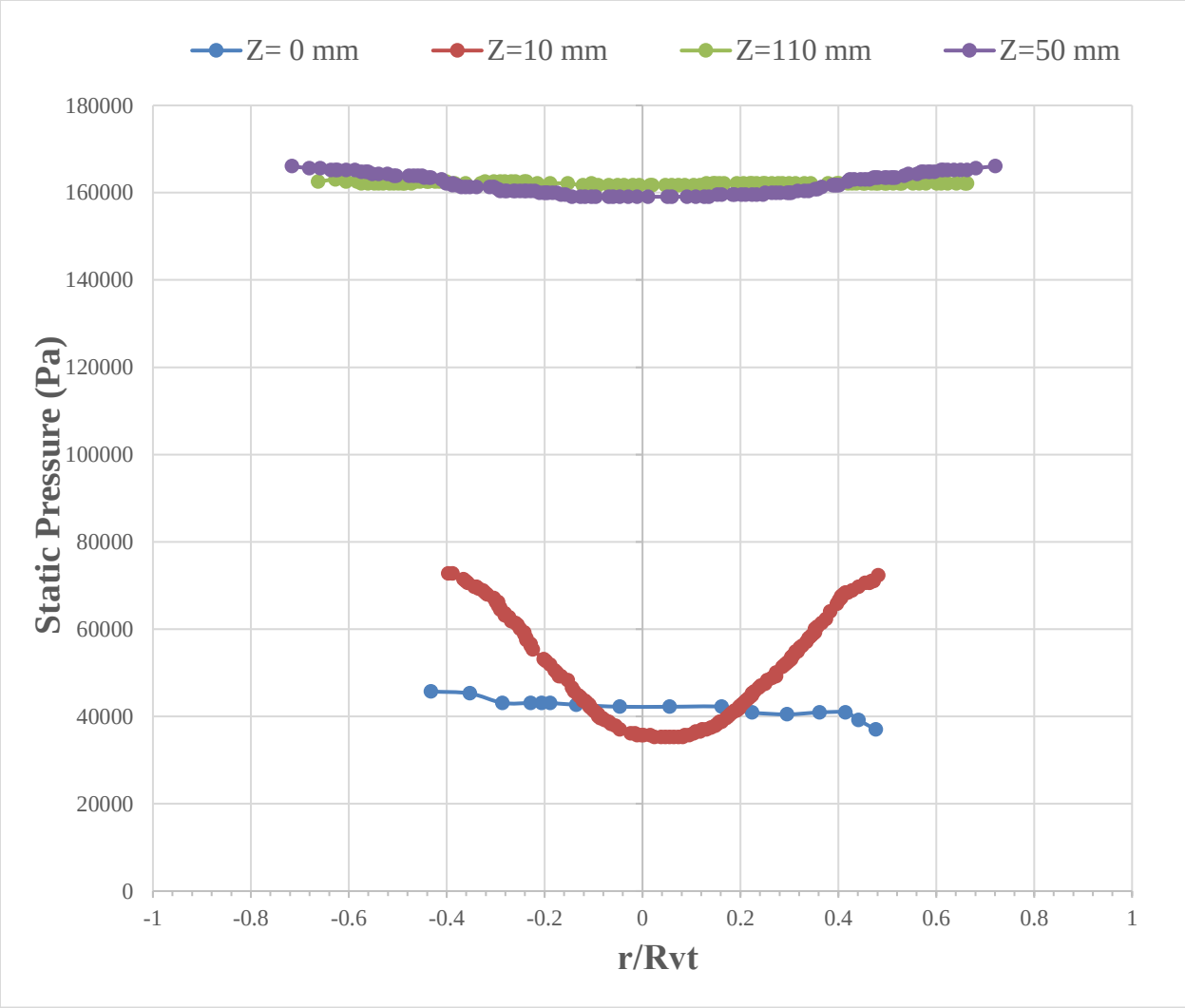

(e)

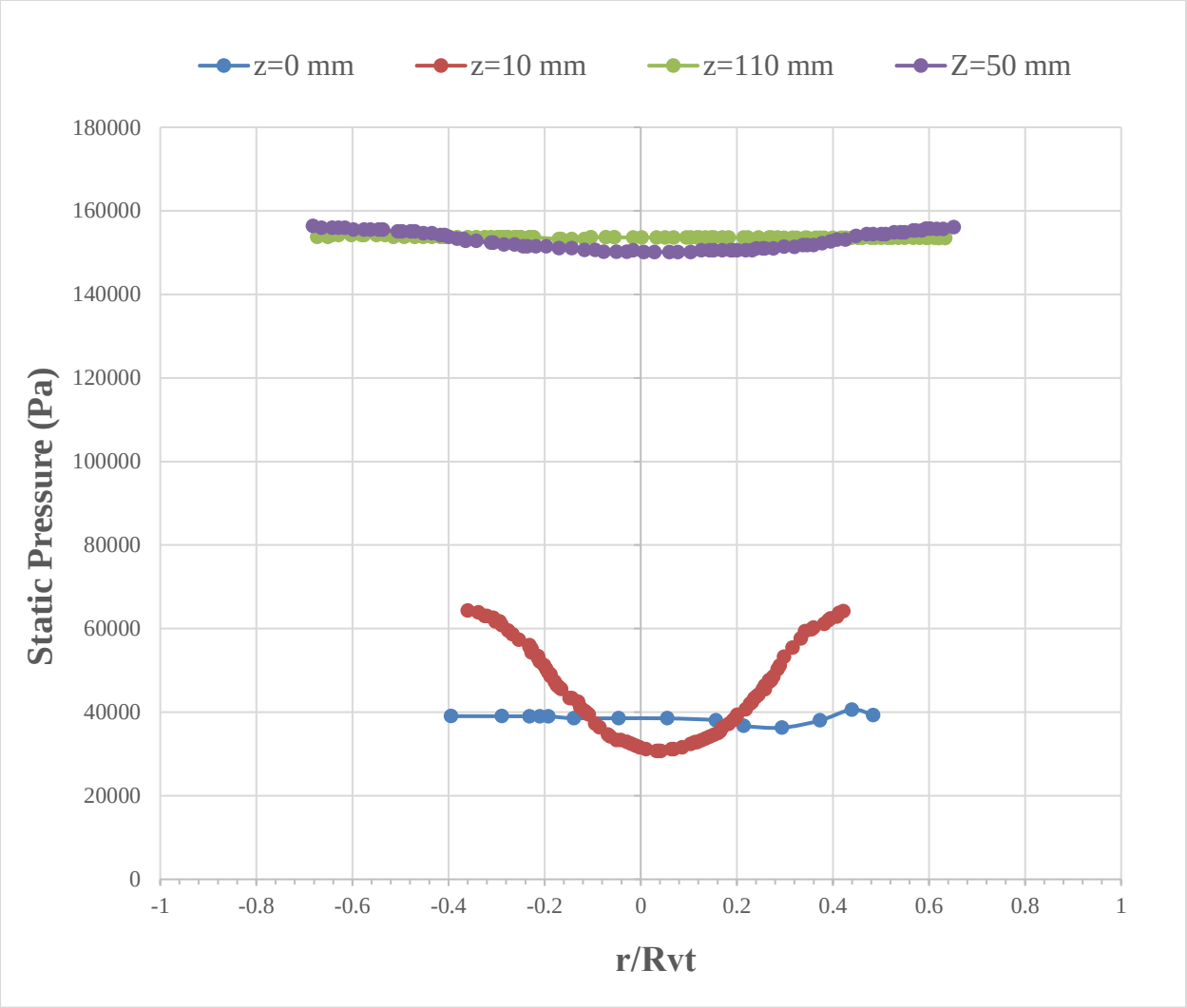

(f)

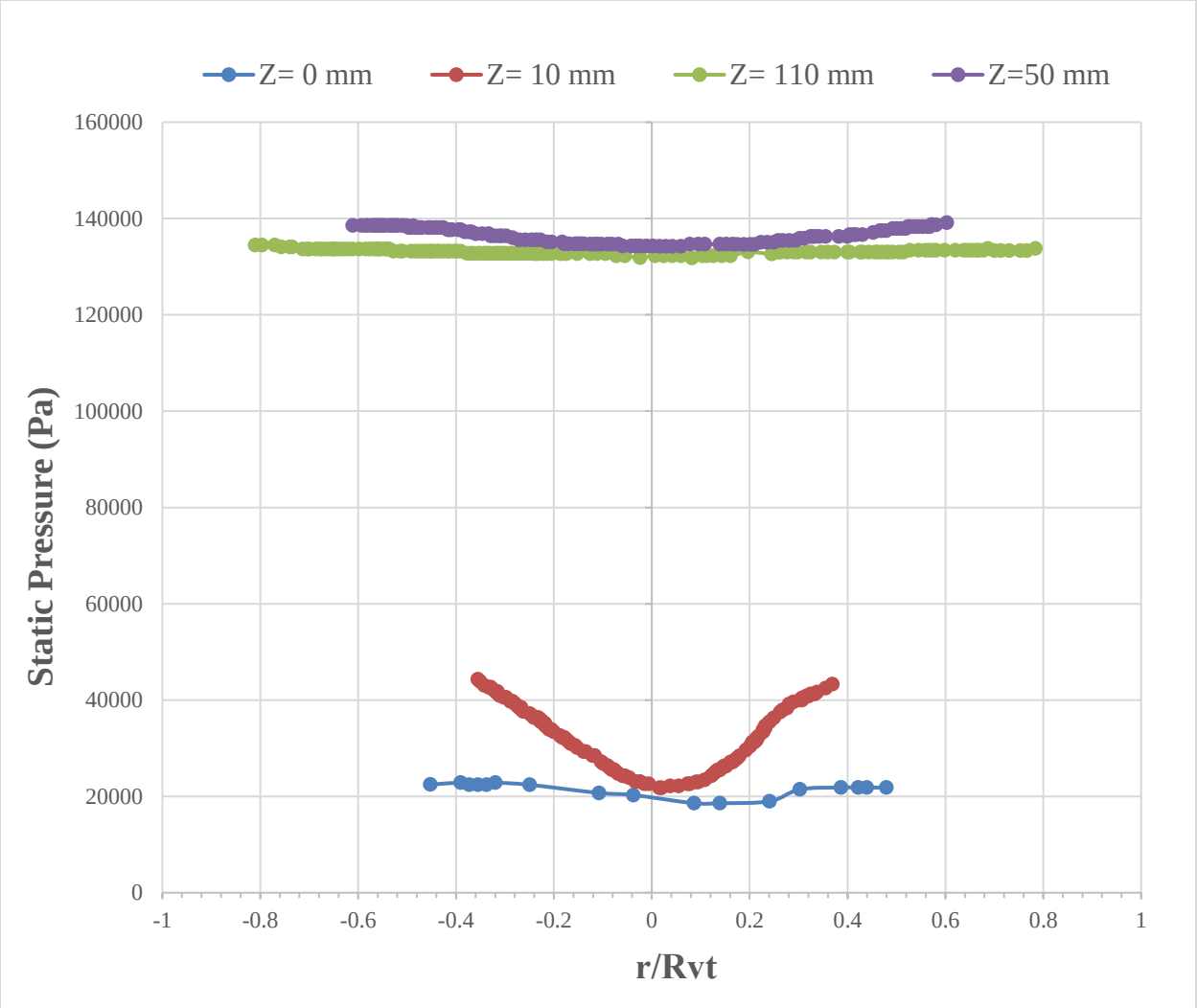

(g)

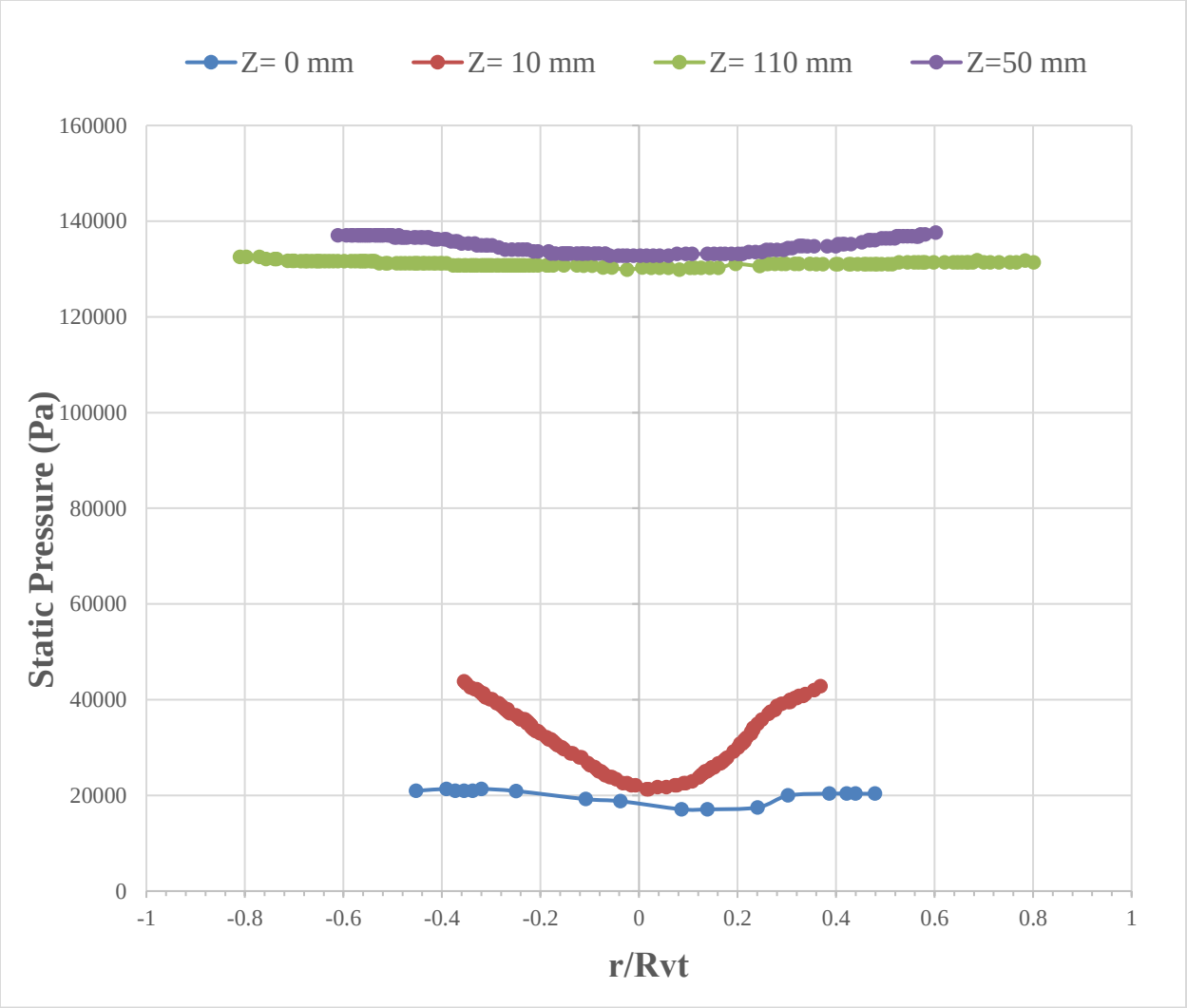

(h)

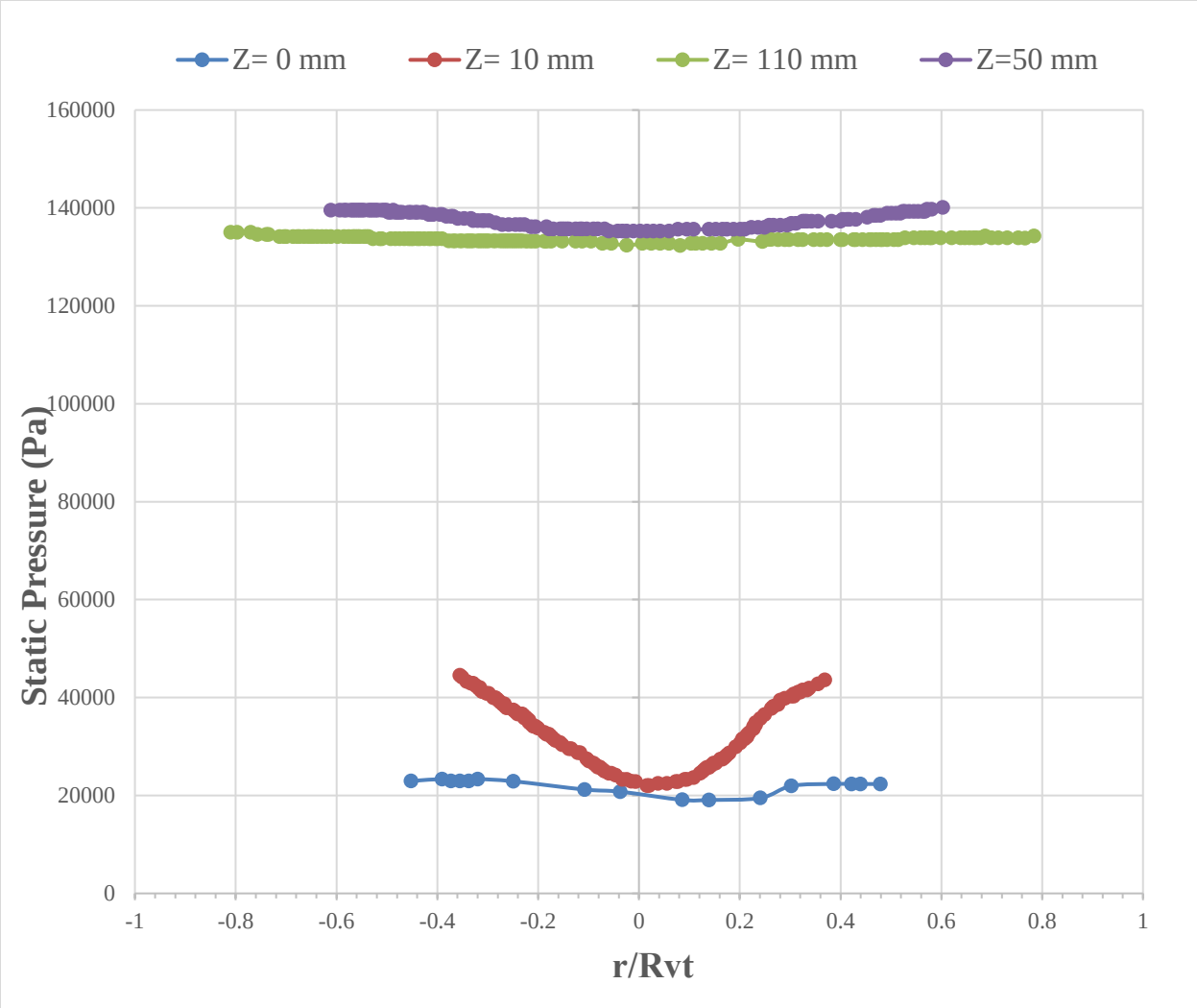

(i)

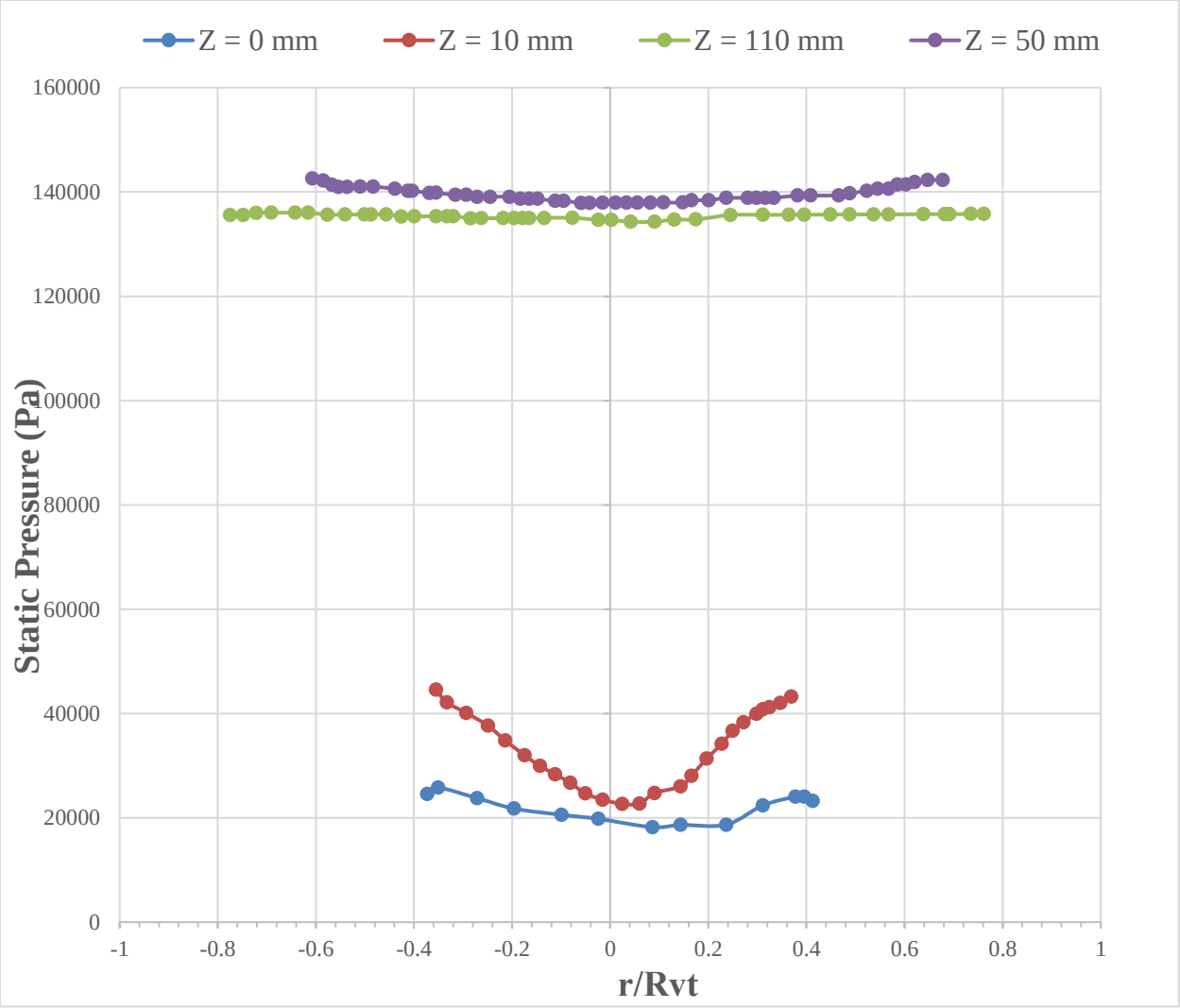

(j)

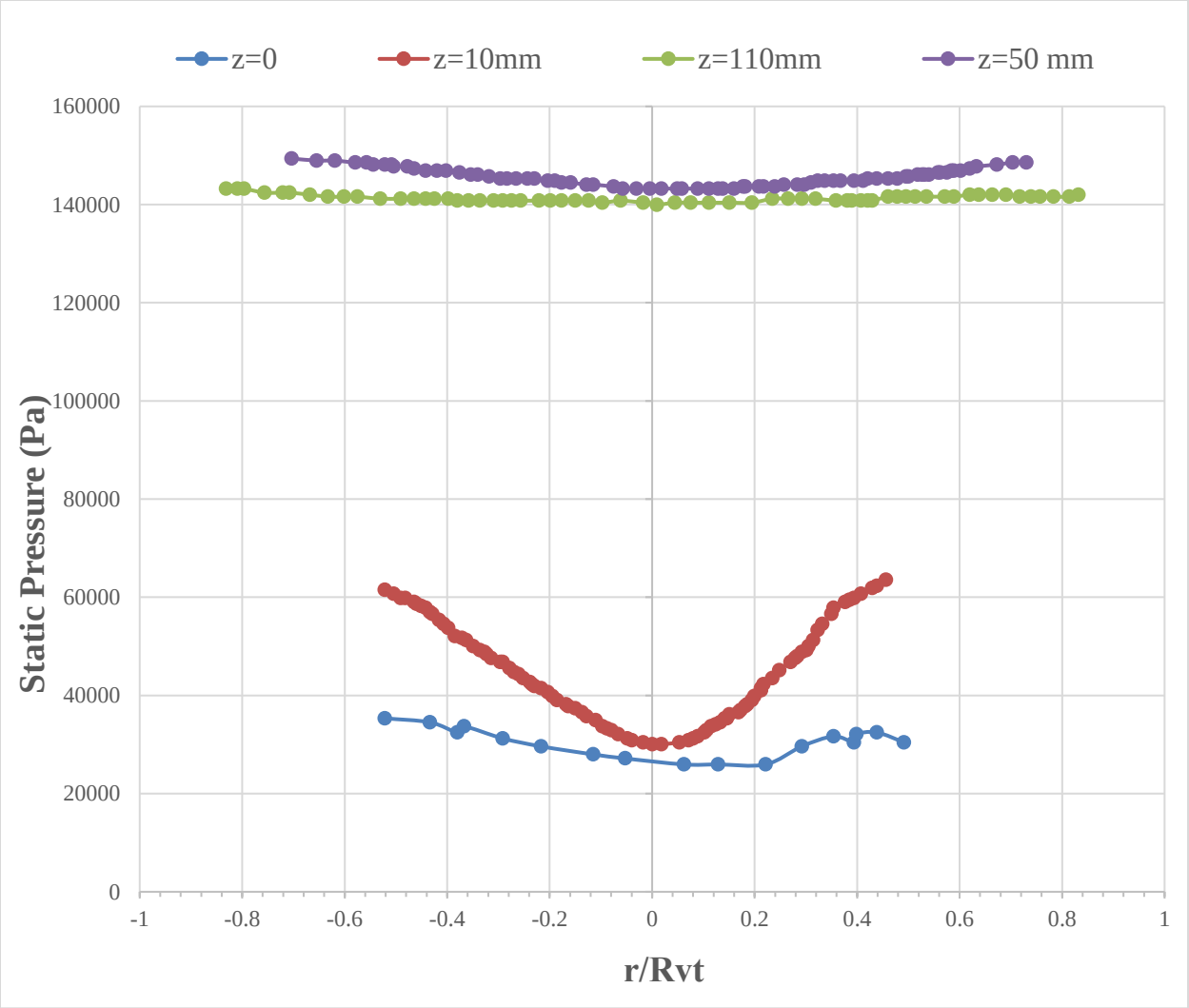

(k)

Fig. 7. Radial profile of static pressure (a) 2°, (b) 1.5°, (c) 1°, (d) 0.8° and (e) 0.5° convergent, (f) straight and (g) 1°, (h) 2°, (i) 3°, (j) 4° and (k) 6° divergent vortex tubes at different cross sections Z = 0, 10, 50, and 110 mm for P = 0.3 MPa.

5.3. Thermal energy and secondary circulation flow

CFD analysis is performed to simulate the influence of divergent and convergent angles of hot- tube on the presence of secondary circulation flow and therefore the influence of secondary flow on energy separation with the straight, divergent and convergent vortex tubes. Fig. 8 shows the radial profiles of the total temperature at different cross section locations (Z = 0, 10, 50 and 110 mm) for 2°, 1.5°, 1°, 0.8° and 0.5° convergent, straight and 1°, 2°, 3°, 4° and 6° divergent vortex tubes, respectively. It can be seen clearly from this figure that the total temperature of the outer peripheral flow is higher than the central core

flow of the vortex tube. In all sections, the divergent tube has the maximum total temperature. Minimum total temperature was observed near exit center of the tube. Also the divergent profiles have minimum total temperature. It was observed that maximum and minimum total temperature gradient are for 2° divergent vortex tube and 2° convergent vortex tube respectively. The temperature gradient for 0.5° convergent vortex tube is higher than 2° convergent vortex tube. The temperature gradient for 2° divergent vortex tube is higher than 6° divergent vortex tube. Also the divergent profiles have higher temperature gradient for all cases of angle of divergences. Furthermore, the convergent profiles have lower temperature gradient than the straight vortex tubes. Therefore, the energy separation in 2° divergent vortex tube is higher than straight vortex tube and the straight vortex tube has higher energy separation than the convergent vortex tubes, under the investigated condition. This also proves that the curvature of the tube greatly influences the flow and performance of vortex tube. To clearly analyze the trend of temperature difference in Fig. 8, the stream lines are drawn in Fig. 9 (a-k) for 2°, 1.5°, 1°, 0.8° and 0.5° convergent, straight and 1°, 2°, 3°, 4° and 6° divergent vortex tubes, respectively. Maximum hot temperatures of 316, 318, 319, 319, 319, 325, 320, 322, 323, 325 and 324 K, and minimum cold temperatures of 290, 289, 287, 286, 284, 283, 281, 277, 281, 281 and 282 K of 2°, 1.5°, 1°, 0.8° and 0.5° convergent, straight and 1°, 2°, 3°, 4° and 6° divergent vortex tubes respectively, was observed for a pressure loss ratio of $\lambda = 0.7$ and P = 0.3 MPa.

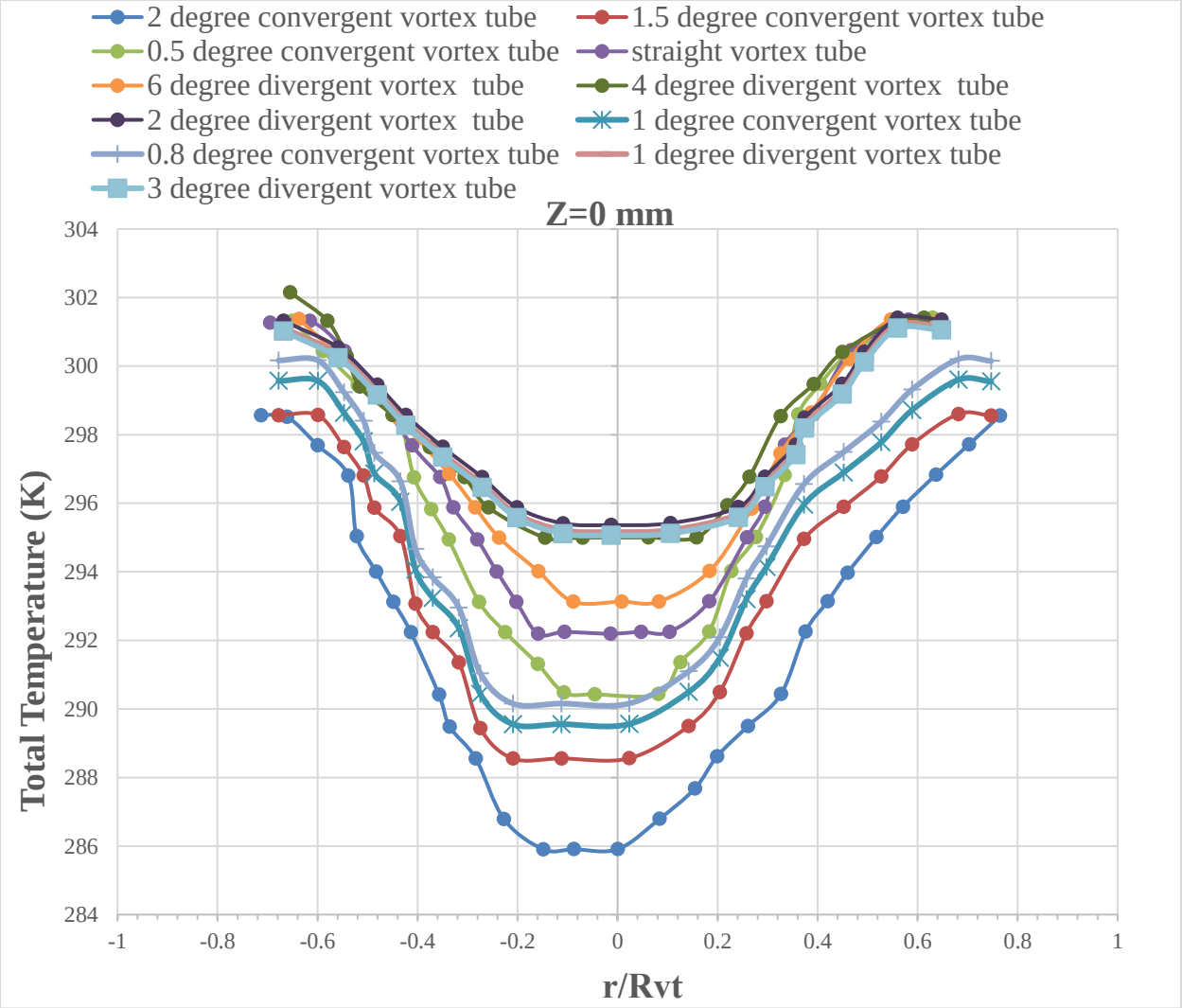

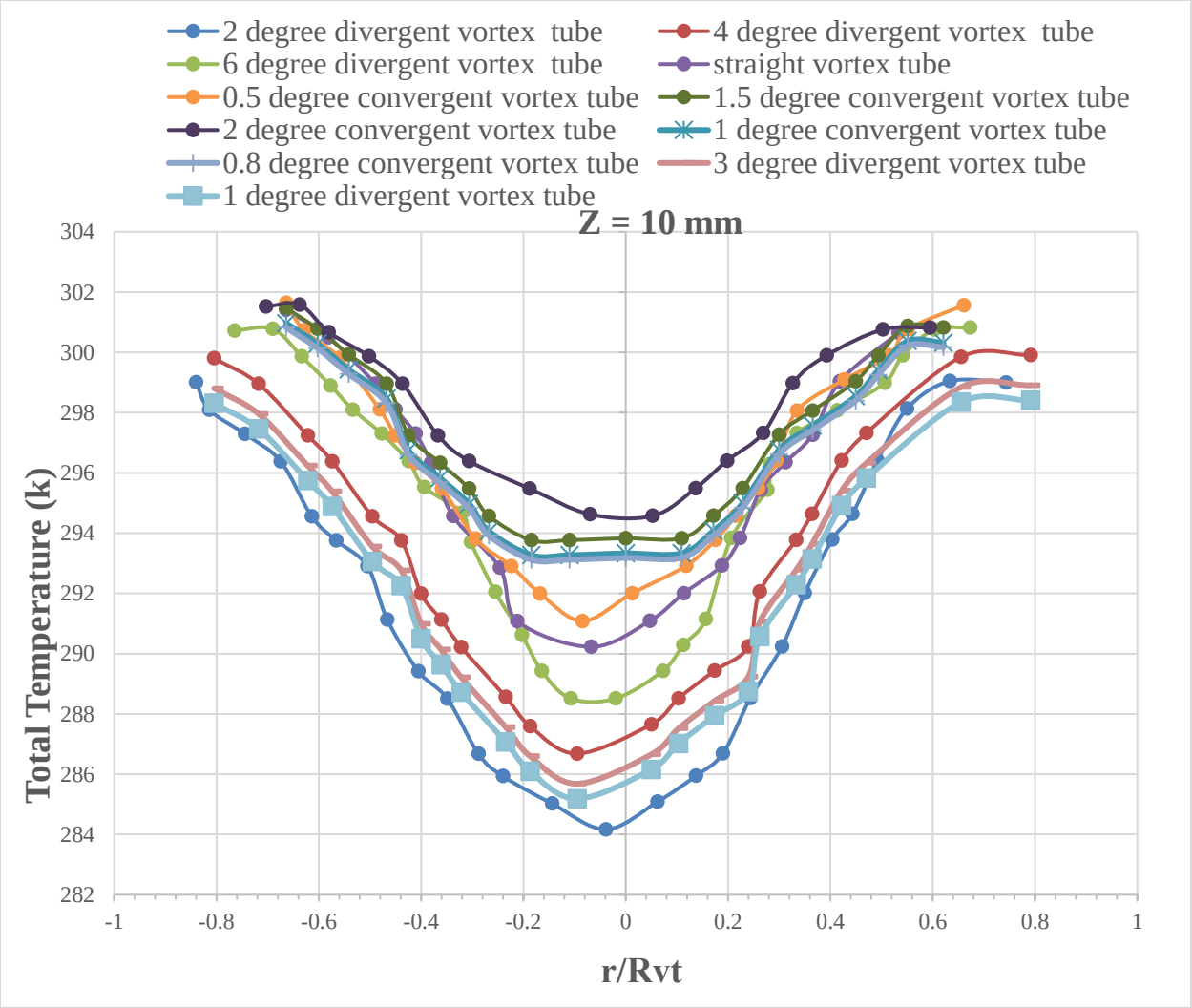

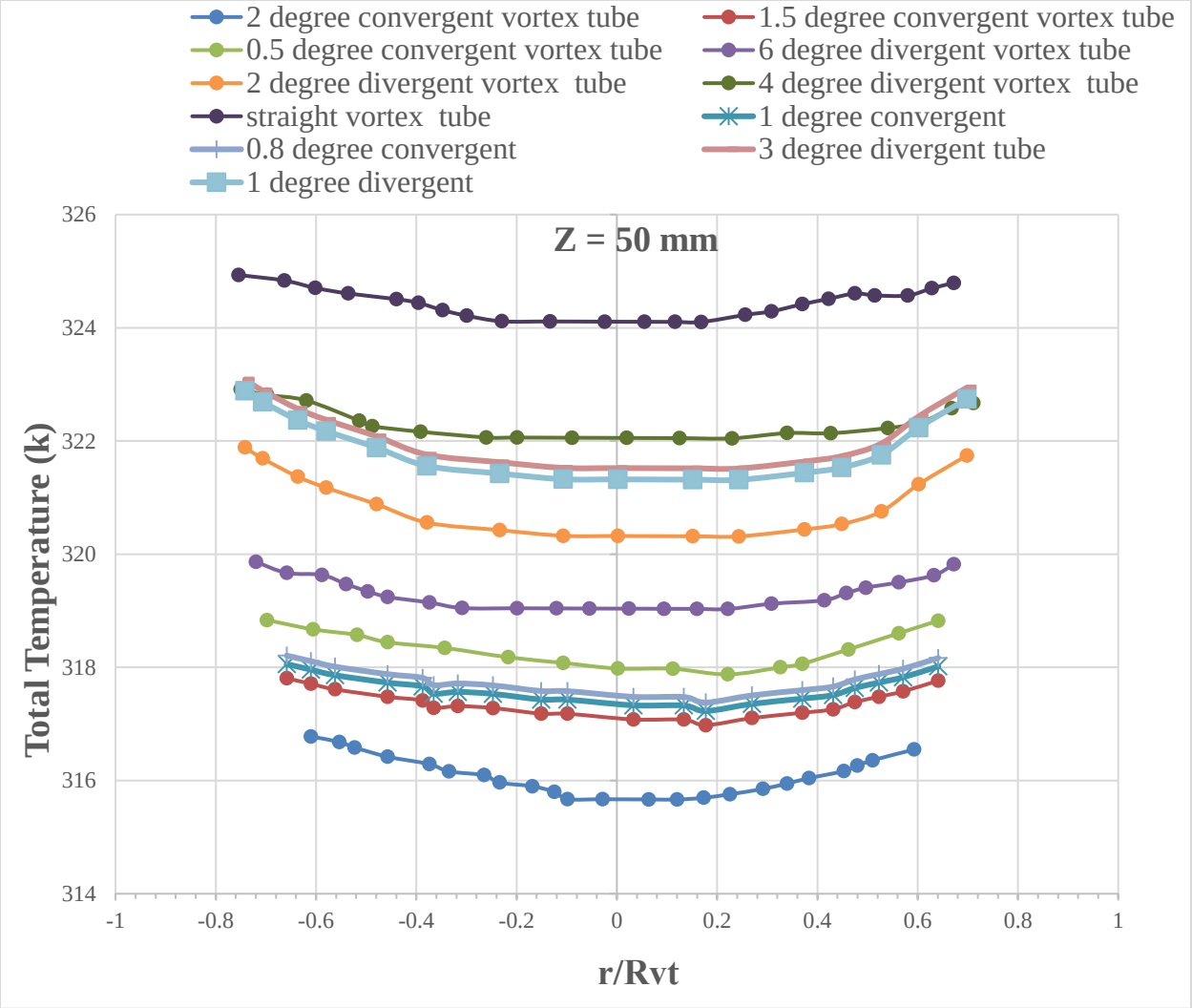

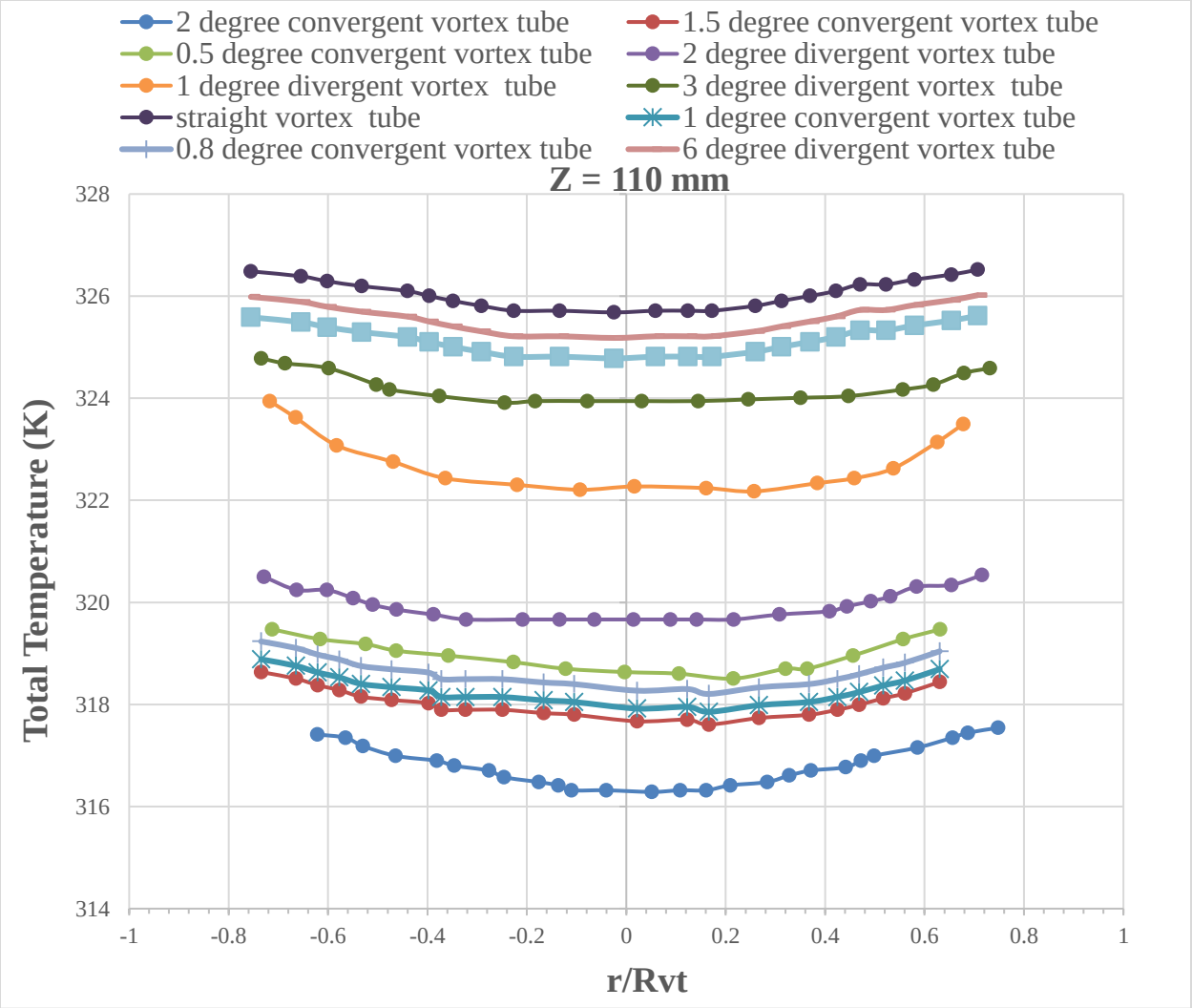

Fig. 8. Radial profile of total temperature at various vortex tubes (2°, 1.5°, 1°, 0.8° and 0.5° convergent, straight and 1°, 2°, 3°, 4° and 6° divergent vortex tubes) at different cross sections Z = 0, 10, 50, and 110 mm.

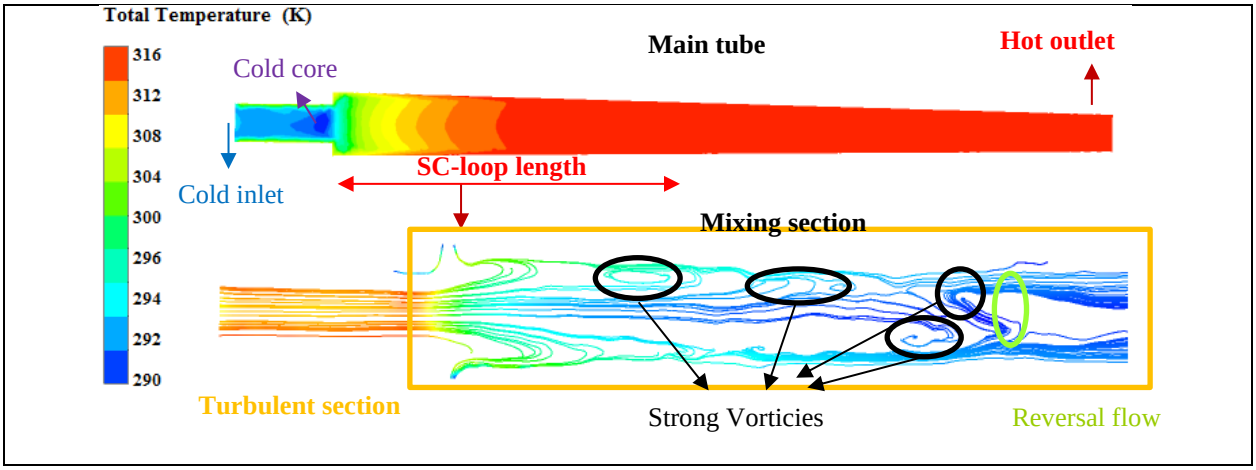

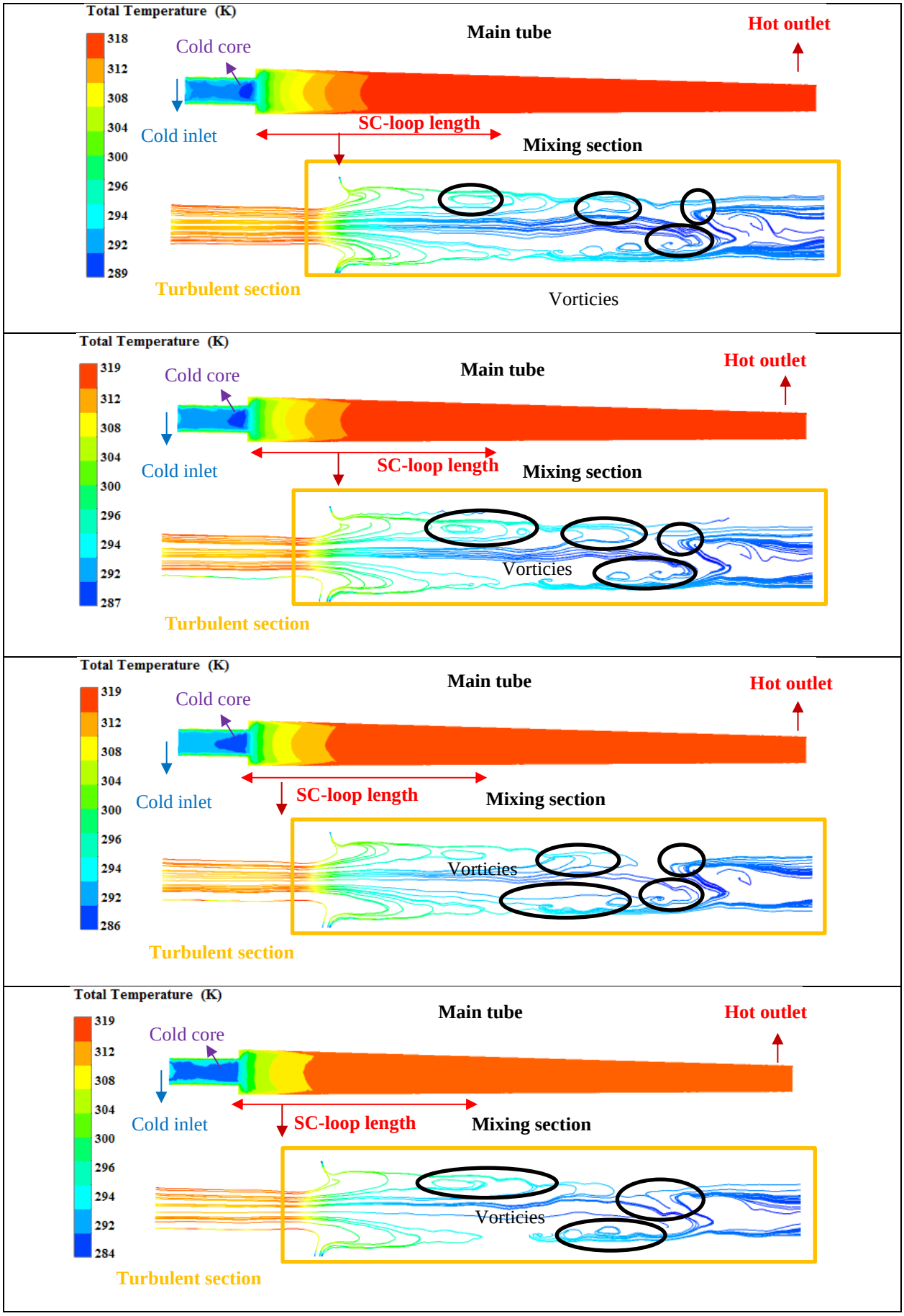

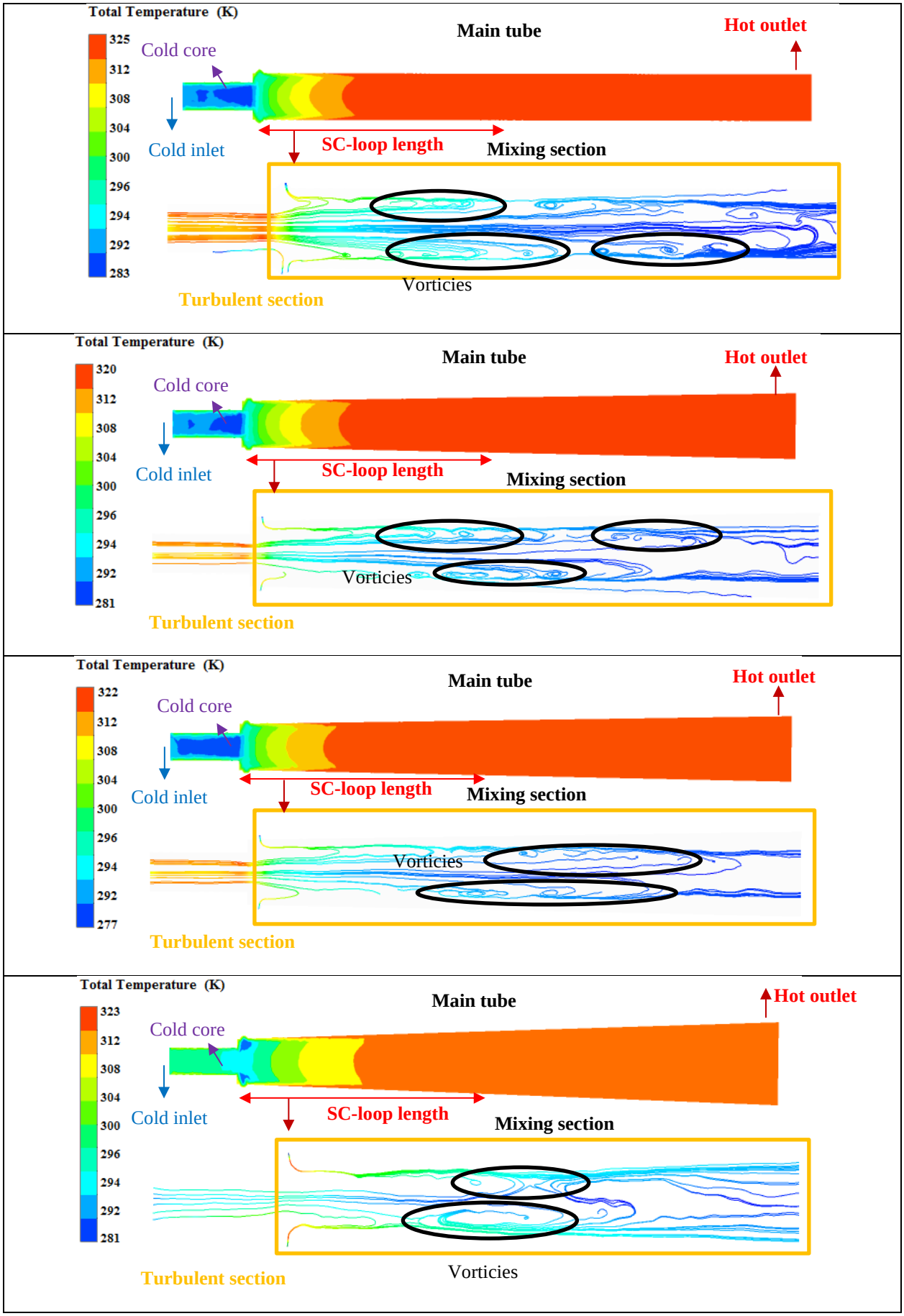

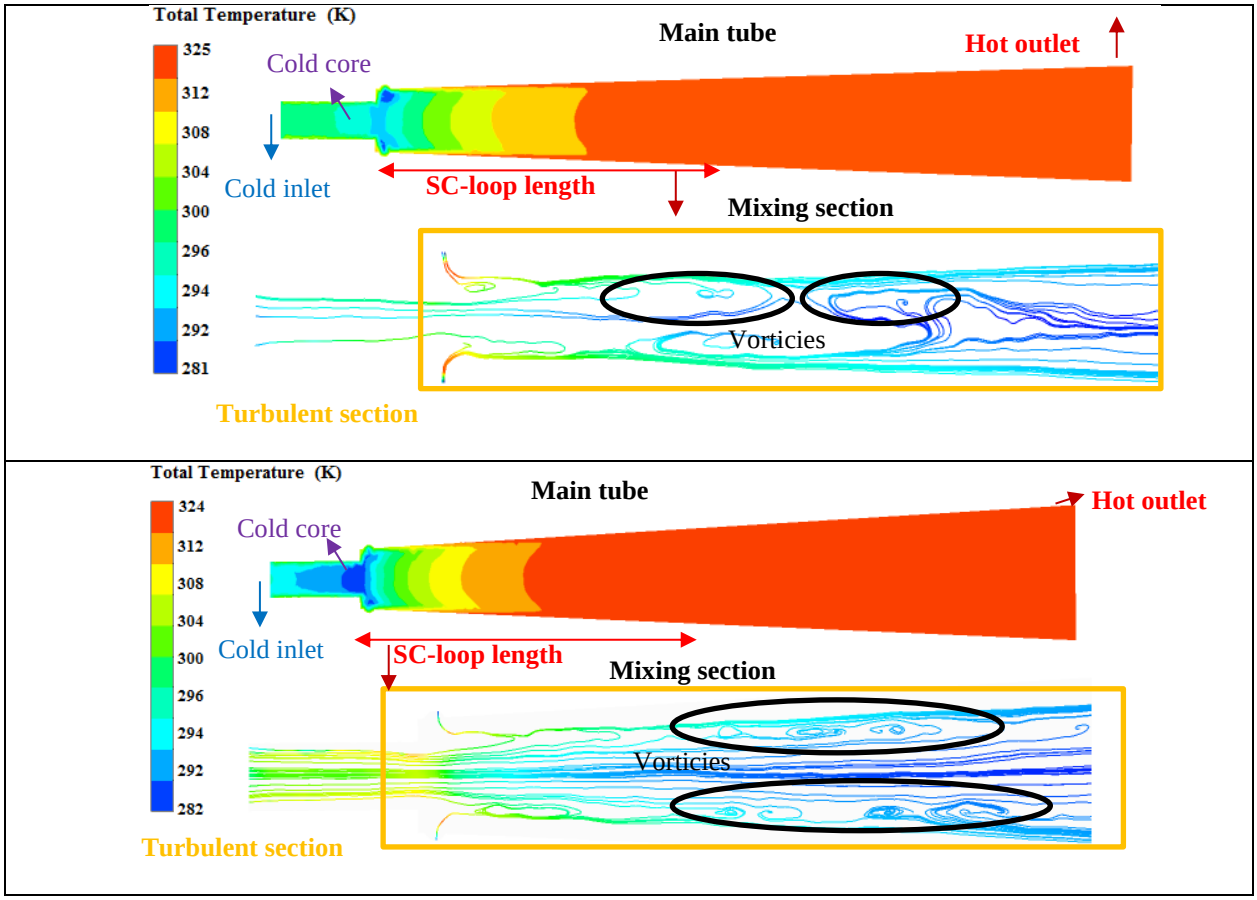

Fig. 9. Total temperature maps with streamline patterns superimposed for (a) 2°, (b) 1.5°, (c) 1°, (d) 0.8° and (e) 0.5° convergent, (f) straight and (g) 1°, (h) 2°, (i) 3°, (j) 4° and (k) 6° divergent vortex tubes.

The existence of secondary circulation flow in vortex tube [4] and its influence on the energy separation within the vortex tubes for different scenarios: straight, divergent and convergent vortex tubes verified from CFD analysis is shown in Fig. 11. In the present study, the motivation is to obtain different flow pattern by changing the curvature of the vortex tube. It would thus more reasonable to define the secondary circulations in terms of the vortices, which represents a characteristic viscous scale appropriate for swirling flow. The stream trace plot (Fig. 11) shows that within the straight vortex tube there exists two swirling flows. One flow swirls to the hot end in the outer peripheral region, named the peripheral swirling flow. The other anti-swirls or reverse to the cold exit in the core region, named the internal swirling flow [25]. Those swirl flows generate the high rotational speed vortex motion inside the vortex tube. This also the obvious case for divergent and convergent vortex tubes too. Fig. 10 displayed the different flow patterns, especially the vortex phenomenon (circulation flow) inside the vortex tube for various angles of divergent and convergent hot-tubes. It is observed that the

stream lines take on a different shape and size for different shape of vortex tubes. Due to strong friction interaction between the central rotation or swirl flow and flow near the tube wall that is caused by the high tangential velocity, as well as the formation of the recirculation flow zones, a form of vortex break down which can cause great energy dissipation, axisymmetric flow distribution will appear easily. As one can see be seen from Fig. 10, there are also three vortices or loop for straight vortex tube. Due to recirculated flow of remained of the flow, named the secondary circulation (SC) loop. Thus flow pattern has been first observed experimentally by Ahlbor and Groves [25] and subsequently by Gao et al. [32]. This loops functions as the high and low temperature environments like to a refrigeration cycle. Internal energy is exchanged between inner and peripheral region via the two loops. The incoming fluid element and the fluid element in the loop mix together. Some fluid elements in this loop first pass the outer peripheral region from the entrance to the hot end, and escape from hot end. Other fluid elements stay in the loop and return axial direction to the cold end in the center and exit via the cold exhaust. As shown in Fig. 10, the number and the size of vortices formed within the main tube are different. The vortices appear to be a characteristic of vortex tube towards energy separation. In fact, vortices in SC-loop cause the mixing process between the cold fluid elements in the core center with hotter fluid element in the outer peripheral region. The mixing process, thus, is increasing by the increase of the number of vortices. The stream function plotting for 2° convergent in Fig. 10 shows four vortices, thus it has lower capacity than straight tube. The 2° divergent vortex tube has two vortices and it shows a higher capacity than the straight and convergent vortex tube. Table (4) presents the cold and hot outlet temperature, number of vortices and length of the SC-loop, where SC-loop is defined as the distance from cold outlet to the end of SC-loop (the point that axial velocity reach to zero) for P = 0.3 MPa and $\lambda = 0.7$. the number of vortices for 2°, 3°, 4° and 6° divergent vortex tubes is two but the length of SC-loop is different which is their main difference thus this parameter plays an important role in cooling performance of these profiles. In other words, the region in SC-loop length is the region where the flow physics in tubes is expected to govern the overall behavior. The reason behind this nature in divergent/convergent vortex tube can be understood by examining the variation of vortices size in tube and its relation with length of SC-loop. By increasing the length of secondary SC-loop, the number of vortices remain constant but growing and it causes the gas element in the loop pass more distance and loss (earn) more energy. The obvious change of number and size of vortices within the vortex tube with different geometrical curvatures indicates that the temperature difference is also due to the partial variation of secondary circulation flow. Taking the fact disclosed in Fig. 7 (c),

we can reasonably concluded the energy separation in vortex tube is mainly due to the strong rotation flow caused by angular momentum transfer from the core to peripheral which can explain well the existence of turbulent vortex flow near front part of vortex tube observed in Fig. 10. However, in the flow part near the hot exit the variation regularity of the tangential velocity in Fig. 7 (c) of Z = 110 mm is not the same as that shown in Fig. 7 (c) for Z = 10 mm. In this axial section, the tangential velocity for 2° divergent is much bigger than that of 2° convergent (and straight) tube. Thus, the tangential velocity profiles in the different sections of the vortex tube show that the temperature rise near the hot end is caused by the energy transformation from the kinetic energy of the peripheral flow and the temperature drop near the cold exit mainly depends on the pressure expansion and angular momentum transfer.

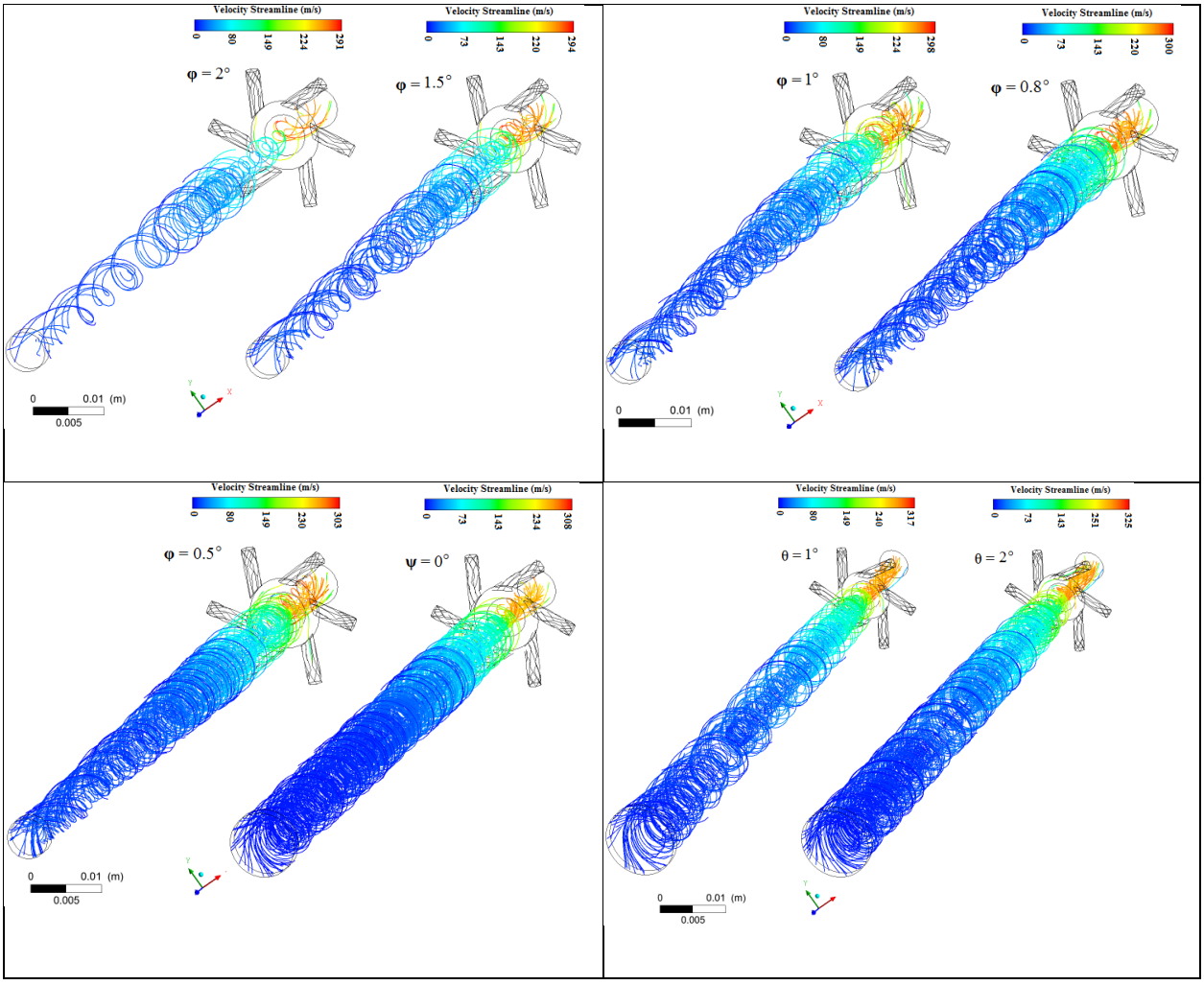

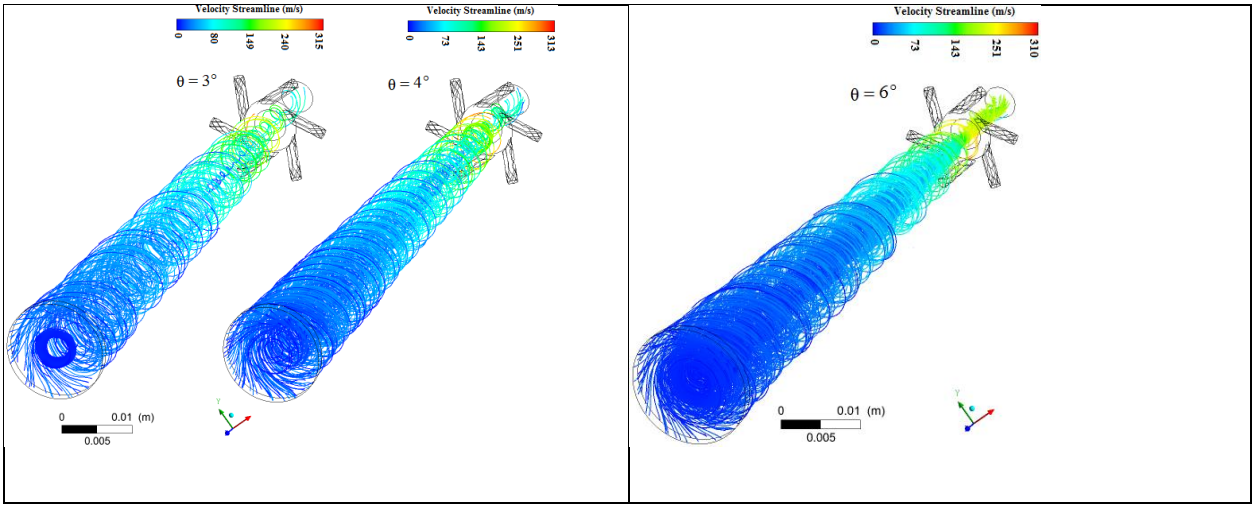

Fig. 10. Stream trace for the inner core fluid flow and peripheral hot fluid flow in the entire 2°, 1.5°, 1°, 0.8° and 0.5° convergent, straight and 1°, 2°, 3°, 4° and 6° divergent vortex tubes in three-dimensional space.

Table 4

Cold and Hot outlet temperatures, number of vortices and length of the SC-loop for different vortex tubes profile at P = 0.3 MPa and λ = 0.65.

Vortex tube profiles	Cold outlet temperature (k)	Hot outlet temperature (k)	Number of vortices	Length of SC – loop (mm)
2º convergent	291.82	315	4	81.4
1.5º convergent	290.84	316	4	77.6
1º convergent	290	317	4	73
0.8º convergent	289.6	318.2	4	71
0.5º convergent	289.2	319.4	3	68.6
Straight	288.73	325	3	67
1º divergent	285.94	321.5	3	48.12
2º divergent	285.1	320	2	43.4
3º divergent	286	320.09	2	55.3
4º divergent	287.4	319	2	59.8
6º divergent	287.96	318	2	63.26

5.4. Thermal analysis (optimization)

The data obtained from the numerical simulation is being utilized further to investigate the optimized thermal performance of the non-uniform curvature hot-tubes. Fig. 11 (a, b) shows the cold temperature difference with respect to the pressure loss ratio at P = 0.3 and 0.4 MPa respectively. As depicted in Fig. 11, the divergent vortex tubes have greater cooling capacity than the straight and convergent vortex tubes. As shown in this

figure, the maximum cold temperature happens for the divergent angle of 2°. The maximum cold temperature difference is about 13.8 K at $\lambda = 0.69$ and 18.71 K at $\lambda = 0.68$ in P = 0.3 and 0.4 MPa for 2° divergent vortex tube respectively. Lowest cold temperature difference is 2.1 K at $\lambda = 0.78$ and 3.6 K at $\lambda = 0.76$ in P = 0.3 and 0.4 MPa for 2° convergent vortex tube respectively. The maximum cold temperature difference at the cold side is located at equal pressure loss ratios at about $\lambda = 0.68$. For $0.68 < \lambda < 0.8$, all divergent vortex tubes have approximately the same cold temperature difference.

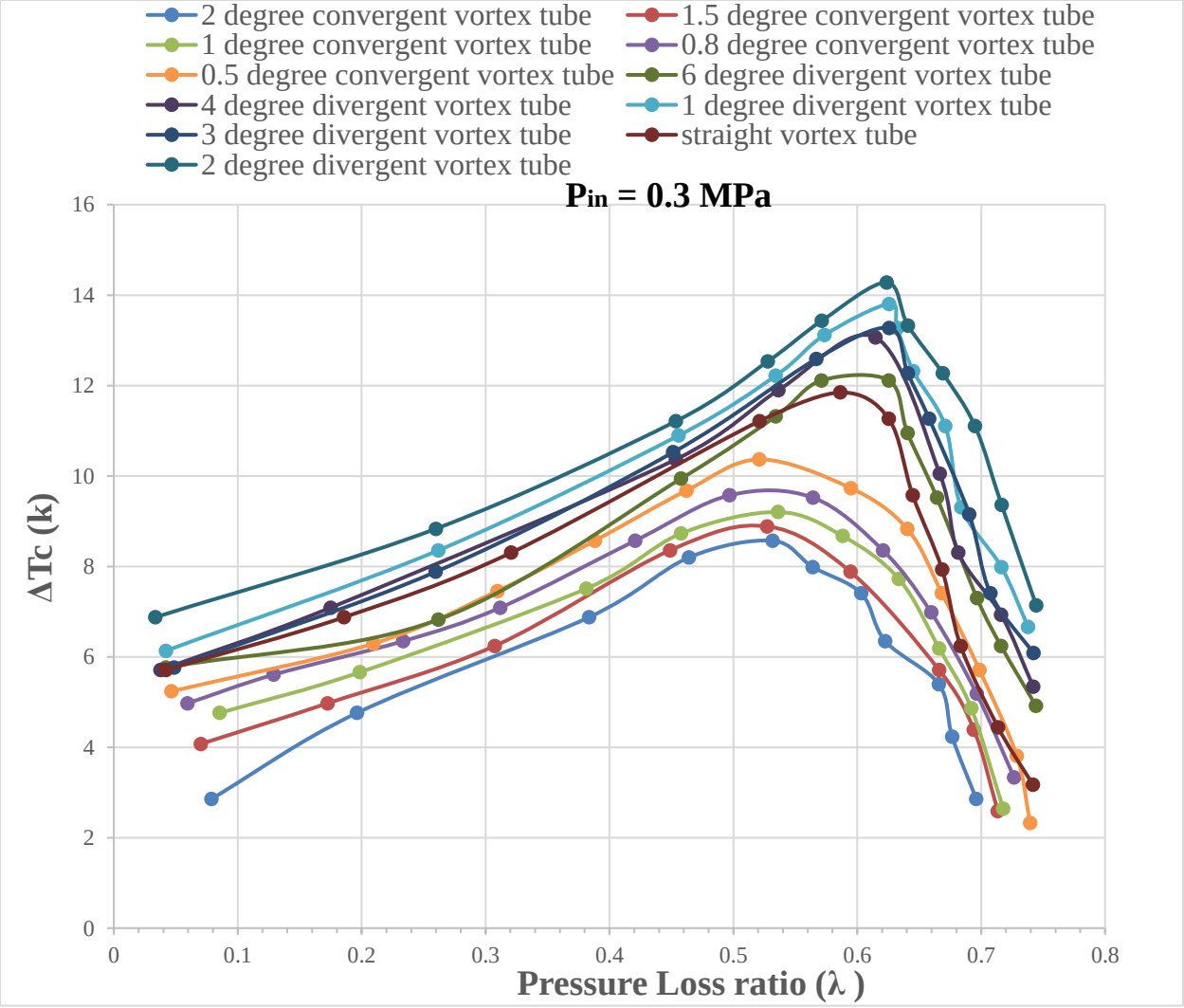

(a)

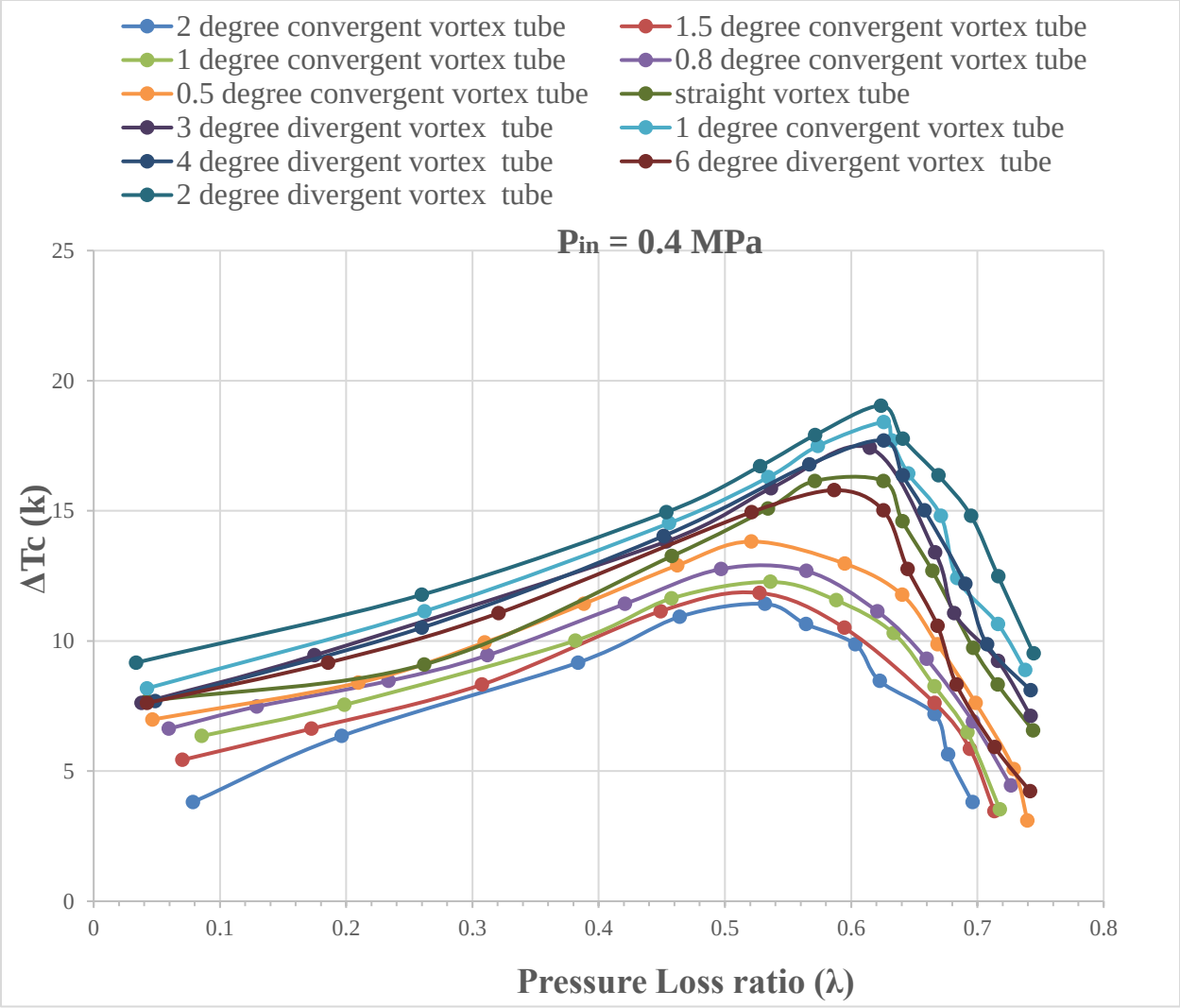

(b)

Fig. 11. Cold temperature difference versus pressure loss ratio for different vortex tubes at P = 0.3 and 0.4 MPa.

Fig. 12 (a, b) shows the efficiency or isentropic cooling performance for vortex tube with different angles of divergent and convergent hot-tubes at inlet pressure of P = 0.3 MPa. The vortex tube with divergence angle of 2° gives the highest efficiency as compared to other vortex tube types, but the vortex tube with convergence angle of 2° gives the lowest efficiency. However, for the investigated conditions, the highest efficiency belongs to the divergent vortex tubes. The highest efficiency takes place for pressure loss ratio at about of λ = 0.66 for all vortex tubes.

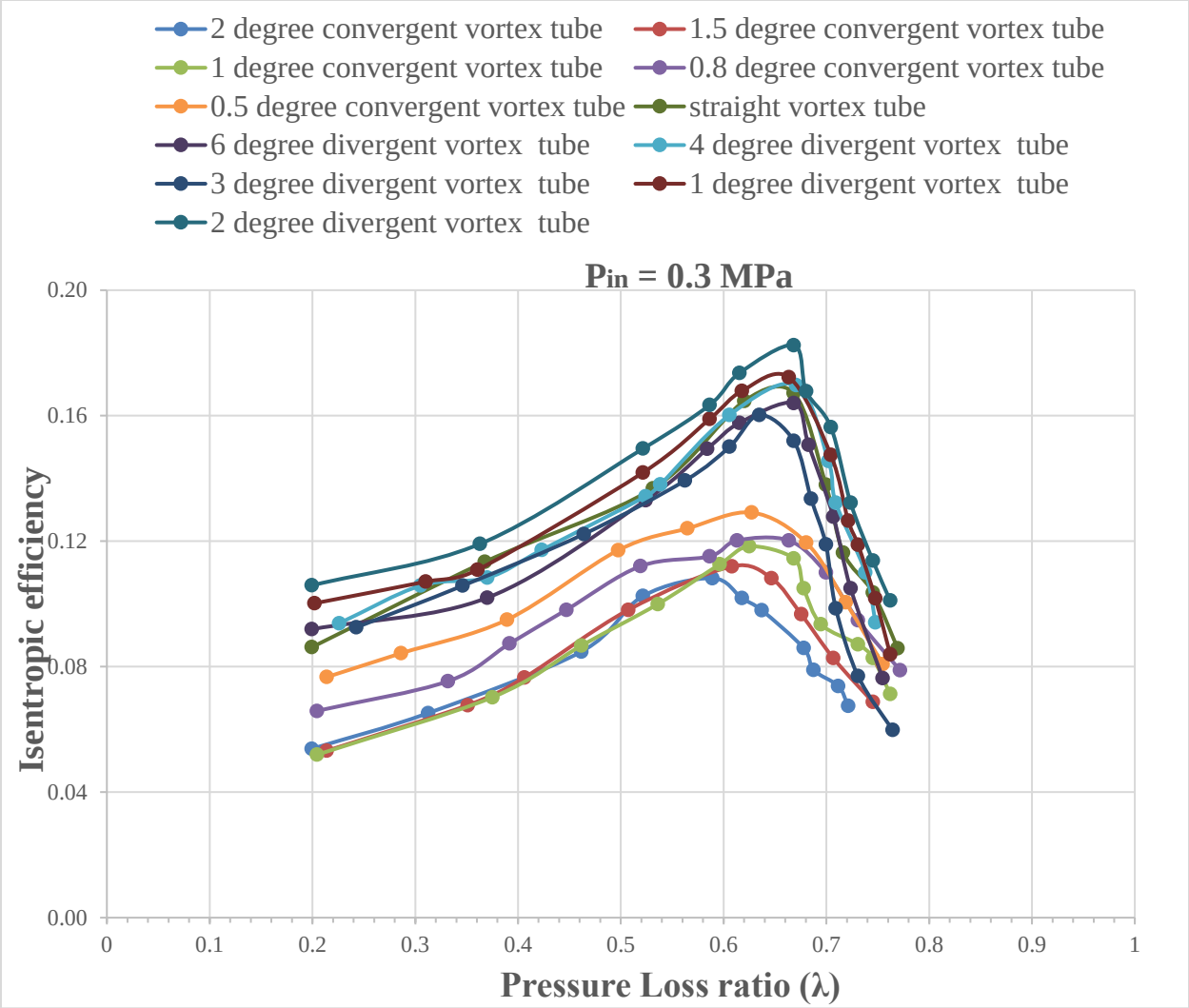

(a)

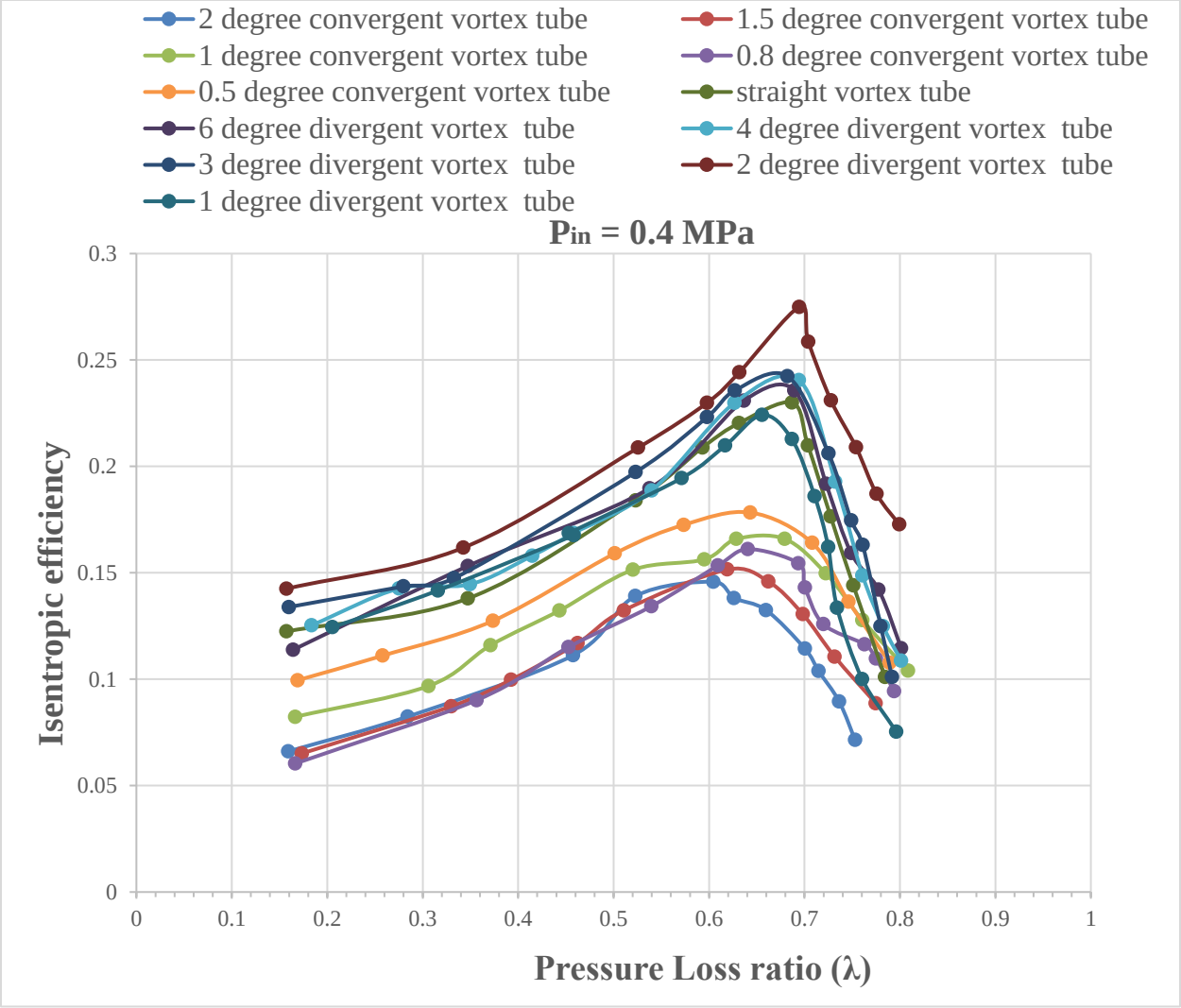

(b)

Fig. 12. Isentropic efficiency versus pressure loss ratios for different vortex tubes at P = 0.3 and 0.4 MPa.

The cooling performance behaviors of the vortex tubes have been estimated by calculating the coefficient of performance (COP). The COP values of the vortex tubes with different angle of convergent and divergent hot-tubes for various pressure loss ratios at the inlet pressure of P = 0.3 MPa are shown in Fig. 13. The 2° divergent vortex tube gives the highest COP and 2° convergent one gives the lowest COP. The optimum COP for all vortex tubes occurs at about $\lambda \approx 0.65$. As seen in Fig. 13, the effect of convergence angle decreases the value of COP and for divergence angle increases the value of COP compared to straight vortex tube, for the investigated condition.

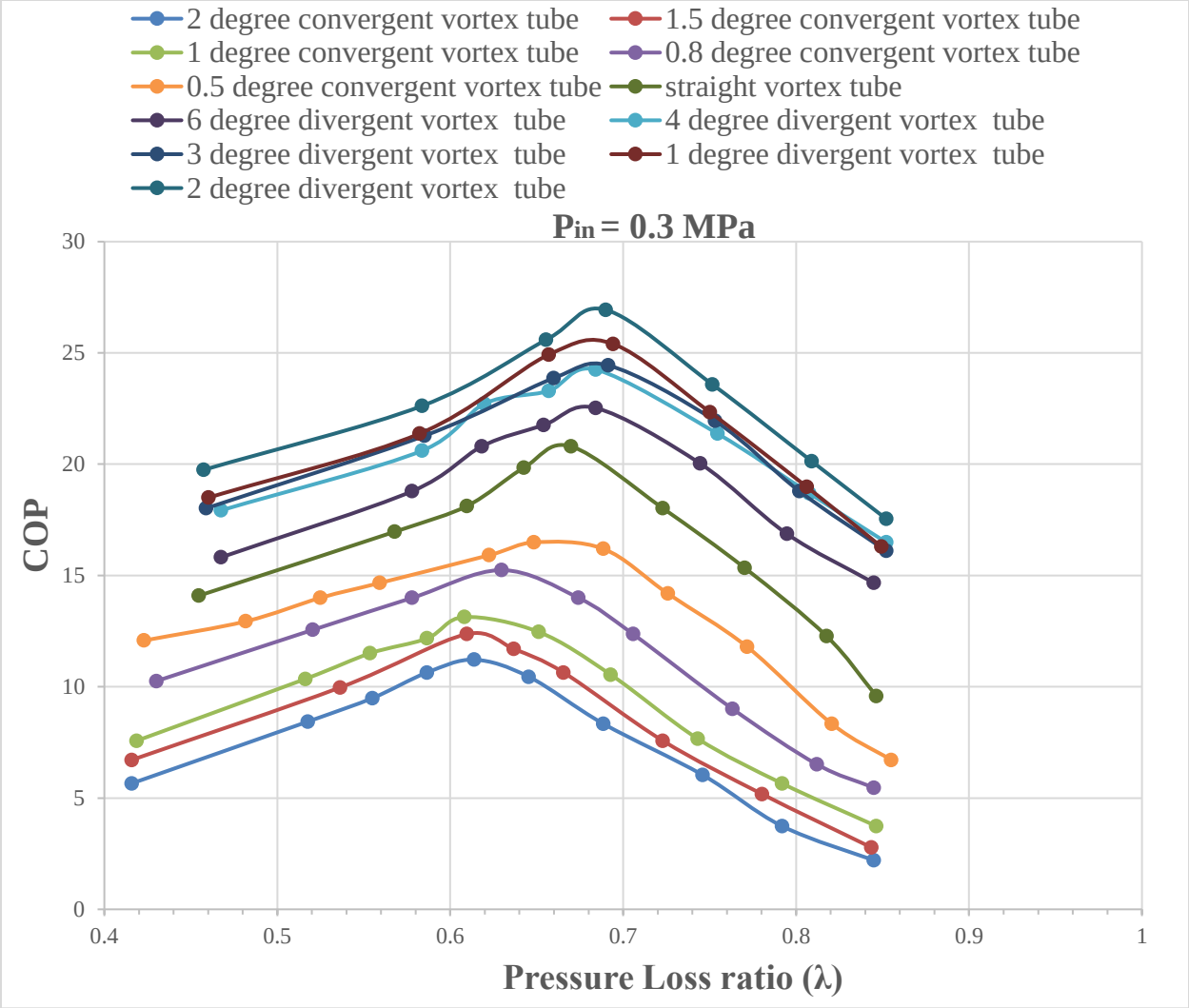

(a)

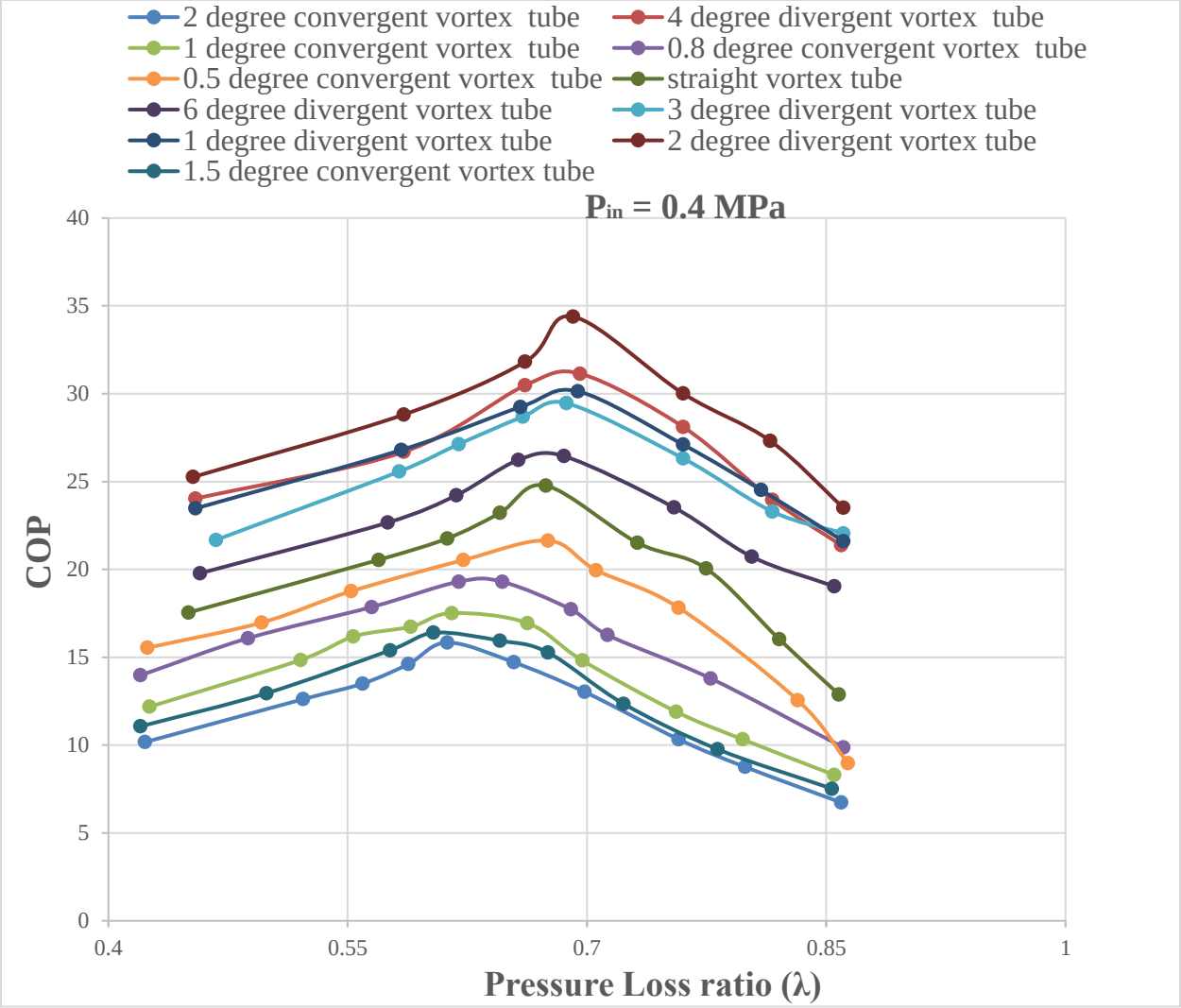

(b)

Fig. 13. Coefficient of performance versus pressure loss ratios for different vortex tubes at P = 0.3 and 0.4 MPa.

Fig. 14 is for investigation the effect of divergence and convergence at constant pressure loss ratios 0.4, 0.5 and 0.6. The models with different L_h/D ratios i.e. 5.31, 6.53, 7.37, 8.45, 9.92, 12, 13.40, 14.41, 15.18, 17.49 and 20.65 with 120 mm length of hot-tube, have been studied. It can be seen clearly from this figure that, for inlet pressure of P = 0.3 MPa, minimum COP points occur for L_h/D = 20.65 (2° convergent vortex tube). By increasing L_h/D from 0 to 8.45 the COP increased, and after region L_h/D = 8.45 the COP decreased.

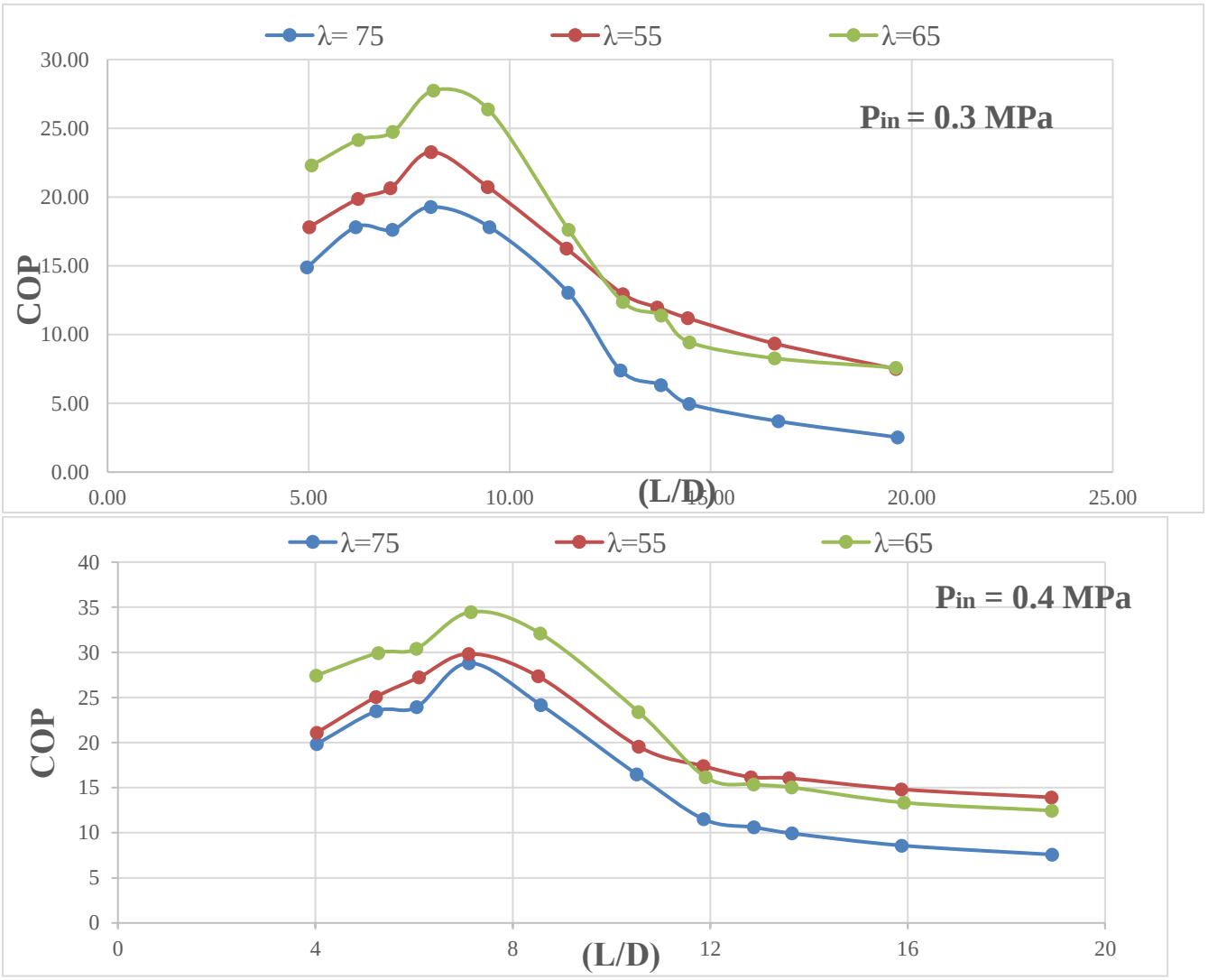

Fig. 14. Numerical coefficient of performance obtained at different L_h/D ratios at P = 0.3 and 0.4 MPa.

6. Conclusions

In the present work, the energy separation inside non-uniform and uniform cross section of vortex tubes are studied in detail. The flow field and energy transfer for the straight, divergent and convergent tube geometries are investigated in order to gain a better insight into physical mechanisms that cause thermal separation. A three-dimensional numerical model of vortex tube has been developed to examine the energy separation mechanism and the swirling flow behavior inside straight and different cross-section of vortex tubes. The mathematical model and proposed numerical solution were first verified by performing grid independence studies and validated by comparing with previous experimental and numerical works for straight vortex tube. The main finding are briefly summarized as follows:

1- The results of proposed CFD model confirm the previous experimental and numerical studies and also provided a detailed insight in the turbulent swirling flow structures.
2- The numerical analysis revealed a stable double helix vortex structure in the vortex tube with different flow features for the investigated scenarios. The axial velocity shows a back flow region in the tube center over the entire length. The results also reveal that the value of axial velocity near cold exit determines the quality of separation process.
3- The results illustrate that the angle in divergent and convergent hot-tubes has a great influence on the temperature difference between the cold gas outlet and hot gas outlet. Under our investigated range, the results show that the divergent hot-tubes can improve the performance of vortex tube. The mean cold gas temperature reduction and efficiency of vortex tubes with divergent angle are higher than those of vortex tube with straight and convergent angle. These results also show that for all angle of convergent a reduction in the performance of vortex tube was observed compared to those of straight and divergent vortex tubes.
4- The analysis illustrates that the divergent tubes have the potential to improves the performance of vortex tubes, significantly. The 2° divergent hot-tube is the optimal angle for obtaining the highest refrigeration performance as a refrigerator. Therefore, divergent vortex tube exhibits better thermo-hydraulic performance compared to the straight and convergent tube.
5- The study of flow structure with different angle of divergent and convergent hot-tubes demonstrates the flow behavior and process. The analysis shows that all different geometrical shapes of vortex tube leads to the formation of recirculation flow zones along the main tube near the inlet. The number, size and shape of these vortices are different for each geometrical shape of vortex tube which greatly influences the vortex tube efficiency. The study also illustrates a reasonable explanation for the operation of vortex tube base on an energy transfer between the cold, hot flow leaving the nozzle and the low velocity flow in the core. This explanation clearly points out that the existence of temperature difference between the cold gas outlet and the hot gas outlet is mainly due to the relative dominance of the vortex effect which comes from the interaction of angular momentum transition and kinetic energy transfer.

Acknowledgements

This paper was partially supported by Petroleum University of Technology (PUT) organization, Department of gas and mechanical engineering of (PUT).

7. References

[1] Ranque G. Expériencesd sur la detente giratoire avec productions simultanes d'un echappment d'air chand et d'un echappment d'air froid. J phys Radium. 1933:112-4.
[2] Hilsch R. Die expansion von Gasen im Zentrifugalfeld als Kälteprozess. Zeitschrift für Naturforschung A. 1946;1:208-14.

[3] Eiamsa-ard S, Promvonge P. Review of Ranque–Hilsch effects in vortex tubes. Renewable and sustainable energy reviews. 2008;12:1822-42.
[4] Gutsol A. The ranque effect. Physics-Uspekhi. 1997;40:639-58.
[5] Thakare HR, Monde A, Parekh AD. Experimental, computational and optimization studies of temperature separation and flow physics of vortex tube: A review. Renewable and Sustainable Energy Reviews. 2015;52:1043-71.
[6] Xue Y, Arjomandi M, Kelso R. A critical review of temperature separation in a vortex tube. Experimental Thermal and Fluid Science. 2010;34:1367-74.
[7] Yilmaz M, Kaya M, Karagoz S, Erdogan S. A review on design criteria for vortex tubes. Heat and mass transfer. 2009;45:613-32.
[8] Ranque G. Experiences sur la d'etente giratoire avec productions simultan\ ees d'un echappement d'air chaud et d'un echappement d'air froid. J Phys Radium. 1933;4:112-4.
[9] Kassner R, Knoernschild E. Friction Laws and Energy Transfer in Circular Flow. Part 1-The Law of Shear Stresses in Circular Flow. Part 2-Energy Transfer in Circular Flow and Possible Applications (Explanation of the Hilsch or Ranque Effect). AIR MATERIEL COMMAND WRIGHT-PATTERSON AFB OH; 1948.
[10] Elser K, Hoch M. Das Verhalten verschiedener Gase und die Trennung von Gasgemischen in einem Wirbelrohr. Zeitschrift für Naturforschung A. 1951;6:25-31.
[11] Deissler R, Perlmutter M. Analysis of the flow and energy separation in a turbulent vortex. International Journal of Heat and Mass Transfer. 1960;1:173-91.
[12] Reynolds AJ. Energy flows in a vortex tube. Zeitschrift für Angewandte Mathematik und Physik (ZAMP). 1961;12:343-57.
[13] Erdélyi I. Wirkung des Zentrifugalkraftfeldes auf den Wärmezustand der Gase, Erklärung der Ranque-Erscheinung. Forschung im Ingenieurwesen. 1962;28:181-6.
[14] Sibulkin M. Unsteady, viscous, circular flow part 3. application to the Ranque-Hilsch vortex tube. Journal of Fluid Mechanics. 1962;12:269-93.
[15] Gulyaev A. Ranque effect at low temperatures. Journal of Engineering Physics and Thermophysics. 1965;9:242-4.
[16] Bruun H. Experimental investigation of the energy separation in vortex tubes. Journal of Mechanical Engineering Science. 1969;11:567-82.
[17] Linderstrøm-Lang C. The three-dimensional distributions of tangential velocity and total-temperature in vortex tubes. Journal of Fluid Mechanics. 1971;45:161-87.
[18] Yokosawa H. Energy Separation in Yerfei Tubes with a Diwergent Chamber. Taper. 1981;8:1.72.
[19] Kurosaka M. Acoustic streaming in swirling flow and the Ranque—Hilsch (vortex-tube) effect. Journal of Fluid Mechanics. 1982;124:139-72.
[20] Stephan K, Lin S, Durst M, Huang F, Seher D. An investigation of energy separation in a vortex tube. International Journal of Heat and Mass Transfer. 1983;26:341-8.
[21] Stephan K, Lin S, Durst M, Huang F, Seher D. A similarity relation for energy separation in a vortex tube. International journal of heat and mass transfer. 1984;27:911-20.
[22] Eckert E. Energy separation in fluid streams. International Communications in heat and mass transfer. 1986;13:127-43.
[23] Balmer R. Pressure driven Ranque Hilsch temperature separation in liquids. Journal of fluids Engineering. 1988;110:161-4.
[24] Ahlborn B, Keller J, Staudt R, Treitz G, Rebhan E. Limits of temperature separation in a vortex tube. Journal of Physics D: Applied Physics. 1994;27:480.
[25] Ahlborn B, Groves S. Secondary flow in a vortex tube. Fluid Dynamics Research. 1997;21:73-86.
[26] Gutsol A, Bakken J. A new vortex method of plasma insulation and explanation of the Ranque effect. Journal of Physics D: Applied Physics. 1998;31:704.
[27] Fröhlingsdorf W, Unger H. Numerical investigations of the compressible flow and the energy separation in the Ranque–Hilsch vortex tube. International Journal of Heat and Mass Transfer. 1999;42:415-22.
[28] Mischner J, Bespalov V. Zur Entropieproduktion im Ranque–Hilsch–Rohr. Forschung im Ingenieurwesen. 2002;67:1-10.
[29] Shannak BA. Temperature separation and friction losses in vortex tube. Heat and mass transfer. 2004;40:779-85.

[30] Aljuwayhel N, Nellis G, Klein S. Parametric and internal study of the vortex tube using a CFD model. International journal of refrigeration. 2005;28:442-50.
[31] Behera U, Paul P, Kasthurirengan S, Karunanithi R, Ram S, Dinesh K, et al. CFD analysis and experimental investigations towards optimizing the parameters of Ranque–Hilsch vortex tube. International Journal of Heat and Mass Transfer. 2005;48:1961-73.
[32] Gao C, Bosschaart K, Zeegers J, De Waele A. Experimental study on a simple Ranque–Hilsch vortex tube. Cryogenics. 2005;45:173-83.
[33] Piralishvili SA, Fuzeeva A. Hydraulic characteristics of Ranque-Hilsch energy separators. High temperature. 2005;43:900-7.
[34] Piralishvili SA, Fuzeeva A. Similarity of the energy-separation process in vortex Ranque tubes. Journal of Engineering Physics and Thermophysics. 2006;79:27-32.
[35] Skye H, Nellis G, Klein S. Comparison of CFD analysis to empirical data in a commercial vortex tube. International Journal of Refrigeration. 2006;29:71-80.
[36] Ui-Hyun J, BHL LG. Experimental and Numerical Studies in a Vortex Tube. Journal of Mechanical Science and Technology.20.
[37] Aydın O, Baki M. An experimental study on the design parameters of a counterflow vortex tube. Energy. 2006;31:2763-72.
[38] Eiamsa-ard S, Promvonge P. Numerical investigation of the thermal separation in a Ranque–Hilsch vortex tube. International Journal of Heat and Mass Transfer. 2007;50:821-32.
[39] Dincer K, Baskaya S, Uysal B. Experimental investigation of the effects of length to diameter ratio and nozzle number on the performance of counter flow Ranque–Hilsch vortex tubes. Heat and Mass Transfer. 2008;44:367-73.
[40] She Z-S, Jackson E, Orszag SA. Intermittant Vortex Structures in Homogeneous Isotropic Turbulence. Nature. 1990;344:226.
[41] Xue Y, Arjomandi M. The effect of vortex angle on the efficiency of the Ranque–Hilsch vortex tube. Experimental Thermal and Fluid Science. 2008;33:54-7.
[42] Secchiaroli A, Ricci R, Montelpare S, D'Alessandro V. Numerical simulation of turbulent flow in a Ranque–Hilsch vortex tube. International Journal of Heat and Mass Transfer. 2009;52:5496-511.
[43] Zin K, Hansske A, Ziegler F. Modeling and optimization of the vortex tube with computational fluid dynamic analysis. Energy research journal. 2010;1:193-6.
[44] Liew R, Zeegers J, Kuerten J, Michałek W. Temperature, Pressure and Velocity measurements on the Ranque-Hilsch Vortex Tube. Journal of Physics: Conference Series: IOP Publishing; 2012. p. 012066.
[45] Liew R, Zeegers J, Kuerten J, Michalek W. Maxwell's demon in the Ranque-Hilsch vortex tube. Physical review letters. 2012;109:054503.
[46] Xue Y, Arjomandi M, Kelso R. Experimental study of the thermal separation in a vortex tube. Experimental Thermal and Fluid Science. 2013;46:175-82.
[47] Liu X, Liu Z. Investigation of the energy separation effect and flow mechanism inside a vortex tube. Applied thermal engineering. 2014;67:494-506.
[48] Xue Y, Arjomandi M, Kelso R. Energy analysis within a vortex tube. Experimental thermal and fluid science. 2014;52:139-45.
[49] Kobiela B. Wärmeübertragung in einer Zyklonkühlkammer einer Gasturbinenschaufel: Verlag Dr. Hut; 2014.
[50] Manimaran R. Computational analysis of energy separation in a counter-flow vortex tube based on inlet shape and aspect ratio. Energy. 2016;107:17-28.
[51] Takahama H. Studies on vortex tubes:(1) experiments on efficiency of energy separation:(2) on profiles of velocity and temperature. Bulletin of JSME. 1965;8:433-40.
[52] Takahama H, Yokosawa H. An experimental study of the vortex tube-Where the vortex chamber includes a divergent tube. Nagoya University Faculty Engineering Memoirs. 1981;33:195-208.
[53] Saidi M, Valipour M. Experimental modeling of vortex tube refrigerator. Applied thermal engineering. 2003;23:1971-80.
[54] Nimbalkar SU, Muller MR. An experimental investigation of the optimum geometry for the cold end orifice of a vortex tube. Applied Thermal Engineering. 2009;29:509-14.
[55] Chang K, Li Q, Zhou G, Li Q. Experimental investigation of vortex tube refrigerator with a divergent hot tube. International journal of refrigeration. 2011;34:322-7.
[56] Uluer O, Kırmacı V, Ataş Ş. Using the artificial neural network model for modeling the performance of the counter flow vortex tube. Expert Systems with Applications. 2009;36:12256-63.

[57] Korkmaz ME, Gümüşel L, Markal B. Using artificial neural network for predicting performance of the Ranque–Hilsch vortex tube. International journal of refrigeration. 2012;35:1690-6.
[58] Khazaei H, Teymourtash AR, Malek-Jafarian M. Effects of gas properties and geometrical parameters on performance of a vortex tube. Scientia Iranica. 2012;19:454-62.
[59] Xue Y, Arjomandi M, Kelso R. Visualization of the flow structure in a vortex tube. Experimental Thermal and Fluid Science. 2011;35:1514-21.
[60] Xue Y, Arjomandi M, Kelso R. The working principle of a vortex tube. international journal of refrigeration. 2013;36:1730-40.
[61] Dos Santos E, Marques C, Stanescu G, Isoldi L, Rocha L. Constructal Design of Vortex Tubes. Constructal Law and the Unifying Principle of Design: Springer; 2013. p. 259-73.
[62] Eiamsa-ard S, Promvonge P. Numerical simulation of flow field and temperature separation in a vortex tube. International communications in heat and mass transfer. 2008;35:937-47.
[63] Bianco V, Khait A, Noskov A, Alekhin V. A comparison of the application of RSM and LES turbulence models in the numerical simulation of thermal and flow patterns in a double-circuit Ranque-Hilsch vortex tube. Applied Thermal Engineering. 2016;106:1244-56.
[64] User's Guide F. 6.3 Documentation. Fluent Inc, Lebanon, NH. 2006.
[65] Choudhury D. Introduction to the renormalization group method and turbulence modeling: Fluent Incorporated; 1993.
[66] Sarkar S, Balakrishnan L. Application of a Reynolds stress turbulence model to the compressible shear layer. 21st Fluid Dynamics, Plasma Dynamics and Lasers Conference1990. p. 1465.
[67] Fluent F. 6.3 user's guide. Fluent Inc. 2006.
[68] Leonard B. Convection-diffusion algorithms. Advances in numerical heat transfer. 1997.

